

ISSN : 2165-4069(Online)

ISSN : 2165-4050(Print)



IJARAI

International Journal of
Advanced Research in Artificial Intelligence

Volume 3 Issue 1

www.ijarai.thesai.org

A Publication of
The Science and Information Organization



INTERNATIONAL JOURNAL OF
ADVANCED RESEARCH IN ARTIFICIAL INTELLIGENCE



THE SCIENCE AND INFORMATION ORGANIZATION
www.thesai.org | info@thesai.org



Editorial Preface

From the Desk of Managing Editor...

"The question of whether computers can think is like the question of whether submarines can swim." — Edsger W. Dijkstra, the quote explains the power of Artificial Intelligence in computers with the changing landscape. The renaissance stimulated by the field of Artificial Intelligence is generating multiple formats and channels of creativity and innovation.

This journal is a special track on Artificial Intelligence by The Science and Information Organization and aims to be a leading forum for engineers, researchers and practitioners throughout the world.

The journal reports results achieved; proposals for new ways of looking at AI problems and include demonstrations of effectiveness. Papers describing existing technologies or algorithms integrating multiple systems are welcomed. IJARAI also invites papers on real life applications, which should describe the current scenarios, proposed solution, emphasize its novelty, and present an in-depth evaluation of the AI techniques being exploited. IJARAI focusses on quality and relevance in its publications.

In addition, IJARAI recognizes the importance of international influences on Artificial Intelligence and seeks international input in all aspects of the journal, including content, authorship of papers, readership, paper reviewers, and Editorial Board membership.

The success of authors and the journal is interdependent. While the Journal is in its initial phase, it is not only the Editor whose work is crucial to producing the journal. The editorial board members, the peer reviewers, scholars around the world who assess submissions, students, and institutions who generously give their expertise in factors small and large— their constant encouragement has helped a lot in the progress of the journal and shall help in future to earn credibility amongst all the reader members.

I add a personal thanks to the whole team that has catalysed so much, and I wish everyone who has been connected with the Journal the very best for the future.

Thank you for Sharing Wisdom!

Editor-in-Chief

IJARAI

Volume 3 Issue 1 January 2014

ISSN: 2165-4069(Online)

ISSN: 2165-4050(Print)

©2013 The Science and Information (SAI) Organization

Editorial Board

Peter Sapaty - Editor-in-Chief

National Academy of Sciences of Ukraine

Domains of Research: Artificial Intelligence

Alaa F. Sheta

Electronics Research Institute (ERI)

Domain of Research: Evolutionary Computation, System Identification, Automation and Control, Artificial Neural Networks, Fuzzy Logic, Image Processing, Software Reliability, Software Cost Estimation, Swarm Intelligence, Robotics

Antonio Dourado

University of Coimbra

Domain of Research: Computational Intelligence, Signal Processing, data mining for medical and industrial applications, and intelligent control.

David M W Powers

Flinders University

Domain of Research: Language Learning, Cognitive Science and Evolutionary Robotics, Unsupervised Learning, Evaluation, Human Factors, Natural Language Learning, Computational Psycholinguistics, Cognitive Neuroscience, Brain Computer Interface, Sensor Fusion, Model Fusion, Ensembles and Stacking, Self-organization of Ontologies, Sensory-Motor Perception and Reactivity, Feature Selection, Dimension Reduction, Information Retrieval, Information Visualization, Embodied Conversational Agents

Liming Luke Chen

University of Ulster

Domain of Research: Semantic and knowledge technologies, Artificial Intelligence

T. V. Prasad

Lingaya's University

Domain of Research: Bioinformatics, Natural Language Processing, Image Processing, Robotics, Knowledge Representation

Wichian Sittiprapaporn

Maharakham University

Domain of Research: Cognitive Neuroscience; Cognitive Science

Yaxin Bi

University of Ulster

Domains of Research: Ensemble Learning/Machine Learning, Multiple Classification Systems, Evidence Theory, Text Analytics and Sentiment Analysis

Reviewer Board Members

- **AKRAM BELGHITH**
University Of California, San Diego
- **ALAA F. SHETA**
Electronics Research Institute (ERI)
- **ALBERT ALEXANDER**
Kongu Engineering College
- **ALPA KALPESH RESHAMWALA**
NMIMS, MPSTME
- **AMIR HAJJAM EL HASSANI**
Université de Technologie de Belfort-Monbéliard
- **AMIT VERMA**
Department in Rayat & Bahra Engineering College, Mo
- **AMITAVA BISWAS**
Cisco Systems
- **ANTONIO DOURADO**
University of Coimbra
- **ASIM TOKGOZ**
Marmara University
- **B R SARATH KUMAR**
LENORA COLLEGE OF ENGINEERING
- **BABATUNDE OPEOLUWA AKINKUNMI**
University of Ibadan
- **BESTOUN S.AHMED**
Universiti Sains Malaysia
- **BHANU PRASAD PINNAMANENI**
Rajalakshmi Engineering College; Matrix Vision GmbH
- **CHIEN-PENG HO**
Information and Communications Research Laboratories, Industrial Technology Research Institute of Taiwan
- **DAVID M W POWERS**
Flinders University
- **DIMITRIS CHRYSOSTOMOU**
Production and Management Engineering / Democritus University of Thrace
- **EHSAN MOHEBI**
University of Ballarat
- **FABIO MERCORIO**
University of Milan-Bicocca
- **FRANCESCO PERROTTA**
University of Macerata
- **FRANK IBIKUNLE**
Covenant University
- **GERARD DUMANCAS**
Oklahoma Medical Research Foundation
- **GORAKSH GARJE**
Pune Vidyarthi Griha's College of Engineering and Technology, Pune
- **GRIGORAS GHEORGHE**
"Gheorghe Asachi" Technical University of Iasi, Romania
- **GUANDONG XU**
Victoria University
- **HAIBO YU**
Shanghai Jiao Tong University
- **HARCO LESLIE HENDRIC SPITS WARNARS**
Budi LUhur university
- **IBRAHIM ADEPOJU ADEYANJU**
Ladoke Akintola University of Technology, Ogbomoso, Nigeria
- **IMRAN CHAUDHRY**
National University of Sciences & Technology, Islamabad
- **JABAR H YOUSIF**
Faculty of computing and Information Technology, Sohar University, Oman
- **JATINDERKUMAR R. SAINI**
S.P.College of Engineering, Gujarat
- **JOSÉ SANTOS REYES**
University of A Coruña (Spain)
- **KRASIMIR YORDZHEV**
South-West University, Faculty of Mathematics and Natural Sciences, Blagoevgrad, Bulgaria
- **KRISHNA PRASAD MIYAPURAM**
University of Trento
- **LIMING LUKE CHEN**
University of Ulster
- **M. REZA MASHINCHI**
- **MALACK OTERI**
jkuat
- **MAREK REFORMAT**
University of Alberta
- **MD. ZIA UR RAHMAN**
Narasaraopeta Engg. College, Narasaraopeta

- **MOHAMED NAJEH LAKHOVA**
ESTI, University of Carthage
- **MOKHTAR BELDJEHEM**
University of Ottawa
- **MONJI KHERALLAH**
University of Sfax
- **PARMINDER SINGH KANG**
De Montfort University, Leicester, UK
- **PETER SAPATY**
National Academy of Sciences of Ukraine
- **PRASUN CHAKRABARTI**
Sir Padampat Singhanian University
- **QIFENG QIAO**
University of Virginia
- **RAJESH KUMAR**
National University of Singapore
- **RASHAD AL-JAWFI**
Ibb University
- **REZA FAZEL-REZAI**
Electrical Engineering Department,
University of North Dakota
- **SAID GHONIEMY**
Taif University
- **SAMARJEET BORAH**
Dept. of CSE, Sikkim Manipal University
- **SAURABH PAL**
VBS Purvanchal University, Jaunpur
- **SECUI DINU CALIN**
IEEE Membership; IEEE Power & Energy
Society Membership; IEEE Computational
Intelligence Society Membership
- **SHAHABODDIN SHAMSHIRBAND**
University of Malaya
- **SHRINIVAS PRABHAKARRAO DESHPANDE**
- **SIMON EWEDAFE**
Baze University
- **SUKUMAR SENTHILKUMAR**
Universiti Sains Malaysia
- **T C.MANJUNATH**
HKBK College of Engg
- **T V NARAYANA RAO**
Hyderabad Institute of Technology and
Management
- **T. V. PRASAD**
Lingaya's University
- **V BABY DEEPA**
- **VIJAY JHA**
BIT MESRA, Ranchi (Jharkhand)
- **VISHAL GOYAL**
- **VITUS S.W. LAM**
- **VUDA SREENIVASARAO**
St. Mary's College of Engineering &
Technology
- **WEI ZHONG**
University of south Carolina Upstate
- **WICHIAN SITIPRAPAPORN**
Mahasarakham University
- **YAXIN BI**
University of Ulster
- **YUVAL COHEN**
The Open University of Israel
- **ZHAO ZHANG**
Deptment of EE, City University of Hong
Kong
- **ZHIGANG YIN**
Institute of Linguistics, Chinese Academy of
Social Sciences
- **ZNE-JUNG LEE**
Dept. of Information management, Huafan
University

CONTENTS

Paper 1: Association Rule Based Flexible Machine Learning Module for Embedded System Platforms like Android

Authors: Amiraj Dhawan, Shruti Bhawe, Amrita Aurora, Vishwanathan Iyer

PAGE 1 – 8

Paper 2: Speed and Vibration Performance as well as Obstacle Avoidance Performance of Electric Wheel Chair Controlled by Human Eyes Only

Authors: Kohei Arai, Ronny Mardiyanto

PAGE 9 – 15

Paper 3: Sensitivity Analysis for Aerosol Refractive Index and Size Distribution Estimation Methods Based on Polarized Atmospheric Irradiance Measurements

Authors: Kohei Arai

PAGE 16 – 21

Paper 4: Vital Sign and Location/Attitude Monitoring with Sensor Networks for the Proposed Rescue System for Disabled and Elderly Persons Who Need a Help in Evacuation from Disaster Areas

Authors: Kohei Arai

PAGE 22 – 34

Paper 5: Method and System for Human Action Detections with Acceleration Sensors for the Proposed Rescue System for Disabled and Elderly Persons Who Need a Help in Evacuation from Disaster Area

Authors: Kohei Arai

PAGE 35 – 41

Paper 6: A New Trust Evaluation for Trust-based RS

Authors: Sajjawat Charoenrien, Saranya Maneeroj

PAGE 42 – 46

Paper 7: Human Lips-Contour Recognition and Tracing

Authors: Md. Hasan Tareque, Ahmed Shoeb Al Hasan

PAGE 47 – 51

Paper 8: New concepts of fuzzy planar graphs

Authors: Sovan Samanta, Anita Pal, Madhumangal Pal

PAGE 52 – 59

Paper 9: Some more results on fuzzy k-competition graphs

Authors: Sovan Samanta, Madhumangal Pal, Anita Pal

PAGE 60 – 67

Paper 10: Zernike Moment Feature Extraction for Handwritten Devanagari (Marathi) Compound Character Recognition

Authors: Karbhari V. Kale, Prapti D. Deshmukh, Shrinivas V. Chavan, Majharoddin M. Kazi, Yogesh S. Rode

Association Rule Based Flexible Machine Learning Module for Embedded System Platforms like Android

Amiraj Dhawan¹ Shruti Bhawe²

Amrita Aurora³ Vishwanathan Iyer⁴

Abstract—The past few years have seen a tremendous growth in the popularity of smartphones. As newer features continue to be added to smartphones to increase their utility, their significance will only increase in future. Combining machine learning with mobile computing can enable smartphones to become ‘intelligent’ devices, a feature which is hitherto unseen in them. Also, the combination of machine learning and context aware computing can enable smartphones to gauge users’ requirements proactively, depending upon their environment and context. Accordingly, necessary services can be provided to users.

In this paper, we have explored the methods and applications of integrating machine learning and context aware computing on the Android platform, to provide higher utility to the users. To achieve this, we define a Machine Learning (ML) module which is incorporated in the basic Android architecture. Firstly, we have outlined two major functionalities that the ML module should provide. Then, we have presented three architectures, each of which incorporates the ML module at a different level in the Android architecture. The advantages and shortcomings of each of these architectures have been evaluated. Lastly, we have explained a few applications in which our proposed system can be incorporated such that their functionality is improved.

Keywords—machine learning; association rules; machine learning in embedded systems; android, ID3; Apriori; Max-Miner

I. INTRODUCTION

Smartphones today are equipped with a number of features which have made it possible for users to obtain information at their fingertips. Incorporation of context aware computing in smartphones can give rise to innumerable new applications in mobile computing. A context aware system uses context to provide information and/or necessary services to users. The information and services provided depend on the current tasks the user is performing on the smartphone [1].

To utilize context awareness to its fullest potential, the system should have knowledge about how the device is used by the user and in what context. This can be achieved through machine learning. In machine learning, the system learns to make associations between the various tasks performed by the user and the corresponding context, which can be the inputs given to the device or other environmental factors. Android being a widely used mobile platform, in this paper, we have proposed methods to incorporate machine learning in the Android architecture. This is achieved through a machine learning (ML) module.

We have identified two major functionalities that the ML module should provide to achieve context awareness in the

system and accordingly have described two modes of operation of the ML module. Next, we have proposed three variations in the Android architecture, which will enable machine learning to be included in the system. In each of these architectures, the ML module is placed at different levels in the Android architecture, which determines how the module will interact with the system as a whole. The placement of the ML module in the Android architecture determines which mode of operation it will be best suited for, as well as the applications that the ML module can be used for.

Finally, we have explained a few applications that can use context aware computing for a more user friendly smartphone experience. These applications make use of the ML module to learn about the device usage patterns and the context of the user. Accordingly, it forms certain associations and rules, using which these applications are prompted to the user proactively.

II. LITERATURE SURVEY

A. Android Architecture

Figure. 1 shows the principal components and levels in the Android architecture.

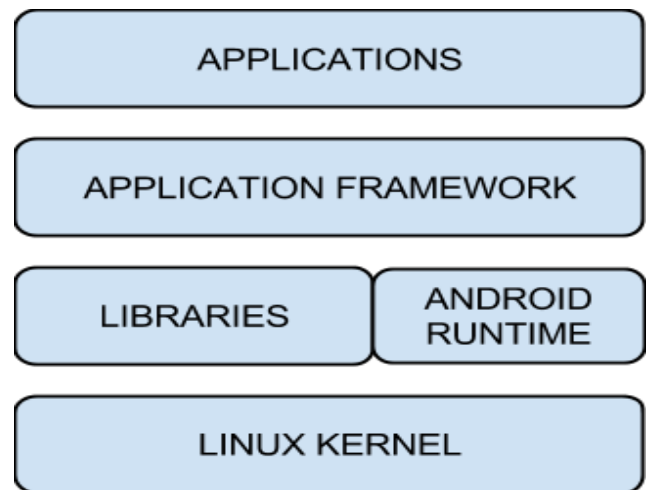


Fig. 1. The Android Architecture

The basic working and functionalities of each component are described as follows [2]:

- Linux Kernel:

Linux kernel forms the bottom layer of the architecture. It provides basic system functionality like process management,

device management and memory management. Also, the kernel handles functions like networking and a huge array of device drivers, to which peripheral hardware is interfaced.

- Libraries:

There is a set of libraries above the linux kernel, which includes WebKit- an open source web browser engine, libc, SQLite database-a useful repository for sharing and storage of application data, libraries to record and play audio as well as video, SSL libraries to monitor internet security, etc.

- Android Runtime:

This is the third section and belongs to the second layer from the bottom. It provides an important component named Dalvik Virtual Machine which is like Java Virtual Machine, designed and optimized specially for Android.

The Dalvik Virtual Machine uses core features of Linux like memory management and multi-threading. The Dalvik Virtual Machine enables every Android application to run in its own process, with its own instance of the Dalvik Virtual Machine. Additionally, the Android runtime provides a set of core libraries. Using these libraries, Android application developers can write Android applications using the standard Java programming language.

- Application Framework:

The Application Framework layer provides a number of higher level services to applications as Java classes. Application developers can use these services to write their applications.

- Applications:

All applications are strictly installed at the top layer. Home, Messages, Contact Books and Games are a few examples of these applications.

B. ID3 (Iterative Dichotomiser 3) Algorithm

ID3, developed by Ross Quinlan, is a decision tree learning algorithm used in the domains of machine learning and language processing. The ID3 algorithm employs a top-down search through the given datasets to test each attribute at every tree node. In this way, a decision tree is constructed. Every tuple in the database is then passed through the tree, which results in its classification.

To determine the input attribute that provides maximum information about the output, a metric called entropy is used. In information theory, entropy is used to measure the order or certainty in a given database set. A higher value of entropy indicates poor classification. A metric called information gain decides which input attribute is to be split. It is calculated as the difference between the entropy of the original dataset and the weighted sum of the entropies of the subdivided datasets. Information gain for each attribute is determined, and the attribute with the highest gain is split [3].

C. Apriori Algorithm

Apriori is a classical algorithm used for association rule learning. This algorithm tries to successively create larger and larger item sets that appear sufficiently in the database.

The algorithm starts with simple association rules of input to output mapping and tries to create more complex rules from these simple rules by increasing the size of the input and output item sets if they appear in the training data sufficient number of times. Every apriori algorithm requires two parameters, first is the support threshold and second is a confidence threshold. Apriori algorithm takes a bottom up approach since it starts with individual items in the item sets and successively adds multiple items in the item sets if they satisfy the support threshold.

This algorithm is one of the most popular association rule generation algorithms. But, the only disadvantage of this algorithm is in its bottom up approach which requires a lot of processing since it enumerates over all the combinations of the item sets [4].

D. Max-Miner Algorithm

Max-Miner algorithm is used to generate association rules with a complexity which is linear to the number of patterns or rules present in the training data.

The complexity is independent of the maximum length of these rules. The algorithm makes use of set-enumeration tree. It heuristically orders the items and dynamically reorders them on a pre-node basis, which leads to an improvement in performance. Hence, this algorithm is preferred [5].

E. Papers

In [6], how context aware systems enhance human computer interaction has been explained. Since context aware computing relies not only on the explicit current input given to a device, but also on the history of actions performed by the device and is capable of modifying the output with changing situations, the unnecessary interaction with the user is reduced.

In [7], the working of 'SenSay' has been described. SenSay is a mobile phone that is capable of manipulating its profile settings in accordance with the user's environment and physiological state. Various sensors, placed on the body give inputs about the users' state to a sensor box mounted on the waist. Based on the sensor information, a decision module computes the resultant action to be taken. However, SenSay does not incorporate machine learning, but relies solely on a set of predefined rules to determine the output. Also, SenSay gets inputs from sensors mounted on the body to obtain information about the user's context. Since our method does not require the user to carry any additional device on their person, it is more convenient to handle.

[8] explores the concept of using machine learning to train a system to choose songs to be played depending on the current activity and physiological state of the user. This device stores all the information relevant to a song, including the time of the day at which it is played, the corresponding activity of the user as well as the user's rating of the song. This is the training period of the system.

Once the training is complete, the device can select and play songs depending on the user's context using machine learning. However, its scope is limited only to song selection and music playlists.

III. PROPOSED SYSTEM

A. Functionalities Required

Broadly, the proposed Machine Learning Module is supposed to provide two major functionalities as described below:

1) *In the first case, any third party application should be able to use the module by providing the following information:*

a) *Set of inputs and/or parameters that are critical for the application.*

b) *Set of valid outputs/actions that the application understands.*

c) *Training data in the form of rules such as:*

Inputs and/or Parameters =>Output/Action, which are used to learn and automatically generate rules with their confidence level.

2) *In the second case, the machine learning module works on its own in a global scope and tries to learn how and in what context the user uses the interface and the android system. Depending on the learning algorithm it should be able to automatically generate rules. Consider an example where the user frequently uses an application near a location (like a train station). Here, the system tries to learn this association. Accordingly, it generates a rule that if the user is near the same location, then the used application is invoked automatically.*

B. Modes of operation of ML module

In order to provide the above mentioned functionalities, the proposed machine learning module has two modes of operation as follows:

- **Application Level Learning:**

The module is used in this mode whenever other applications are to use the learning module for purposes internal to the application. This mode fulfills the first required functionality.

- **System Level Learning:**

The module constantly monitors the system and checks if the current context i.e., the current inputs and/or parameters match an already learned generated rule. If a match is found, then the required output/action is performed. Also, if an event occurs due to the users' intervention, like invocation of an application, the module adds the current inputs and/or parameters and the action i.e., the invocation of application as an entry in the training data. In this manner, the system learns new rules on the runtime.

C. Steps to be followed by the third party application in order to use the ML Module

To effectively use the ML module, any third party application needs to follow a set of steps to ensure proper configuration of the module and explain the kind of input and the expected list of outputs to the module. Since multiple applications should be able to use the ML module, a method is required through which the ML module can uniquely identify each application.

Accordingly, the module will load the proper context and use the inputs provided by the application. The process is as follows:

- **Register_App:**

In this step the third party application is required to call the Register_App API of the ML module in order to register itself with the ML module. This procedure generates a random alphanumeric string and stores this alphanumeric string along with the application name passed. This random alphanumeric string (identification key) is passed to the third party application which is required to remember this string. In any further communication with the ML module, this string is to be passed. The string helps the ML module to uniquely identify applications when the requests are coming through a common API.

In all the further requests, the string helps the ML module to load the proper context of the application for proper usage. This step needs to be done only once for initialization. After this step, the third party application is always required to send the identification key with the requests.

- **Set_Input_Output:**

In this step the third party application is required to send an array of parameters with their data types that are supposed to be used as inputs for the ML algorithm. It should also send an array of data types of the outputs which the ML module should produce, along with the identification key with which the applications are registered. This key helps the ML module to know which application is trying to access the API. This request is supposed to be sent only once, before calling Generate_Rules.

- **Load_Training_Data:**

In this step the third party can send any training data if available, to the ML module. This data should be in the format specified in the Set_Input_Output call. This step can be skipped and the data for generating the rules can be set as and when it is available as individual rows/tuples.

- **Set_Training_Data_Row:**

This step can be done repeatedly at any time or even skipped. This request is used to insert a new row in the training data for the applications, determined by the accompanying identification key. The format of the row should be as per the structure defined using Set_Input_Output.

Either Load_Training_Data or Set_Training_Data_Row should be performed (single or multiple times) to ensure that the ML module has some training data to generate rules. If the application does not have a training data set available then it can insert rows of training data whenever an event occurs. Hence this step is essential.

- **Generate_Rules:**

This step asks the ML module to generate the rules as per the support threshold and confidence threshold provided by the third party application. This request returns 'False' if the training data set is empty. If the training data for the application has at least one row, the returned data is the set of

rules generated according to the support and confidence thresholds passed along with the request. This request also stores the generated rules along with the identification key of the application for use. The design decision of allowing the application to provide the required support threshold and confidence threshold is to allow various applications to generate rules with a confidence level which is required by the application. This ensures that the generated rules are flexible according to the need of the application.

Consider a case in which an application does repeated calls to `Generate_Rules` with varying support and confidence threshold to smartly select which rule to follow and give some response to the event. This request is essential to be called at least once with success. This request can be configured in two modes:

1) *Automated*: In this mode, the request is generated internally by the ML module whenever `Set_Training_Data` or `Set_Training_Data_Row` is called. The third party applications do not need to call this function directly

2) *Manual*: In this mode, the application is required to call this request explicitly whenever required.

- `Get_Current_Output`:

The application after generating the rules from the training data can then use the rules internally to get the output for a given set of inputs. Else, it can ignore the returned rules and call this request `Get_Current_Output` and pass an array of the inputs to get the inferred output from the ML module. The module on receiving this request first loads the context of the application with the help of the identification key.

Next it loads the generated rules for this application and parses the rules to check if it has a rule with the inputs passed along with the request. If such a rule is found then the output of the rule is sent back to the application else 'Null' is passed. The application, depending on the expected output sent by the ML module can then take actions for the event(s) (set of inputs passed to this request).

- `Send_Feedback_Last_GCO_Request`:

This stands for send feedback of last `Get_Current_Output` request. This request is used to send a feedback to the ML module for the last call to the request `Get_Current_Output`. If the output expected by the ML module was correct then a positive feedback is sent to the module else a negative feedback is sent. For a positive feedback, the module increases the confidence of the rule by a predefined amount. For a negative response the confidence of the rule is dropped by some predefined amount. This request is optional.

Some more non critical requests are as follows:

- `Delete_Training_Data`:

This request is used to delete all the training data.

- `Delete_Training_Data_Row`:

This request is used to delete a row from the training data. The set of inputs needs to be provided to find the row required

for deleting. Either the first matched row is deleted or all the rows with the same values of the set of inputs are deleted.

- `Change_Inputs_Outputs`:

In case the application requires to change the structure of the training data then this request can be used to specify the new structure of the training data required. The missing inputs from the new structure are deleted from the training data and any new input is kept as null for the previous training data. Any changes in the output are also handled the same way as inputs.

D. System Level Learning: A special case of Application Level Learning

System level learning is a special case of application level learning in which the entire system is one application and the requests are auto generated by listeners on the sensors (inputs/parameters) and events (outputs like vibrator or speakers, invocation of an application). If there is an event like invocation of an application by the user, the state of the sensors with some other parameters like time etc, are used as the input. The current inputs are monitored constantly. At any point if the inputs match a rule, the output as per the rule can be used to automatically generate an event without the users' intervention.

E. Architectures

Placing the Machine Learning Module in the android architecture is a critical decision to be made. The placement affects the way other applications would interact with the ML module and also how the module can work independently in the System Level Learning mode.

- Application Level Architecture

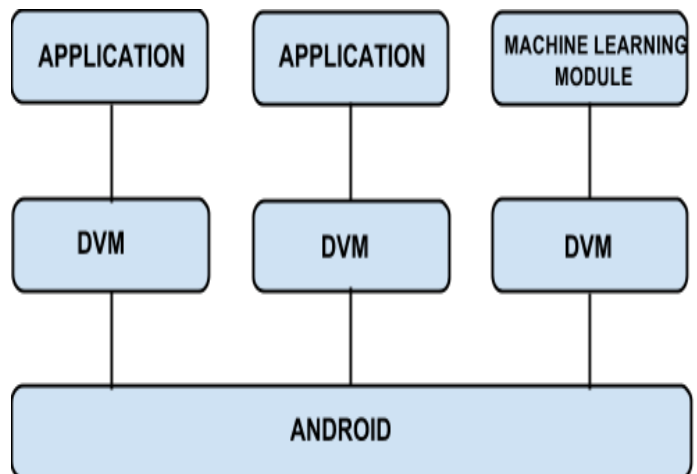


Fig. 2. Application level architecture

In this proposed architecture, the machine learning module is used as an application which executes over its own Dalvik Virtual Machine (DVM). The third party applications would be required to communicate with the Machine Learning Module Application (MLMA). This can be achieved using the Intent class of the Android Framework for Inter Application Communication.

The following snippet shows how inter application communication can be achieved.

```
<activity android:name=".SecondActivity">  
<intent-filter>  
<action  
android:name="com.machineLearning.action.REGISTER_AP  
P_ML" />  
<action  
android:name="com.machineLearning.action.SET_INPUTS_  
OUTPUTS" />  
<action  
android:name="com.machineLearning.action.GET_CURREN  
T_OUTPUT" />  
/* and so on for all the requests mentioned above */  
</intent-filter>  
</activity>
```

This method requires the third party applications to specify an action for each of the functions provided by the MLMA. This approach is not preferable since it requires a lot of effort from the third party application. Also in this approach since the ML module runs as an independent application, it cannot access all the various sensors and input data sources without proper permissions. Thus in this case the ML module would require access to all the sensors and in return permissions to all the sensors which is difficult to manage.

In this case since the ML module works as a separate application, using the module for system wide learning is difficult. For system level learning the operating system would be required to use the functionality of the module as if it is another third party application. Thus system level learning cannot work independently without the need for the operating system to use it.

- System Level Architecture

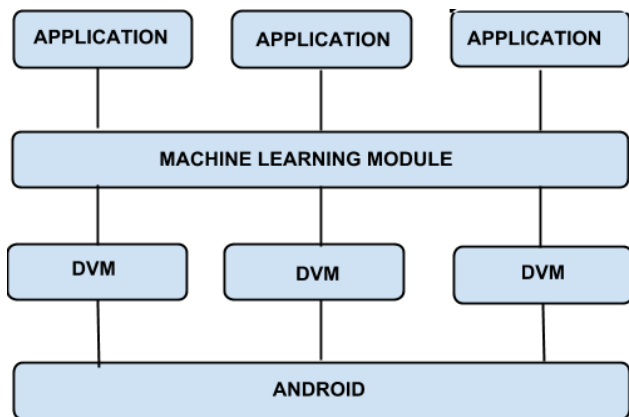


Fig. 3. System Level Architecture

In this approach, the ML module works as a layer between the DVM and the applications. This gives easy access to the machine learning module from the applications.

In this case since the ML module does not act as a standard application, it can be bundled with the operating system itself and surpass the permissions required as in the previous approach.

The module being part of the operating system can easily access any sensor. Since in this approach the ML module is between the DVM and the third party applications, it can easily monitor the usage of the applications and can work well for system level learning. However since the ML module is shared across the third party applications, providing access to the module from the applications for application level learning is challenging. Separating the applications context from each other would be difficult since all the applications share the same ML module layer.

This approach would require a lot of change in how the applications interact with the DVM instances. The module would be required to monitor all the interactions between the applications and the corresponding DVM machine. This would require changes in the core android operating system.

- Hybrid Architecture

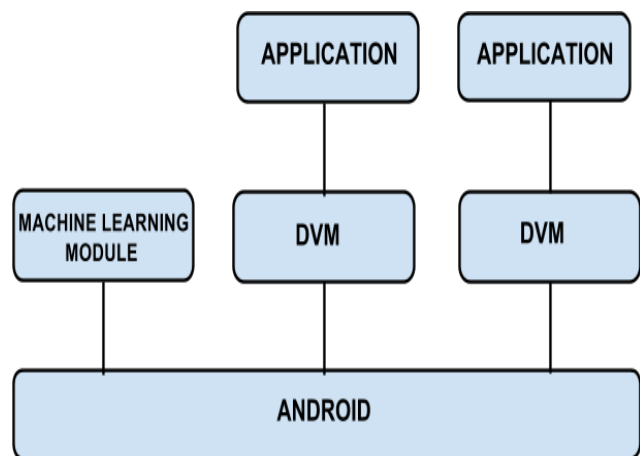


Fig. 4. Hybrid Architecture

In this approach, the module works as an independent system level library which is available as an API for applications for usage. Since the module is an independent library, the operating system too can use the functionality and perform system level learning. This approach can be used effectively for both system level as well as application level learning. Since the ML module is a library, it does not require permissions to access the sensors or other input sources. The applications can communicate with the module using all the requests explained earlier.

The operating system can register itself and send training data to learn usage patterns. Thus, it can deduce which application is highly likely to be used at the current instance. This output or deduced information can be used to automatically start applications as per the current input and sensor state. This architecture not only provides a good and clean interface for application level learning but also supports system level learning.

F. Generation of Rules

Once the application (or operating system in case of system level learning) creates a training data set for the ML module using either Load_Training_Data or Set_Training_Data_Row, it can instruct the machine learning

module to generate association rules. These can be used to predict the current usage output as per the current input state. This procedure may take considerable time depending on the size of the training data. The module at this point starts parsing the training data for the particular application and tries to generate association rules that cross the support and confidence threshold values. The ML module generates these association rules by using algorithms like Apriori, ID3 or Max-Miner, which are popular association rule generation algorithms. For this application Max-Miner algorithm would be preferable since it uses less resources to come up with good association rules as compared to Apriori algorithm. Since embedded systems have lesser resources, performance should be the most important criteria while selecting the association rule generation algorithm.

Once the rules are generated for an application, it can then request for the current output possible according to the rules generated by providing the input list. If a rule exists with similar input state as provided by the application, the corresponding output is returned by the machine learning module along with its confidence level. The application can then decide what is supposed to be done with the output.

In case of the system level learning, the operating system performs all the tasks just like an ordinary application can work.

The actual end action is decided by the applications depending on the output of the machine learning module. This output can also be ignored by the application thus proving flexible usage of the module.

IV. APPLICATIONS

The following examples provide an overview of the varied use of the machine learning module in mobile applications. Depending on the users everyday usage of the device, the machine learning module trains itself and provides an output that saves time and is comfortable to access by the user.

A. Music player application

A user has an everyday schedule of listening to particular songs at particular instants of time, for example, while travelling to work at 8:00 AM or returning home at 7:00 PM. The machine learning module stores all the information relevant to opening of the music player and playing the song.

This includes the time at which it is played and the activity of the user at that time. Inputs of inserting the headphones in the device and opening the player at that particular time are provided to the module. It then trains itself according to this users schedule and generates an application ID which denotes that the music player application is running currently. If the same task is performed by the user every day at the same time after the training period, the module automatically provides a widget to the user at that time of the day to open the player thus saving his time.

B. Automatic Profile Settings

Automatic profile settings can be extremely beneficial to students in schools and colleges as well as employees in companies. The predefined time of a daily lecture or meeting

is known to the user. Inputs of these lecture/meeting timings as well as the location of the school/office is provided as input to the machine learning module. Combining the users' environmental location and the timing of the users usage on the mobile device, the module trains itself and depending on the application ID provided, it displays a widget suggesting to the user to change the phone settings to silent mode. This prevents the unnecessary ringing of mobiles in important meetings and lectures making it immensely user friendly.

C. Task List

The user experience can be drastically improved by displaying relevant information on the device's screen rather than spending time searching for that information. Machine learning module takes input of a task list and the time for execution of this task from the user. Following the users usage pattern, it trains itself to display a widget of this task list needed at the time of its implementation. For example, if the user purchases groceries from the market every Friday at 7:00 PM, then the mobile will automatically display the list of groceries to be purchased by the user at this time every week. This saves time and makes it user friendly for the user.

D. Messaging

The user habitually sends the same alert message at a particular instant every day at the same time for a week. For example, a user before leaving for school/work informs his parents/spouse that he has left home. The ML module saves a draft of this message. The time, day and message are provided as the input to the ML module. Depending on the time span when the user leaves for school/work, the module displays an output i.e., the drafted message on the users screen with the recipients entered. The user can then just press the send option to send the message thus saving his time rather than retyping the same message every day and then searching for the recipients.

E. Location Based Profile Settings

If the user traverses the same path every day eg: from home to work or vice versa, the ML module keeps a record of his path taken regularly which is provided as input. With the help of Google plus, if there is a huge amount of traffic on that path on any particular day, it informs the user to traverse another path with lesser traffic. Thus the users' energy and time are saved.

F. Alarm

The user sets the alarm every day in a specific span of time. Thus the time and date of entering the event is provided to the ML module as input. The ML module then learns and trains itself according to the input of these events. The module provides an application ID which indicates the application being that of the alarm. The output is provided to the user in form of a widget that suggests the needed occurrence of the alarm. Thus the module trains itself to display a widget of the alarm every day at certain time interval before the person sets the alarm.

V. CONCLUSION

Incorporation of context awareness in mobile computing has a wide scope in a number of smartphone applications. The

ability to learn about users' preferences and usage patterns and suggest services accordingly will facilitate a more user-friendly smartphone experience.

Although this paper describes context awareness and machine learning specific to the android framework, it can also be extended to include other embedded systems like set-top box or a set-top unit. The machine learning module can learn about the channel preferences of the viewer, on the basis of the previous viewing history, time as well as day of the week. Accordingly, it can suggest which channel is to be played at what time. As most viewers have fixed television schedules as well as fixed preferences in terms of channels and television shows, the channels can be tailored according to each user's needs and demands. Thus, the machine learning module can be incorporated in various embedded systems for a more personalized and simplified usage experience.

VI. FUTURE WORK

The paper in its current scope focuses on the importance of a machine learning module in an embedded system platform like android. The main focus is on how to design the module to be flexible so that it can be used by other applications as well as by the system. It also deals with the interface of the module to allow maximum flexibility and allow efficient use of the module.

Taking this proposed system as the base, future efforts include generalizing the module for generic embedded system platforms, analyze and compare the performance of the module using various association rule generation algorithms like ID3, Apriori and Max-Miner from a qualitative perspective. The future work on this system also includes working on the privacy issues of this machine learning module since it handles user data. Another research area could be to design and implement the machine learning module in a hardware integrated circuit to offload the heavy processing required by the module from the main processing unit. The

hardware IC can be designed to support processors based on the ARM architecture which is widely used on embedded systems. This could lead to better support for machine learning on such systems and provide unparalleled support to understand the user/environment better in order to take smart decisions by the embedded platforms.

Robotic platforms can leverage the machine learning capabilities to be slightly closer to achieving artificial intelligence. This is because these platforms can then accurately predict future events based on past events. If the module is implemented as a hardware IC, then the interface between the robotic platforms and this module can be simplified.

REFERENCES

- [1] G. D. Abowd, A. K. Dey, P. J. Brown, N. Davies, M. Smith, and P. Steggle, "Towards a Better Understanding of Context and Context-Awareness," in Proceedings of the 1st international symposium on Handheld and Ubiquitous Computing Karlsruhe, Germany: Springer-Verlag, 1999.
- [2] "Android Architecture," http://www.tutorialspoint.com/android/android_architecture.htm
- [3] KalpeshAdhatrao, Aditya Gaykar, AmirajDhawan, RohitJha and VipulHonrao, "Predicting Students' Performance Using ID3 and C4.5 Classification Algorithms," in International Journal of Data Mining & Knowledge Management Process (IJDKP) Vol.3, No.5, September 2013.
- [4] "Apriori Algorithm," http://en.wikipedia.org/wiki/Apriori_algorithm
- [5] Roberto J, and BayardoJr, "Efficiently Mining Long Patterns from Databases," IBM Almaden Research Center.
- [6] H. Lieberman, T. Selker, "Out of Context: Computer Systems that Adapt to and Learn from, Context," in IBM Systems Journal, Volume 39, Nos. 3 and 4, 2000.
- [7] DanielSiewiorek, AsimSmailagic, Junichi Furukawa, NeemaMoraveji, Kathryn Reiger, and Jeremy Shaffer, "Sen-Say: A Context-Aware Mobile Phone," Human Computer Interaction Institute and Institute for Complex Engineered Systems, Carnegie Mellon University.
- [8] SandorDornbush, Jesse English, Tim Oates, ZarySegall and Anupam Joshi, "XPod: A Human Activity Aware Learning Mobile Music Player," University of Maryland, Baltimore County.

Speed and Vibration Performance as well as Obstacle Avoidance Performance of Electric Wheel Chair Controlled by Human Eyes Only

Kohei Arai ¹

Graduate School of Science and Engineering
Saga University
Saga City, Japan

Ronny Mardiyanto

Department of Electric and Electronics
Institute Technology of Surabaya
Surabaya, Indonesia

Abstract—Speed and vibration performance as well as obstacle avoidance performance of the previously proposed Electric Wheel Chair: EWC controlled by human eyes only is conducted. Experimental results show acceptable performances of speed vibration performance as well as obstacle avoidance performance for disabled persons. More importantly, disabled persons are satisfied with the proposed EWC because it works by their eyes only. Without hands and finger, they can control EWC freely.

Keywords—Human Computer Interaction; Gaze; Obstacle Avoidance; Electric Wheel Chair Control

I. INTRODUCTION

The Electric Wheel Chair: EWC controlled by human eyes only is proposed previously. It works well in principle. Some experiments show acceptable performances previously. This paper describes the performance of speed control and vibrations as well as obstacle avoidance performance.

The proposed system consists of forward and backward looking Web cameras mounted glass and pocket PC that allows Bluetooth communications. Thus users can be moved using the system. Pocket PC can be communicated with not only with Input and Output devices but also the other pocket PCs mounted on the other Electric Wheel Chairs: EWCs so that created and updated map information can be shares with many EWCs. The system provides obstacle finding with forward-looking camera so that EWCs can avoid obstacles. Location information of obstacles is uploaded to the other EWCs through Bluetooth communications. Thus all the EWCs can be controlled safely avoiding obstacles with the shared map information.

The following section describes the proposed system followed by experiments for the proposed system in terms of control performance of EWC, in particular, obstacle avoidance performance.

II. THE PROPOSED COMPUTER INPUT SYSTEM WITH HUMAN EYES-ONLY

A. Hardware configuration

Hardware configuration is shown in Figure1. The proposed system consists of (1) two Web cameras mounted glass, (2) Pocket PC, (3) Ultrasonic Sensor. One of two Web cameras

looks forward and the other one looks backward (acquires users' eye image). The web camera used 1.3 Mega pixel OrbiCam (Visible camera) and The Pocket PC used Sony VAIO UX180P with Intel Solo Processor U1400 1.20GHz and 512 MB RAM. First camera is used for acquired eye behavior and other camera is used for detect the obstacle. The Electric Wheel Chair used Yamaha JW-I type.

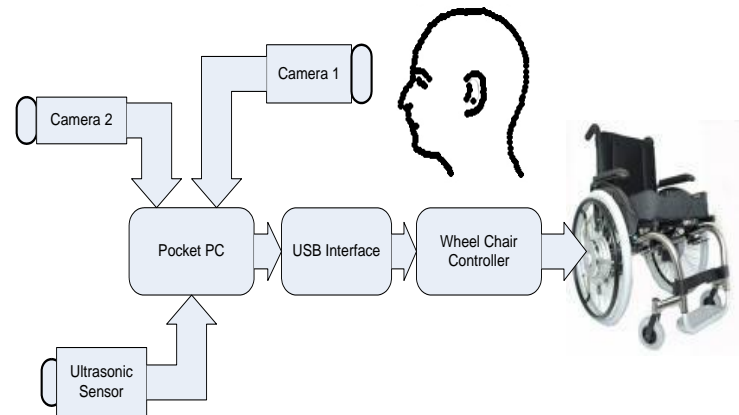


Fig. 1. Hardware configuration

B. The method used and system parameters

In order to control EWC, at least four keys, move forward, turn right, turn left and stop are required. For the safety reason, users have to look forward so that the key layout that is shown in Figure 2 is proposed.

Stop		
Turn left	Move forward	Turn right
Stop		

Fig. 2. 3 by 3 of key layout for EWC control

Namely, key consists of 9 keys (3 by 3). Move forward and turn left/right are aligned on the middle row. Stop key is aligned on the other rows, top and bottom rows. Users understand the location of desired key so that it can be selected with users' eye-only. The backward looking Web camera whose resolution is 640 by 480 pixels acquires users' eye and its surrounding. Using OpenCV⁽¹⁴⁾ of eye detection and tracking installed on the Pocket PC, users' eye is detected

and tracked. If the OpenCV cannot detect users' eye, then EWC is stopped for safety reason. EWC is also stopped when users look at the different location other than the three keys aligned on the center row. When users are surprised human eyes used to be large. Such a situation can be detected with acquired image with backward looking Web camera so that EWC is stopped.

Intentional blink can be detected if the eye is closed for more than 0.4 seconds because accidental blink is finished within 0.3 seconds. In this connection, it is easy to distinguish between intentional and accidental blink. Also, key selection can be done every 0.4 seconds. Thus the system recognizes user specified key every 0.4 seconds. In order to make sure the user specified key, 10 frames per seconds of frame rate is selected for backward looking camera.

C. Eye Detection and Tracking⁽¹⁷⁾

Figure 3 shows the process flow of eye detection and tracking. Eye is detected by Viola-Jones classifier. The viola-Jones classifier employs ADABOOST at each node in the cascade to learn a high detection rate the cost of low rejection rate multi-tree classifier at each node of the cascade. To apply the viola-Jones classifier on the system, we use viola-Jones function in OpenCV⁽¹⁵⁾. Before use the function, we should create xml file data. The training sample (face or eye image) must be collected. There are two sample types: negative and positive sample. Negative sample correspond to non-object images. Positive sample correspond to object image. After acquired image, OpenCv will search the face center location and continue with search the eye center location. Advantage this function is fast and robust.



Fig. 3. Eye detection and tracking

D. Template Matching

Eye behavior is detected by template matching. Template matching which used is not based on histograms; the function matches an actual image patch against an input by sliding the patch over the input image. There are several template matching methods:

1) Square difference matching methods

These methods match the square difference, so perfect match will be 0 and bad matches will be large.

$$R_{sq_diff}(x, y) = \sum_{x', y'} [T(x', y') - I(x + x', y + y')]^2 \quad (1)$$

This method will obtain good result only if both images have same pixel intensity. Because of output result only 0 and 1, it not sophisticated for the proposed system.

2) Correlation matching methods

These methods multiplicatively match the template against the image, so a perfect match will be large and bad matches will be small or 0.

$$R_{corr}(x, y) = \sum_{x', y'} [T(x', y') \cdot I(x + x', y + y')]^2 \quad (2)$$

3) Correlation coefficient matching methods.

These methods match a template relative to its mean against the image relative to its mean, so a perfect match will be 1 and a perfect mismatch will be -1; a value of 0 simply means that there is no correlation.

$$R_{coeff}(x, y) = \quad (3)$$

$$\sum_{x', y'} [T'(x', y') \cdot I'(x + x', y + y')]^2 \quad (4)$$

$$T'(x', y') = \frac{1}{(w \cdot h) \sum_{x'', y''} T(x'', y'')} \quad (5)$$

$$I'(x + x', y + y') = \frac{1}{(w \cdot h) \sum_{x'', y''} I(x + x'', y + y'')}$$

In this system we used Correlation coefficient methods and give additional normalized to reduce the effects of lighting difference between the template and the image.

$$z(x, y) = \sqrt{\sum_{x', y'} T(x', y')^2 \cdot \sum_{x', y'} I(x + x', y + y')^2} \quad (6)$$

Result values for this method that give the normalized computation are:

$$R_{coeff_norm}(x, y) = \frac{R_{coeff}(x, y)}{z(x, y)} \quad (7)$$

In this system, four template images are used to determine eye gaze. These images are acquired during calibration step. The best result will obtain eye gaze. The threshold is set to 90% match.

E. Calibration Step

Eye gaze measurements that apply template matching methods will does work on fix illumination and fix condition. Illumination changes, shadow, different of eye shape when it is used by other users, and others difference condition will obtain mismatch result.

This problem can be solved by calibration step. The calibration step consists of acquiring template image and self evaluation as is shown in Figure 4.

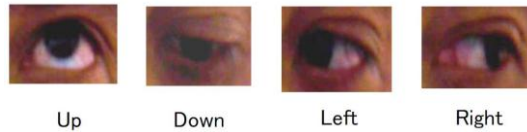


Fig. 4. Result of calibration step. These steps obtain up, down, left, and right image. Up image is used for move forward, down is used for stop, left is used for turn left, and right is used for turn right

System will acquire eye image when looking at down, up, left, and right keys. Next, system will evaluate template image. If template image is good template, it will be used. If not, system will acquire eye image again until good template are obtained. When system is started, it will check that template images are proportional. Illumination, shadow, and eye shape will compare with current eye image. If there are not proportional image, calibration step will be ran.

F. Custom Microcontroller

Yamaha JW-I Electric wheel chair type is used. To control EWC using Pocket PC, custom microcontroller circuit is used. USB interface on pocket PC is used to connect with other peripheral. The custom microcontroller circuit is use RS232 communication. Microcontroller AT89S51 type is used. To connect between pocket PC and custom microcontroller circuit, USB to Serial communication is used. The microcontroller will drive relay to move the EWC. Microcontroller connection is shown in Figure 5.

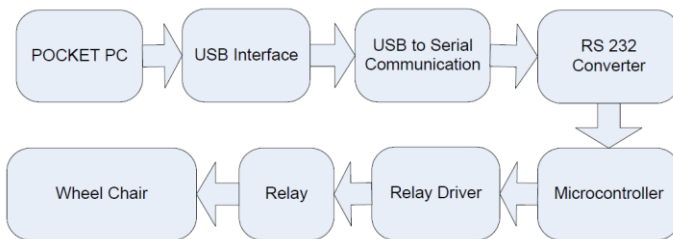


Fig. 5. Microcontroller AT89S51 connects to other peripheral through serial communication. Serial communication type should be converted to USB communication using USB to serial converter.

G. Obstacle Avoidance

In order to safety reason, obstacle avoidance system is implemented in our system. Obstacle avoidance system will able to identify the obstacle in front of EWC and avoid it. This system consists of two approaches: (1) Obstacle detection, and (2) Best Path Finding.

H. Obstacle Detection

Obstacle detection is consisting of image processing based and ultrasonic sensor based. Image processing based utilizes background subtraction between current image $I(x, y)$ and background image $B(x, y)$. Background subtraction method will obtain black-white image $S(x, y)$ which represent obstacle. On this image, obstacles appear as white pixel. By using searching of outer line from white pixels, we can determine position and size of obstacle.

$$S(x, y) = 0, \text{ if } |I(x, y) - B(x, y)| < \text{threshold} \quad (8)$$

$$S(x, y) = 255, \text{ if } |I(x, y) - B(x, y)| \leq \text{threshold} \quad (9)$$

Weakness of background subtraction method is working only if two images have same position of translation, scale, shear, and rotation. To solve these problems, we utilize affine transformation. This transformation requires 3 points that appears on both images as is shown in Figure 6.



Fig. 6. Background subtraction method, left-top is background image and right-top is current image. Background subtraction method will obtain black-white image (bottom)

Translation, scale, share, and rotation parameter can be determined from these points. Affine transformation required at least three noticeable important points. These points should be appears on both images. It can be detected by several ways: corner, edge, specific object, and etc. Corner and edge have many points and its will create computation problem. In our system, we decide to use specific object. The specific object can be an easily recognized object, text character, chessboard wall, and etc. Flow process of obstacle detection using affine transformation is shown in Figure 7.

The specific object will obtain one coordinate from center of area. Obstacle detection using affine transformation requires identifying at least three kind of object, so it will obtain three noticeable important points.

First step of obstacle detection is convert source image into gray image. By using template matching, system will find specific object position. Using six noticeable points, system calculate translation, share, scale, and rotation parameter. These parameters will used for creating affine matrix.

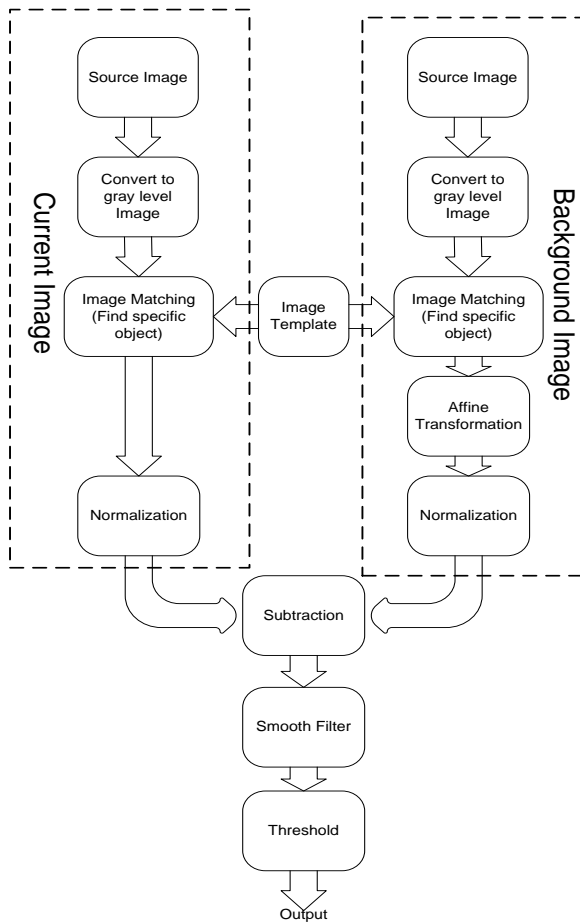


Fig. 7. Obstacle Detection. This methods rely on subtraction between two images and affine transformation.

Affine matrix apply on background image will obtain affine image. Normalization is used to eliminate disturbance such shadow, noise, and etc. Next, subtract between output form current image and background image. Smooth filter is used to reduce noise which is caused by subtraction process. Last step is applying threshold on image and it will obtain black and white image. Obstacle will be signed as group of white pixel. After black white image is obtained, we should return center of white pixel area into current coordinate and coordinate of obstacle is founded. Because of so many type of specific object, we got best performance of specific object by using chessboard wall. The advantage of the chessboard (Figure 8) is easily detected and robust on distance changes. We use 3 types of chessboard: 3 by 4, 3 by 5, and 3 by 6 as are shown in Figure 9. The other obstacle detection is use ultrasonic sensor. This sensor has advantage when visual system does not work. In case EWC move into surrounding glass door, smoke condition, and minimum lighting will caused visual system of obstacle detection fail. Ultrasonic sensor consists of transmitter and receiver part. We use ultrasonic sensor with 40 kHz frequency resonance.

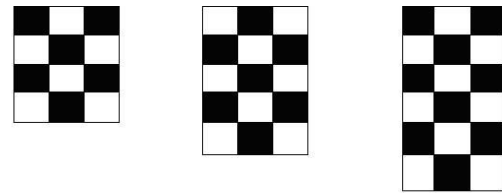


Fig. 8. Chessboard as specific point

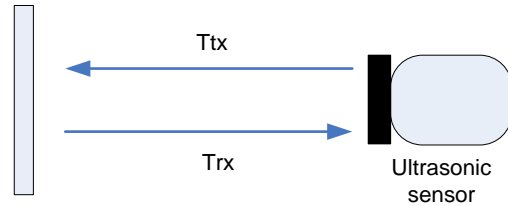


Fig. 9. Ultrasonic sensor, distance is measured by converting half of Tx transmitting time and Trx receiving time

I. Best path finding

When EWC detect the obstacle, it must understand where the best path should be chosen if EWC want to go into specific place. Best path will be chosen based on floor layout map and image map. Image map is created by acquiring background images in every 1 m as is shown in Figure 10. In every location (x, y) have one image. Instance, if the location has size 10 x 10 m, it will have 100 images. After acquire background images, floor layout map will be added manually as initial condition. This map is setup manually based on room layout. Example is shown in Figure 11.

Combination between background images and layout path will obtain main map. EWC will move consider the main map. After obstacle is detected in current path, EWC will switch to another path which have same destination. Obstacle avoidance methods are also useful when user is not confident to pass the obstacle. EWC will take over and pass the obstacle. Best path is chosen based on Dijkstra algorithm. Furthermore, System also able to renew existing map.

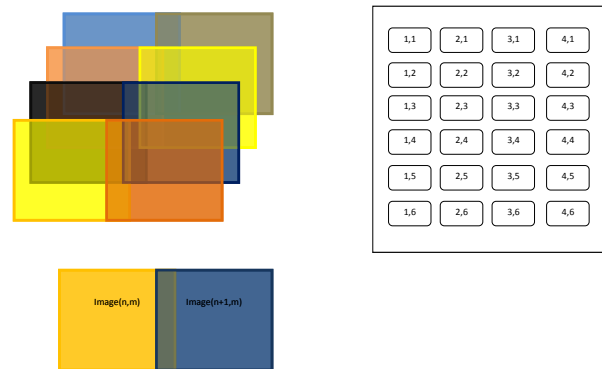


Fig. 10. Image map, created by acquire image in every 1m.

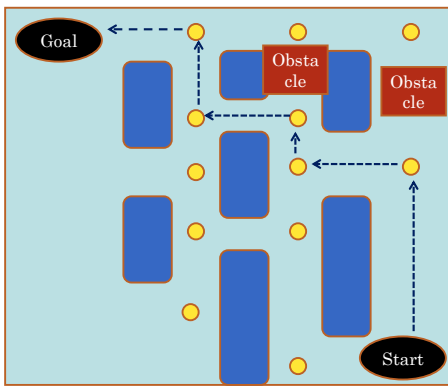


Fig. 11. Best path finding using Dijkstra, best path is chosen based on shortest distance

III. EXPERIMENTS

A. Key selection

The proposed method experiments by measuring success rate eye gaze detection as hit keys selection. Success rate of eye gaze detection is measured by change user distance to camera. Experiments say that minimum distance of success rate is 13 cm and maximum distance is 38 cm. The distance beyond these, OpenCV will not detect the eye and caused the system fail to measure eye gaze. Hit keys selection experiment was done by using real time video 640 by 480 pixels. Data experiments when measure hit keys selection on range distance 24 – 30 cm is shown in Table 1.

TABLE I. HIT KEYS MEASUREMENT

Distance (cm)	Success Rate			
	Stop (%)	Move Forward (%)	Turn Left (%)	Turn Right (%)
24	100	100	100	100
25	100	100	100	100
26	100	100	100	100
27	100	100	100	100
28	100	100	100	100
29	100	100	100	100
30	94.12	100	100	100

The result of hit key measurement is shown almost perfectly, Error which cannot understand the eye input is caused by the system fail to verify the template image. Error will zero if good quality template is used. To make sure that good quality template is used; System will always verify every template and analyzed it. If templates have poor quality, system will conduct calibration step again. This step will repeat until good quality template is obtained.

B. Obstacle avoidance performance.

Experiment of obstacle avoidance is conducted by acquiring image in corridor with distance 1m per images. Location which image was acquired, is set with (x, y) coordinate. So, in every (x, y) location will have 1 background image. This image will be used as background reference. Obstacle is detected by subtract background image with current image. To eliminate problem which caused by different position between these images, affine transformation is used to transform background image to affine image which

have same position with current image. Applying affine transformation will does work if only if three noticeable important points are appears on both images. These important points are represented by three types of chessboard. If the chessboard is successful detected, then by using affine transformation and subtraction between background image and current image, obstacle is founded. Experiments of chessboard detection is conducted by measuring maximum location which still detected by system. Chessboard is put in fix location. After that, EWC is move around the chessboard. Maximum location which detected by system is recorded. Data experiments are shown in Figure 12.

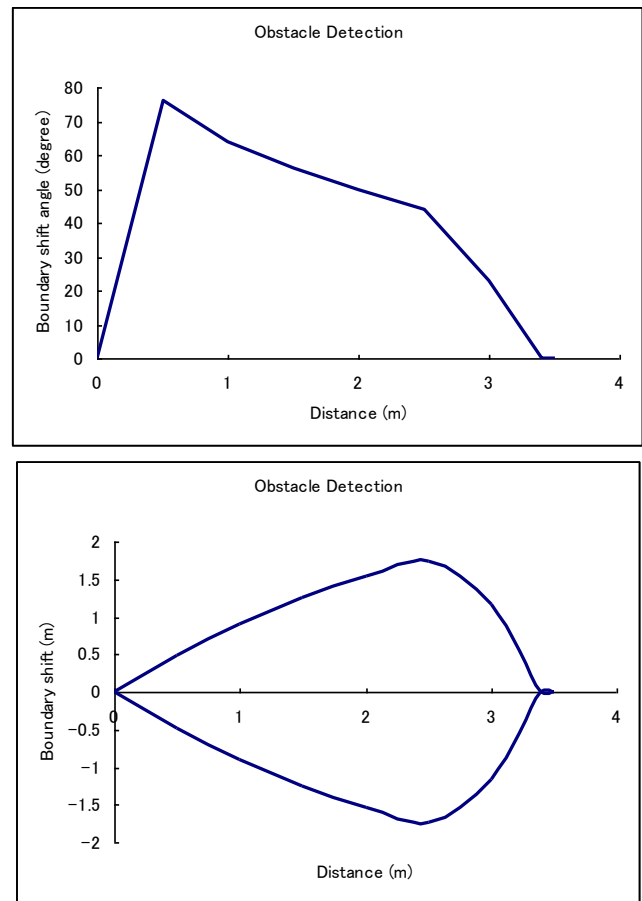


Fig. 12. measuring obstacle avoidance performances

Data show that boundary shift will decrease when distance between camera and chessboard is increase. This experiment is equal to obstacle detection. After three types of chessboard are detected, affine transformation will use these points (three chessboard center of areas) to subtract with current image and obstacle position will be found.

C. Ultrasonic Sensor

Objective of this experiment is measure accuracy of ultrasonic sensor before used in the system. This experiment is conducted by measure sensor output for measuring distance and comparing with real data. Some object is put on front of sensor with varies distances and measure it. The experiment is conducted on distance 0 cm until 3 m.

Ultrasonic sensor use PING type parallax product and microcontroller AT89S51 as processing data (convert from time value to distance output). Graph of accuracy sensor is shown in Figure 13.

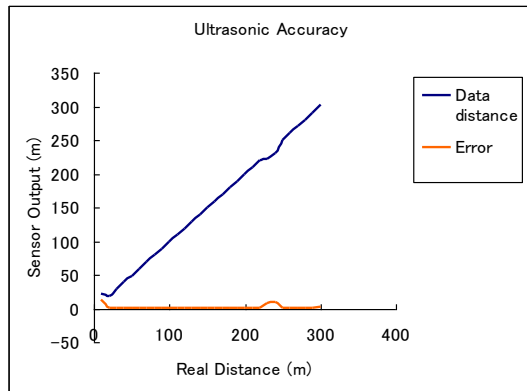


Fig. 13. Experiment of ultrasonic accuracy. This shown that minimum distance is around 3 cm and maximum distance is 3 m. This range is appropriate for detect the object.

Elevation angle is require to know how width of the beam sensor. Ultrasonic sensor with width beam is not benefit to our system. Narrow beam will obtain good result because it will not influence with any disturbance. This experiment is conducted by measure elevation angle from 0 cm until 3 m. Graph of elevation angle is shown in Figure 14.

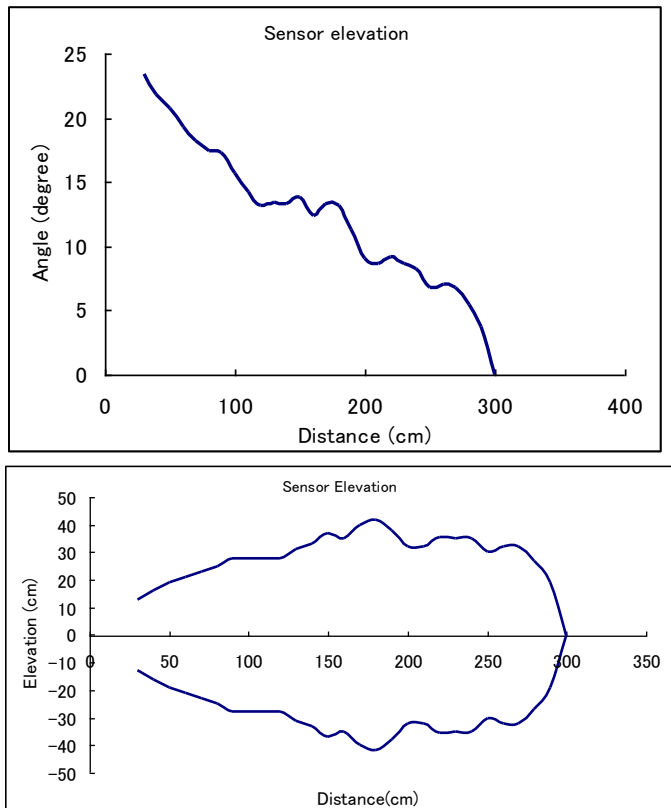


Fig. 14. Experiment of Elevation angle. Top side is distance versus angle, and bottom side is distance versus distance elevation.

D. Performance of Electric Wheel Chair

This experiment is conducted for measure EWC performance on starting up acceleration, forward and backward breaking deceleration. Also conducted speed measurement when EWC move forward, backward, turn left, and turn right. EWC is drive by user who has weight is 73 kg. We record the duration time and convert it into speed value. Experiment data of speed measurement is shown in Table 2. Graph of EWC acceleration and deceleration when start and stop duration is shown in Figure 15.

TABLE II. SPEED MEASUREMENT

Moving	Speed (m/s)
Forward	0.29
Backward	0.26
Turn Left	0.11
Turn Right	0.11

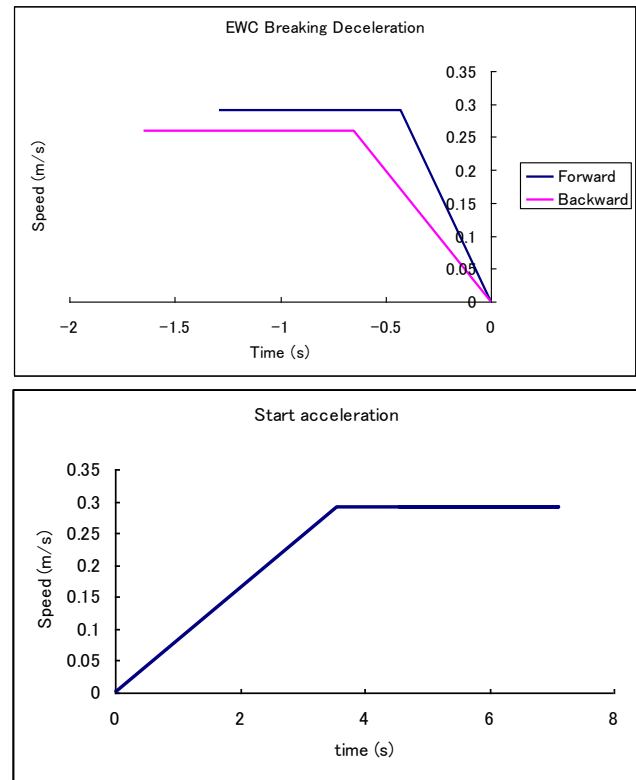


Fig. 15. Experiment of EWC acceleration and deceleration

E. Processing time each process

In order to apply whole method into EWC application, processing time should be measured to identify performance of our real time system. Figure 16 shows transient time of eye detection and tracking, n the beginning of chart, it seem this method take long time around 300 ms. In this time, system still process face detection, eye detection and others process before running template matching method. After eye location is founded, then system bypass previous step and cause process working fast.

Meanwhile, Figure 17 shows processing time of eye detection and tracking on steady state condition, it looks faster than transient condition.

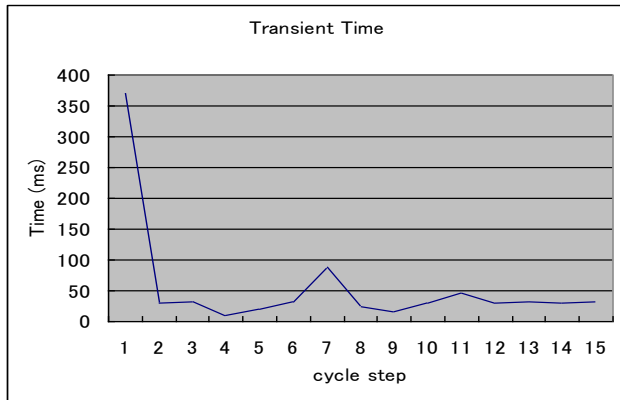


Fig. 16. Transient time of eye detection and tracking, n the beginning of chart, it seem this method take long time around 300 ms. In this time, system still process face detection, eye detection and others process before running template matching method. After eye location is founded, then system bypass previous step and cause process working fast.

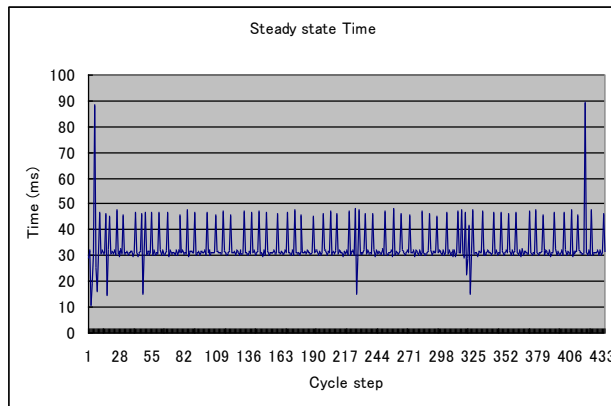


Fig. 17. Processing time of eye detection and tracking on steady state condition, it looks faster than transient condition.

F. Eye detection and tracking

This experiment is conducted using Optiplex 755 Dell computer with Intel Core 2 Quad CPU 2.66 GHz and 2G of RAM. We use NET COWBOY DC-NCR131 camera as visual input. Experimental result show average steady state processing time is 32.625 ms. it also shows difference processing time between transient and steady state condition. Transient time require more time than steady state time.

G. Eye gaze measurement

Objective of this experiment is measure processing time on Eye gaze identification. It is conducted by using ACER computer ASPIRE 5572 Series Core Duo T2050 1.6 GHz CPU

and 1G of RAM. Result data show average processing time of this method is 342.379 ms. Figure 18 shows processing time of Eye gaze method.

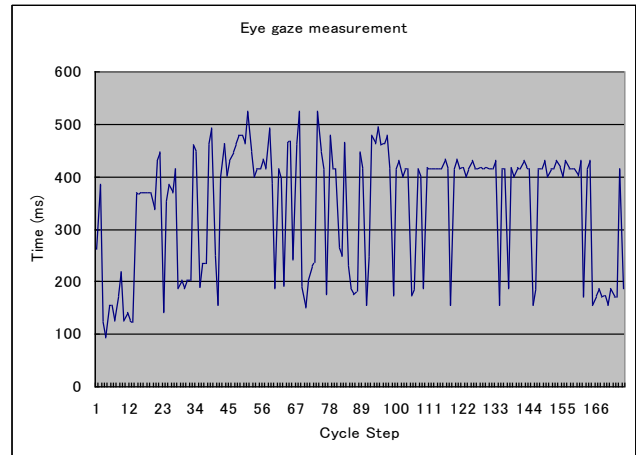


Fig. 18. processing time of Eye gaze method

H. Obstacle detection

This experiment also was conducted using Optiplex 755 Dell computer with Intel Core 2 Quad CPU 2.66 GHz and 2G of RAM. NET COWBOY DC-NCR131 camera as visual input is also used. Experimental result show average processing time is 32.625 ms. Figure 19 shows processing time of obstacle detection.

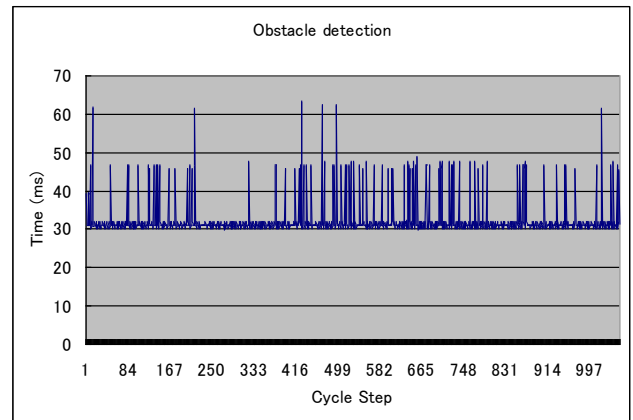


Fig. 19. processing time of obstacle detection

I. Ultrasonic sensor

We implemented ultrasonic sensor parallax PING type. This sensor is controlled by using custom microcontroller AT89S51. Data was stored into computer by using USB communication. Result data show average processing time is 568.658 ms. Figure 20 also shows processing time of ultrasonic sensor, it look take longer time than others.

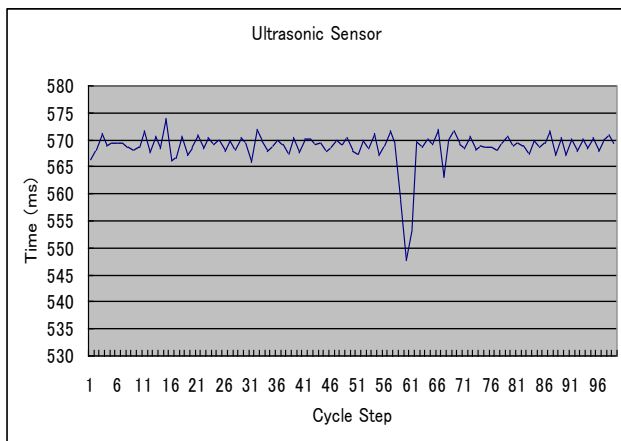


Fig. 20. processing time of ultrasonic sensor, it look take longer time than others.

IV. CONCLUSION

It is concluded that the proposed key-in system with human eyes only works 100% perfectly for the number of keys is four, start, stop, turn right and left. Also it is concluded that the proposed EWC control system does work in a real basis avoiding obstacles on range bellow 3.4 m using image processing method and bellow 3 m using ultrasonic sensor. By the proposed system, EWC is able to identify obstacle and avoid them. Obstacle avoidance can assist user into interest place although undesired condition such as dark areas, glass wall or door, smoke area, and etc. By implemented this system, EWC will move more safely and comfortable.

ACKNOWLEDGMENT

The author would like to thank Dr.Djoko of Institute of Technology Surabaya, Indonesia for his efforts through experiments and simulations.

REFERENCES

- [1] Park, K.S., and Lee K.T., Eye controlled human/computer interface using the line of sight and intentional blink, *Computer Ind. Eng.*, 30, 3, 463-473, 1996.
- [2] Ito, Sudo, the Ifuku part: "The look input type communication equipment for serious physically handicapped persons", the Institute of Electronics, Information and Communication Engineers paper magazine, J83D1, 5, 495.503, 2000.
- [3] Yamada, Fukuda: "The text creation and the peripheral equipment control device" by eye movement, the Institute of Electronics, Information and Communication Engineers paper magazine , J69D, 7, 1103-1107, 1986.

- [4] Mitsunori Yamada, the research trend of the latest eye movement, an electric information-and-telecommunications academic journal, MBE95-132, NC95-90, 145-152, 1995.
- [5] K.Abe, S.Ohiamd M.Ohyama: "An Eye-gaze Input System based on the Limbus Tracking Method by Image Analysis for Seriously Physically Handicapped People", 7th ERCIM Workshop "User Interface for All" Adjunct Proc., 185-186, 2002.
- [6] <http://www.creact.co.jp/jpn/por.pdf>
- [7] Kuno, Yagi, Fujii, Koga, Uchikawa: "Development of the look input interface using EOG", the Information Processing Society of Japan paper magazine, 39, 5, 1455-1462, 1998.
- [8] D.A.Robinson: A method of measuring eye movement using a sclera search coil in a magnetic field, *IEEE Trans. on Biomedical Electronics*, 10, 137-145, 1963.
- [9] <http://webvision.med.utah.edu/>
- [10] Ito, Nara: "Eye movement measurement by picture taking in and processing via a video capture card", an Institute of Electronics, Information and Communication Engineers technical report, 102, 128, 31-36, 2002.
- [11] Kishimoto, Yonemura, Hirose, Changchiang: "Development of the look input system by a cursor move system", and the Institute of Image Information and Television Engineers, 55, 6, 917-919, 2001.
- [12] Corno, L.Farinetti, I. Signorile: "A Cost-Effective Solution for Eye-Gaze Assistive Technology", *Proc. IEEE International Conf. on Multimedia and Expo*, 2, 433-436, 2002.
- [13] Abe, Ochi, Oi, Daisen: "The look input system using the sclera reflection method by image analysis", and the Institute of Image Information and Television Engineers, 57, 10, 1354-1360, 2003.
- [14] Abe, Daisen, Oi: "The multi-index look input system which used the image analysis under available light", and the Institute of Image Information and Television Engineers, 58, 11, 1656-1664, 2004.
- [15] Abe, Daisen, Oi: "The look input platform for serious physically handicapped persons", *Human Interface Society Human interface symposium 2004 collected papers*, 1145-1148, 2004.
- [16] http://homepages.inf.ed.ac.uk/rbf/CVonline/LOCAL_COPIES/GONG1/cvOnline-skinColourAnalysis.html.
- [17] Gary Bradski, Andrian Kaebler, "Learning Computer Vision with the OpenCV Library", O'REILLY, 214-219, 2008.

AUTHORS PROFILE

Kohei Arai, He received BS, MS and PhD degrees in 1972, 1974 and 1982, respectively. He was with The Institute for Industrial Science and Technology of the University of Tokyo from April 1974 to December 1978 also was with National Space Development Agency of Japan from January, 1979 to March, 1990. During from 1985 to 1987, he was with Canada Centre for Remote Sensing as a Post Doctoral Fellow of National Science and Engineering Research Council of Canada. He moved to Saga University as a Professor in Department of Information Science on April 1990. He was a councilor for the Aeronautics and Space related to the Technology Committee of the Ministry of Science and Technology during from 1998 to 2000. He was a councilor of Saga University for 2002 and 2003. He also was an executive councilor for the Remote Sensing Society of Japan for 2003 to 2005. He is an Adjunct Professor of University of Arizona, USA since 1998. He also is Vice Chairman of the Commission "A" of ICSU/COSPAR since 2008. He wrote 30 books and published 478 journal papers

Sensitivity Analysis for Aerosol Refractive Index and Size Distribution Estimation Methods Based on Polarized Atmospheric Irradiance Measurements

Kohei Arai¹

¹ Graduate School of Science and Engineering
Saga University
Saga City, Japan

Abstract—Aerosol refractive index and size distribution estimations based on polarized atmospheric irradiance measurements are proposed together with its application to reflectance based vicarious calibration. A method for reflectance based vicarious calibration with aerosol refractive index and size distribution estimation using atmospheric polarization irradiance data is proposed. It is possible to estimate aerosol refractive index and size distribution with atmospheric polarization irradiance measured with the different observation angles (scattering angles). The Top of the Atmosphere (TOA) or at-sensor radiance is estimated based on atmospheric codes with estimated refractive index and size distribution then vicarious calibration coefficient can be calculated by comparing to the acquired visible to near infrared instrument data onboard satellites. The estimated TOA radiance based on the proposed method is compared to that with aureole-meter based approach which is based on refractive index and size distribution estimated with solar direct, diffuse and aureole (Conventional AERONET approach). It is obvious that aureole-meter is not portable, heavy and large while polarization irradiance measurement instruments are light and small (portable size and weight).

Keywords—Degree of Polarization; aerosol refractive index; size distribution

I. INTRODUCTION

Earth observation satellites have a long history of being characterized by vicarious methods. These include the Marine Observation Satellite-1 [Arai, 1988], Landsat-7 Enhanced Thematic Mapper Plus [Barker, et al., 1999], SeaWiFS [Barnes, et al., 1999], SPOT-1 and 2 [Gelleman, et al., 1993], Hyperion [Folkman, et al., 1997], and POLDER [Hagolle, et al., 1999]. Vicarious approaches also provide a cross-comparison between sensors to characterize mission instruments onboard the same satellite [Arai, 1997] via the use of well-understood ground areas such as desert sites [Cosnefroy, et al., 1996]. Arai and Thome [2000] published an error budget analysis of solar reflectance-based vicarious calibration. The most dominant factor for vicarious calibration is surface reflectance measurement, followed by optical depth measurement, estimation of refractive index, aerosol size distribution, and identification error in test site pixels. Typical vicarious calibration accuracy is around 4%. Onboard calibrators cannot provide results of a higher accuracy than the preflight laboratory calibration. This means that the accuracy

of the in-flight (absolute) calibration is inferior to the preflight results. This is because the preflight calibration source is used to calibrate the onboard calibrators. In addition, the uncertainty of the onboard calibrator typically increases with time. Hence, it makes good sense to include additional calibration approaches that are independent of the preflight calibration. Besides the normal and expected degradation of the onboard calibrators, they also run the risk of failing or operating improperly. Therefore, vicarious approaches are employed to provide further checks on the sensor's radiometric behavior. Given the understanding that the orbiting sensor's response will change over time, the ASTER science team developed a methodology, based on OBC results, to update preflight RCCs that are input to generate the Level-1B product [Thome, Arai et al., 2008]. The OBC results are also combined with vicarious calibration to produce the most accurate knowledge of ASTER's radiometric calibration.

The solar radiometers are relatively calibrated immediately prior to, during, or after each field campaign via the Langley method or Modified Langley method, and this allows for the determination of spectral atmospheric optical depths [Arai, et al., 2005]. The optical depth results are used as part of an inversion scheme to determine ozone optical depth and an aerosol size distribution. The aerosols are assumed to follow a power law distribution, also referred to as a Junge distribution. Columnar water vapor is derived from the solar extinction data using a modified-Langley approach. The atmospheric and surface data are used in a radiative transfer code. There are a variety of codes available that satisfy all the requirements of predicting the at-sensor radiance to the required accuracy. It has shown that similar conclusions are drawn for other code types such as doubling-adding, and the methods used in the 6S code [Lenoble 1985]. Besides these, another method takes into account polarizations in the calculation of down-welling and up-welling radiation [Arai et al., 2003]. It uses ground-based solar direct, diffuse and aureole radiance measurements as well as polarized radiance with several polarization angles [Arai and Liang, 2005, and Liang and Arai, 2005]. It is obvious that aureole-meter is not portable, heavy and large while polarization irradiance measurement instruments are light and small (portable size and weight). This study is based on a Lambertian view of the surface. The near-nadir view for the majority of the ASTER overpasses reduces the uncertainty of this assumption since the dominant direct-reflected solar

irradiance is correctly taken into account. Strong gaseous absorption effects due to water vapor are determined using MODTRAN to compute transmittance for the sun-to-surface-to-satellite path for 1-nm intervals from 350 to 2500 nm. Also ozone absorption is taken into account based on MODTRAN with measured column ozone using atmospheric extinction measurements. This sun-to-ground-to-sensor transmittance is multiplied by the at-sensor radiance output from the radiative transfer code to correct the radiances for this strong absorption. While this approach is an approximation that excludes interactions between diffusely scattered radiances and absorption, it does not cause large uncertainties for ASTER applications because of the small absorption effect within most of the bands, and the typically high surface reflectance of the test sites used in this work.

For the multiple-scattering components calculation, it is easy to estimate Rayleigh scattering (molecule) with measured atmospheric pressure. Meanwhile Mie scattering (aerosol) is not so easy to estimate. Aerosol parameters, refractive index, size distribution, etc. have to be estimated. AERONET (Holben B.N. et al., 1998) and SKYNET Aoki, K. et al., 2005) allows for the estimation of aerosol parameters at the specific locations. They use aureole-meters and sky-radiometers which allow solar direct, diffuse and aureole irradiance. These ground-based instruments are heavy and large so that they equip them at the specific sites. Small and light portable polarization irradiance measuring instrument, on the other hand, is proposed by Arai (2009) for estimation of aerosol parameters. With a measured polarized irradiance at the specific observation angles (scattering angles) allows estimation of aerosol refractive index and size distribution. Estimated aerosol parameters are a little bit differing from those which are derived from AERONET as well as SKYNET. This paper describes at-sensor radiance of ASTER/VNIR with the estimated aerosol parameters derived from AERONET and SKYNET as well as the proposed method together with a sensitivity analysis.

II. PROPOSED MODEL

Reflectance based vicarious calibration method proposed here is based on MODTRAN with the following input parameters, Measured surface reflectance (Lambertian surface), Calculated molecule scattering based on a measured atmospheric pressure, Calculated aerosol scattering with the aerosol parameters, refractive index and size distribution which are estimated with measured polarized irradiance at several scattering angles (for instance seven scattering angles which ranges from 60 to 120 with 10 degree step) based on the proposed method, Calculate absorbance due to water vapor and ozone with measured column water and ozone.

At-sensor radiance is estimated based on MODTRAN and is compared to the actual ASTER/VNIR data derived radiance. The most influencing factor of the proposed method is

estimation accuracy of aerosol parameters, refractive index and size distribution.

Therefore, sensitivity of aerosol parameters on TOA radiance should be analyzed. Figure 1 shows the calculated TOA radiance in unit of $[W/cm^2/sr/\mu m]$ with the parameter of real and imaginary parts of refractive index while Figure 2 shows the calculated TOA radiance with the parameters of size distribution.

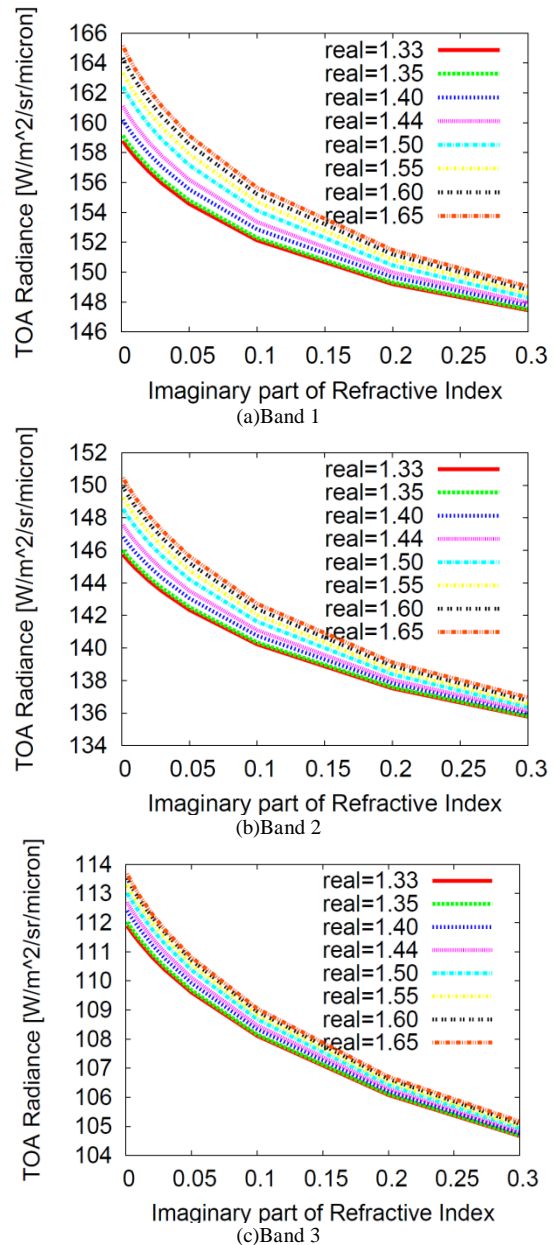


Fig. 1. Calculated TOA radiance derived from the field campaign which was conducted at Railroad valley on September 21 2008 with the parameters of real and imaginary parts of refractive index.

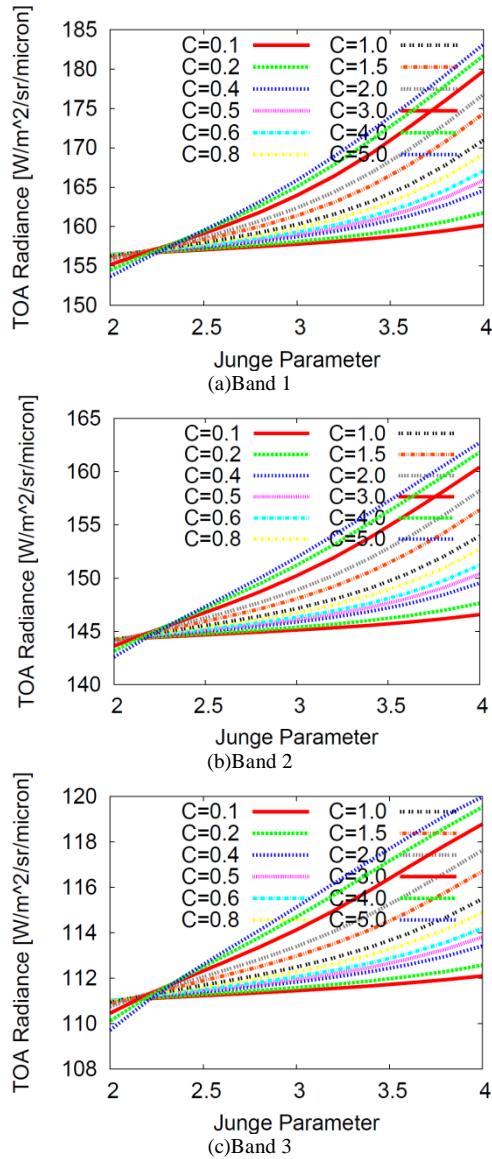


Fig. 2. TOA radiance as a function of Junge parameter

These examples are derived from the field campaign which was conducted at Railroad valley on September 21 2008. Junge distribution, one of power law distributions is assumed as is expressed as the equation (1).

$$\frac{dN}{d \ln(r)} = Cr^{-\alpha}, \alpha = -(\nu + 1) \quad (1)$$

where α denotes the slope of the relation between volume and radius of aerosol particles and ν is Junge parameter as are shown in Figure 3. Figure 3 also shows a typical aerosol density vertical profile. TOA radiance is increased with increasing of real part of refractive index and is decreased with increasing of imaginary part of refractive index. The TOA radiance-increasing ratio at shorter wavelength (Band 1) is much greater than that in the longer wavelength (Band 3N: Nadir view). Figure 1 and 2 also show that the calculated TOA radiance is changed below 2% when the estimated refractive index and Junge parameter are changed within a range of

$\pm 10\%$ from the assumed typical values, 1.44 of real part of refractive index, 0.05 of imaginary part of refractive index and 3 of Junge parameter. This implies that required estimation accuracy of refractive index and size distribution is not so high; about $\pm 10\%$ would be enough if 2% were the required TOA radiance estimation accuracy.

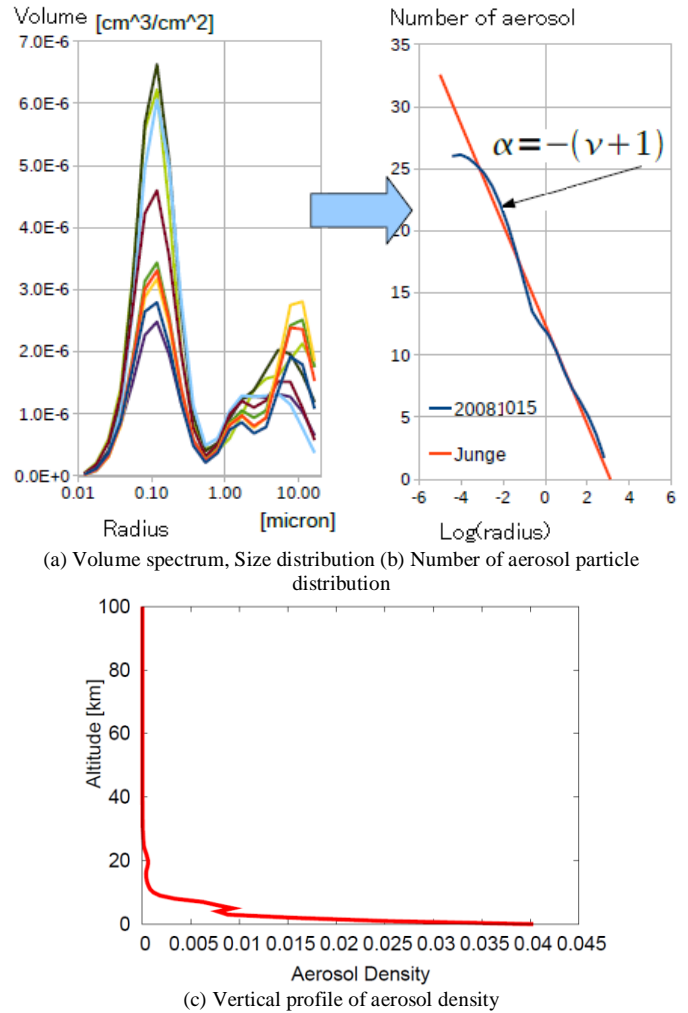


Fig.3. Volume spectrum and corresponding power law distribution, representation of aerosol size distribution with Junge parameter with corresponds to slope of the power law distribution together with aerosol density profile (an example of Saga (33:14.46N, 130:17.3E, 29m) field campaign which was conducted on October 15 2008).

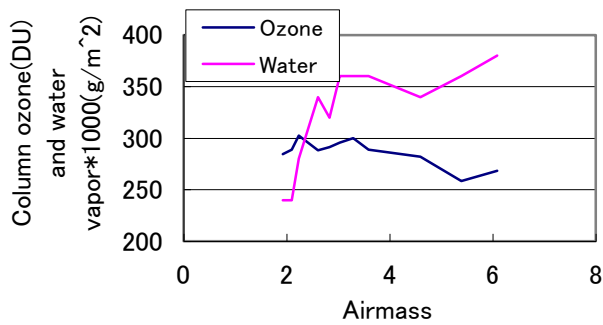
III. EXPERIMENTL

Field campaigns were conducted at Roach Lake on December 3 2008 and at Coyote Lake on December 10 2008, respectively. Table 1 shows the detailed information of the field campaigns.

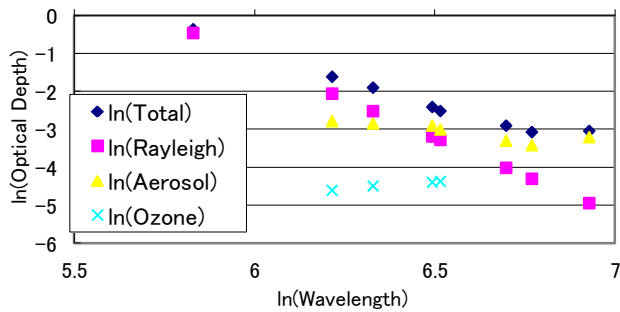
Measured column ozone and water vapor are shown in Figure 4 (a) while relation between $\ln(\text{wavelength})$ and $\ln(\text{optical depth})$ are shown in Figure 4 (b), respectively. Also measured surface reflectance as well as estimated refractive index and size distribution are shown in Figure 4 (c) to (f). These are measured and estimated values for Roach Lake field campaign that was conducted on December 3 2008.

TABLE I. DETAILED INFORMATION OF THE FIELD CAMPAIGNS CONDUCTED.

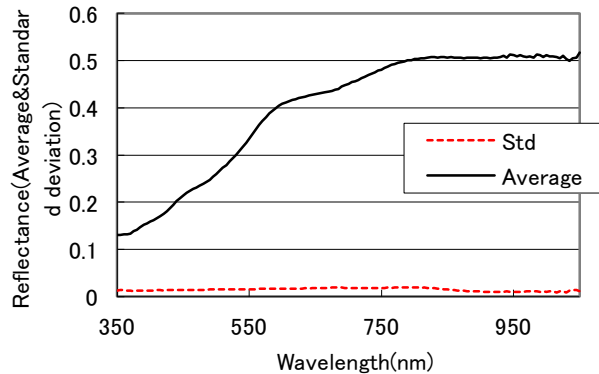
Date and time (UTM)	December 3 2008, 18:38:34	December 10 2008, 18:38:34
Solar azimuth and zenith angles	154.48, 59.84	163.92, 59.61
Location	Roach Lake(38:30:18N,115:41:29W)	Coyote Lake(35:03:53N,116:44:50W)
Air-temperature, atmospheric pressure	22.5, 933hPa	22.1, 974hPa
Junge parameter(370/870, 500/870)	2.73, 3.15	5.89, 7.21
Ozone(DU), Water vapor(g/cm ²)	284.7, 0.24	271.6, 0.46



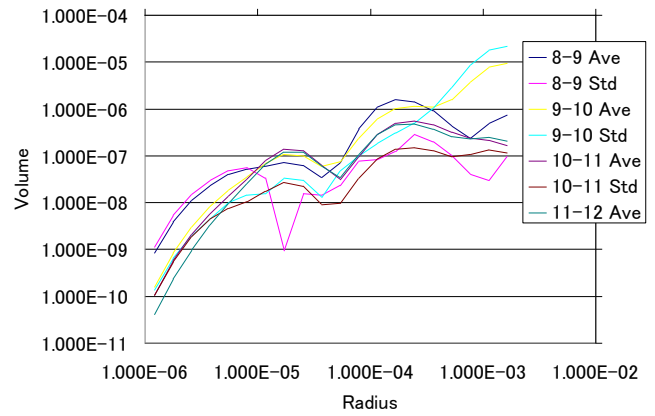
(a) Column ozone and water vapor



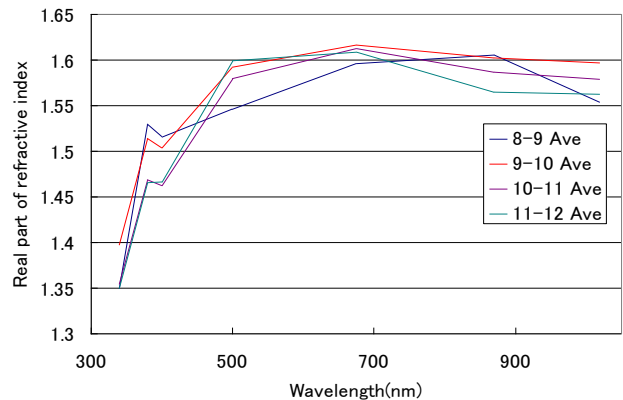
(b) Angstrom exponent and Junge parameter



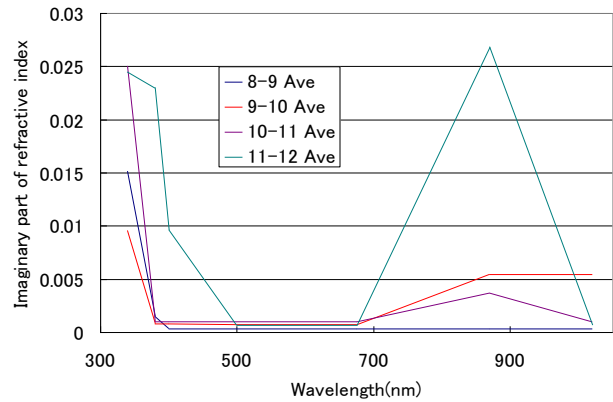
(c) Surface reflectance



(d) Volume spectrum (Size distribution)



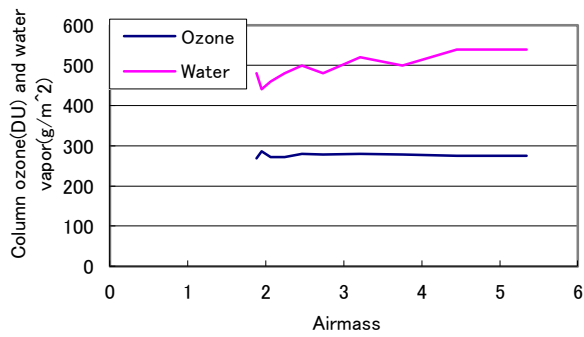
(e) Real part of refractive index



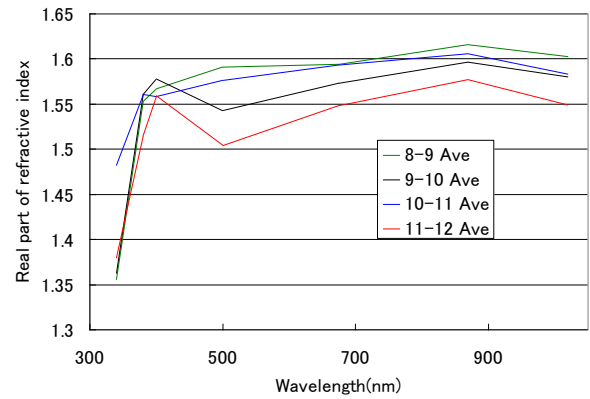
(f) Imaginary part of refractive index

Fig. 4. Atmospheric and surface characteristics of the test site at Roach Lake measured on December 3 2008.

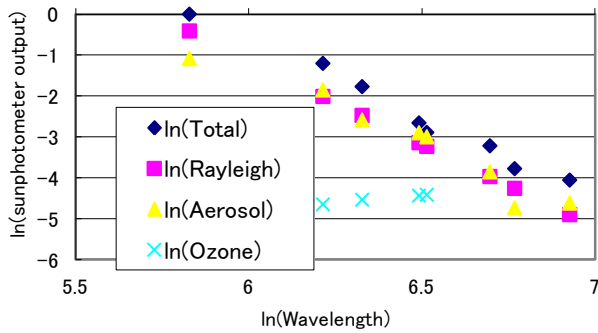
Meanwhile those for Coyote Lake campaign are shown in Figure 5. Atmospheric optical depth for Coyote Lake campaign was very thin compared to Roach Lake campaign. In particular, Junge parameter for Coyote Lake campaign is twice much greater than that for Roach Lake campaign. This implies that small size of aerosol particles is dominant for Coyote Lake campaign in comparison to Roach Lake campaign.



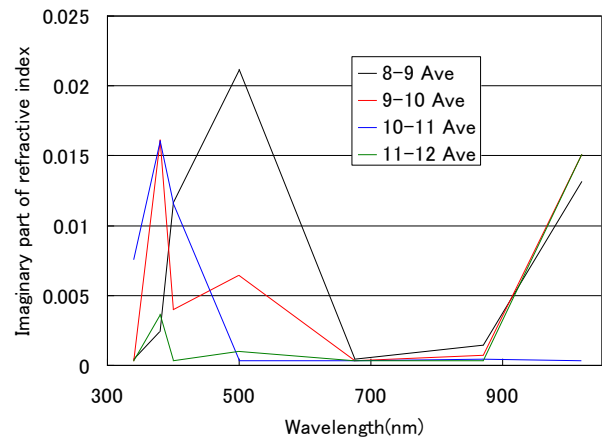
(a) Column ozone and water vapor



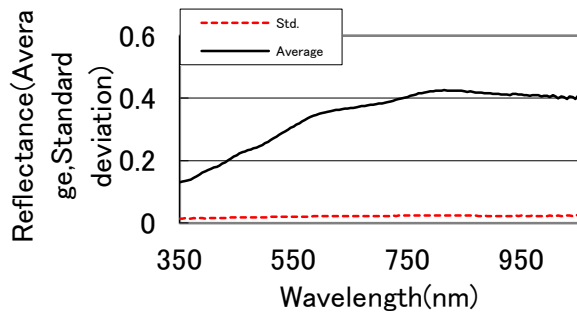
(e) Real part of refractive index



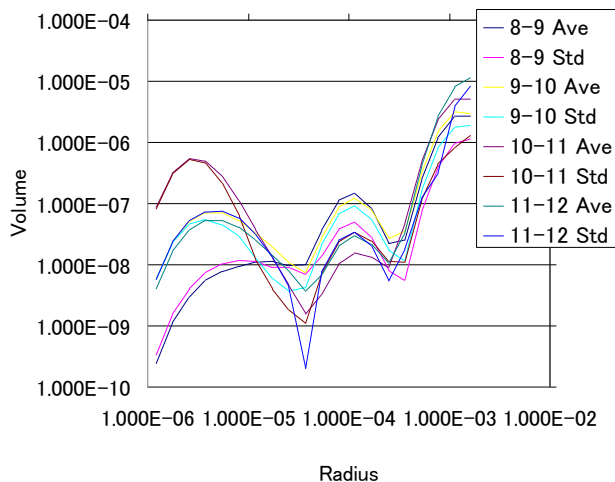
(b) Angstrom exponent and Junge parameter



(f) Imaginary part of refractive index



(c) Surface reflectance

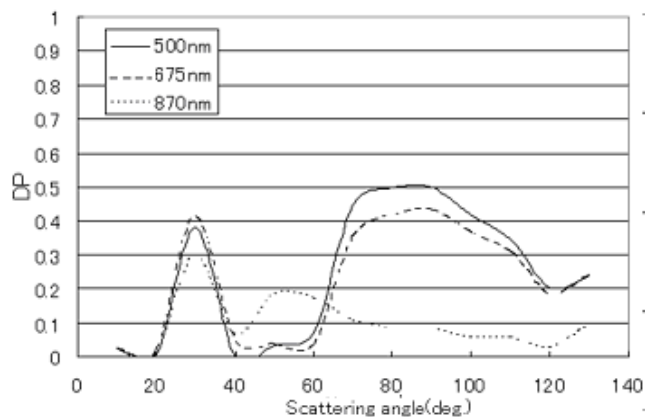


(d) Volume spectrum (Size distribution)

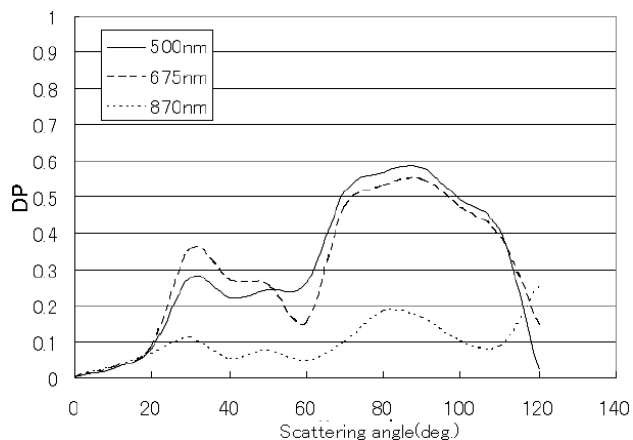
Fig. 5. Atmospheric and surface characteristics of the test site at Coyote Lake measured on December 10 2008.

Refractive index and size distribution are estimated with skyradiometer data which allows measure solar direct, diffuse and aureole irradiance on the ground surface. Dr.Tsuchida and Dr.Kamei provided Skyradiometer data with their courtesy [Tsuchida and Kamei, 2009]. Using the modified skyrad.pack of software code, refractive index and size distribution are retrieved with these data. Although the original skyrad.pack provided by Dr.Nakajima (Nakajima et al., 2000) does not care about polarized radiance from the surface, the modified Arai-Ryo model takes p and s polarization of irradiance and radiance in the radiative transfer (Arai and Liang, 2005). On the other hand, measured scattering angle characteristics of Degree of Polarization (DP) are shown in Figure 6. Using curve-fitting algorithm of iterative method, most appropriate refractive index and size distribution (Junge parameter) is estimated. Through a comparison between estimated refractive index and Junge parameter by Arai-Ryo model with skyradiometer data and by curve fitting algorithm with seven scattering angles (60,70,80,90,100,110,120) of DP, it is found that both shows good coincidence (difference between both is within a range of $\pm 5\%$). In accordance with the previous research, it is known that the estimation accuracy of refractive index and Junge parameter is approximately 6%. $\pm 10\%$ of refractive index and Junge parameter estimation accuracy

causes $\pm 2\%$ of TOA radiance estimation accuracy so that 6% of accuracy of refractive index and Junge parameter would cause below 2% of TOA radiance estimation accuracy.



(a) Roach Lake campaign



(b) Coyote Lake campaign

Fig. 6. DP measured for field campaigns at Roach Lake and Coyote Lake which were conducted on December 3 and 10 2008.

Using estimated refractive index and size distribution derived from skyradiometer data and DP data as well as surface reflectance, column ozone and water vapor, atmospheric pressure (Rayleigh scattering) TOA radiance is estimated based on MODTRAN. Table 2 shows the estimated refractive index and size distribution with skyradiometer data and DP data for Roach Lake and Coyote Lake campaigns. Both show a good coincidence, discrepancy of real part of refractive index ranges from -4.65 to 2.566%, difference of imaginary part of refractive index ranges from -5.86 to 3.846%, and discrepancy of Junge parameter ranges from 0.013 to 3.653%, respectively.

Meanwhile Table 3 shows the estimated TOA radiance with refractive index and size distribution derived from DP data and skyradiometer data. Also both show a good coincidence, below 15.22% of discrepancy. In particular, discrepancy at the shorter wavelength, 560 and 660nm of Bands 1 and 2 for Coyote Lake campaign is much greater than those for Band 3 for Coyote field campaign and Roach Lake campaign.

TABLE II. COMPARISON OF JUNGE PARAMETER AND REFRACTIVE INDEX DERIVED FROM SKYRADIOMETER DATA AND DP DATA

	Method	Junge	Real	Imaginary
08/12/03	Skyradiometer	3.372	1.582	0.0004
Roach	DP	3.365	1.501	0.0003
08/12/10	Skyradiometer	5.213	1.574	0.0068
Coyote	DP	5.214	1.541	0.0066

TABLE III. COMPARISON OF TOA RADIANCE DERIVED FROM SKYRADIOMETER DATA AND DP DATA

2008/12/3	L_DP	L_skyrad	% difference
B1(560)	111.75	110.47	1.145
B2(660)	114.4	113.65	0.656
B3N(810)	95.2	94.84	0.378
B3B(810)	94.58	94.56	0.021
2008/12/10	L_DP	L_skyrad	% difference
B1(560)	109.08	92.48	15.22
B2(660)	99.22	89.67	9.625
B3N(810)	76.7	73.22	4.537
B3B(810)	76.12	73.92	2.89

This is caused by relatively large Junge parameter, small size of aerosol particles are greater than large size of those for Coyote Lake campaign. Except these, the discrepancy between two methods for estimation of TOA radiance with skyradiometer data and DP data is below 4.5%. Due to the fact that aerosol optical depth increases in accordance with decreasing wavelength sharply for Coyote Lake field campaign, the discrepancy between estimated TOA radiance between two methods is greater than those in the longer wavelength regions. Also it is true that Junge parameter for Coyote Lake campaign is twice much greater than Roach Lake campaign. TOA radiance is sensitive to Junge parameter, in particular, greater Junge parameter regions as is shown in Figure 7 (which was derived from the field campaign which was conducted at Railroad valley on September 21 2008). In accordance with increasing of Junge parameter, the calculated TOA radiance is increased sharply. For these reasons, the discrepancy between two methods for Coyote Lake campaign is greater than that of Roach Lake.

IV. CONCLUSION

The estimated refractive index and size distribution using the proposed DP based method shows a good coincidence with the estimated those by the conventional skyradiometer (POM-01 which is manufactured by Prede Co. Ltd.), or aureole meter based method so that the proposed method does work well. The Junge parameter estimated by skyradiometer based method is derived from Angstrom exponent that is calculated with aerosol optical depth measured with skyradiometer while that by the proposed DP based method is derived from Angstrom exponent that is calculated with aerosol optical depth measured with polarized irradiance measuring instrument (MS720 which is manufactured by EKO Co. Ltd.).

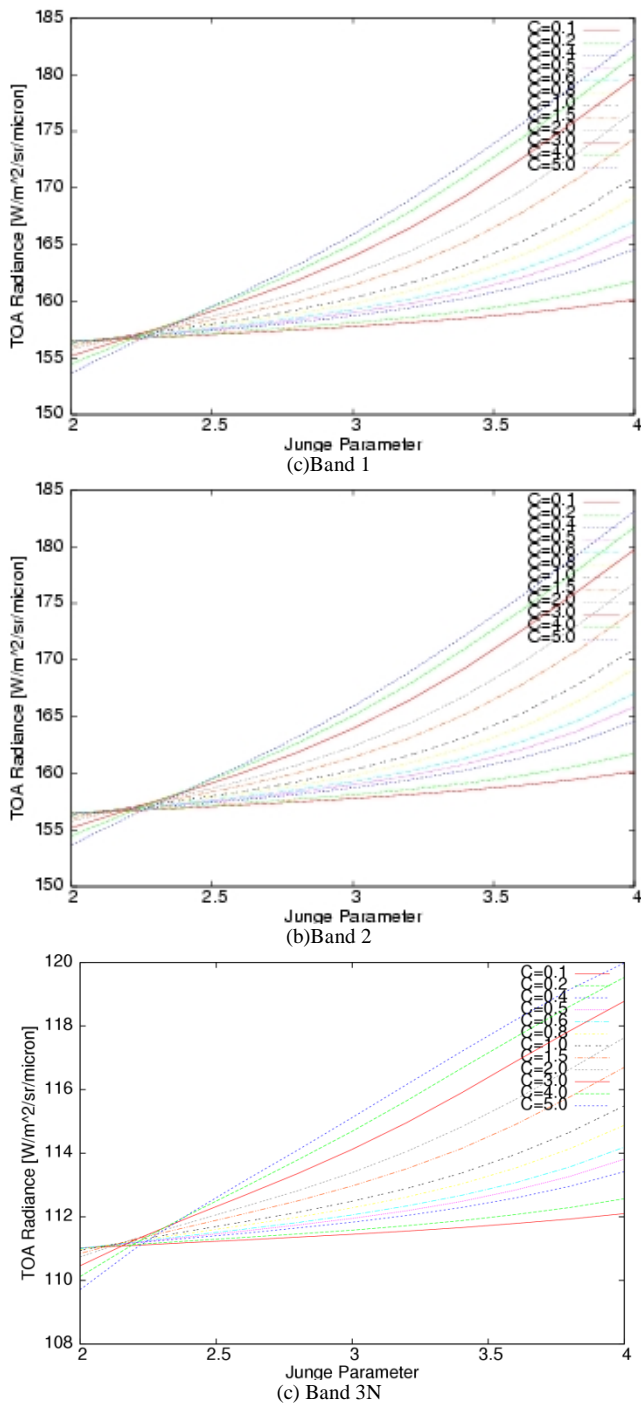


Fig. 7. Relation between TOA radiance and Junge parameter (Example of the calculated TOA radiance for the field campaign which was conducted at Railroad valley on September 21 2008)

The difference between both is caused by the difference of gain/offset of the two instruments, POM-1 and MS720. On the other hand, the differences of estimated refractive index between skyradiometer based and the proposed DP based methods are mainly caused by the estimation methods, inversion of radiance to refractive index for skyradiometer based method while least square method minimizing the discrepancy between the actual and simulated DP at the seven different scattering angles based on MODTRAN.

The difference of TOA radiance derived from the proposed DP based method and the conventional skyradiometer based method is within the range of 1.2% for relatively high reflectance and comparatively thin aerosol optical depth as well as small Junge parameter case (relatively large aerosol particles are dominant) and is within the range of 2.9 to 15.2% for relatively low reflectance and comparatively thick aerosol optical depth as well as large Junge parameter case (relatively small aerosol particles are dominant). Due to the fact that p and s polarized irradiance is relatively small for relatively high reflectance and comparatively thin aerosol optical depth as well as small Junge parameter case (relatively large aerosol particles are dominant), it is understandable.

It is obvious that skyradiometer and aureole meter is typically large and heavy in comparison to the polarized irradiance measuring instruments. It is possible to bring the polarized irradiance measuring instrument at anywhere easily. p and s polarized irradiance measurement at the seven different scattering angle takes around three minutes so that it has to be assumed that the atmosphere is stable for more than three minutes. p and s polarized irradiance is sensitive to the surface reflectance so that it is recommendable to use the proposed method for widely homogeneous ground cover targets.

ACKNOWLEDGMENT

The author would like to thank Mrs. Yui Nishimura for her efforts through experiments and simulations.

REFERENCES

- [1] Aoki, K., T. Takamura, and T. Nakajima, Aerosol optical properties measured by SKYNET sky radiometer validation network. *Proc. of the 2nd EarthCARE Workshop*, 133-134, 2005.
- [2] Arai K., Preliminary assessment of radiometric accuracy for MOS-1 sensors, *International Journal of Remote Sensing*, 9, 1, 5-12, 1988.
- [3] Arai, K., In-flight test site cross calibration between mission instruments onboard same platform, *Advances in Space Research*, 19, 9, 1317-1328, 1997.
- [4] Arai K., Post Launch Calibration of ASTER with MODIS data, *Proceedings of the 3rd Annual IR Calibration Symposium in Utah State University*, 1992.
- [5] Arai K., A.Ono and Y.Yamaguchi, Accuracy Assessment of the Interactive Calibration of ASTER/TIR with MODIS, *Proceedings of the IGARSS'93*, pp.1303-1305, 1993.
- [6] Arai K., H.Fujisada, ASTER Level 1 WG, ATBD: Analytical Theoretical Basis Document for Level 1 Products, 1995.
- [7] Arai K., and K.Thome, Error budget analysis of the reflectance based vicarious calibration for satellite-based visible to near infrared radiometers, *Journal of the Japanese Society for Photogrammetry and Remote Sensing*, 39, 1, 99-105, 2000.
- [8] Arai K. and X.Liang, Method for the top of the atmosphere radiance estimation taking into account the polarization in down and up welling radiance calculations, *Journal of the Japanese Society for Photogrammetry and Remote Sensing*, 44, 3, 4-12, 2005.
- [9] Arai and H.Tonooka, Radiometric performance evaluation of ASTER/VNIR, SWIR and TIR, *IEEE Trans. on GeoScience and Remote Sensing*, 43,12,2725-2732, 2005.
- [10] Arai.K. and X.Liang, Characterization of aerosols in Saga city areas, Japan with direct and diffuse solar irradiance and aureole observations, *Advances in Space Research*, 39, 1, 23-27, 2006.
- [11] Arai, K., Vicarious calibration for solar reflection channels of radiometers onboard satellites with deserted area of data, *Advances in Space Research*, 39, 1, 13-19, 2006.

- [12] Arai, Atmospheric Correction and Residual Errors in Vicarious Cross-Calibration of AVNIR and OCTS Both Onboard ADEOS, *Advances in Space Research*, 25, 5, 1055-1058, 1999.
- [13] Barker, J.L., S.K. Dolan, et al., Landsat-7 mission and early results, *SPIE*, 3870, 299-311, 1999.
- [14] Barnes, R.A., E.E.Eplee, et al., Changes in the radiometric sensitivity of SeaWiFS determined from lunar and solar based measurements, *Applied Optics*, 38, 4649-4664, 1999.
- [15] Cosnefroy, H., M.Leroy and X.Briottet, Selection and characterization of Saharan and Arabian Desert sites for the calibration of optical satellite sensors, *Remote Sensing of Environment*, 58, 110-114, 1996.
- [16] Folkman, M.A.,S.Sandor, et al., Updated results from performance characterization and calibration of the TRWIS III Hyperspectral Imager, *Proc. SPIE*, 3118-17, 142, 1997.
- [17] Gellman, D.I., S.F. Biggar, et al., Review of SPOT-1 and 2 calibrations at White Sands from launch to the present, *Proc. SPIE, Conf.No.1938*, 118-125, 1993.
- [18] Hagolle, O., P.Galoub, et al., Results of POLDER in-flight calibration, *IEEE Trans. On Geoscience and Remote Sensing*, 37, 1550-1566, 1999.
- [19] Holben, B. N., et al., AERONET- A federated instrument network and data archive for aerosol characterization, *Remote Sens.*, 12, 1147-1163, 1991.
- [20] Holben, B.N., and Coauthors, AERONET-A federated instrument network and data archive for aerosol characterization. *Remote Sens. Environ.*, 66, 1-16. 1998.
- [21] Lenoble, J., Edt. Radiative transfer in scattering and absorbing atmospheres: Standard computational procedures, A.Deepak Publishing Co.,Ltd.,
- [22] Liang X. and K.Arai, Method for aerosol refractive index and size distribution with the solar direct, diffuse, aureole and polarization radiance, *Journal of Remote Sensing Society of Japan*, 25, 4, 357-366, 2005.
- [23] Nakajima, T., M.Tanaka and T. Yamauchi, Retrieval of the optical properties of aerosols from aureole and extinction data, *Applied Optics*, 22, 19, 2951-2959, 1983.
- [24] Ono.A., F.Sakuma, K.Arai, et al.,Pre-flight and Inflight Calibration for ASTER, *Journal of Atmospheric and Ocean Technology*, Vol.13, No.2, pp.321-335, Apr.,1996.
- [25] Slater P., K.Thome, A.Ono, F.Sakuma, K.Arai, et al., Radiometric Calibration of ASTER, *Journal of Remote Sensing Society of Japan*, Vol.15, No.2, pp.16-23, June 1995.
- [26] Thome, K., K. Arai, et.al., ASTER preflight and in-flight calibration and validation of level 2 products, *IEEE Trans. on Geoscience and Remote Sensing*, 36, 4, 1999.
- [27] Thome, S.Schiller, J.Conel, K.Arai and S.Tsuchida, Results of the 1996 Earth Observing System vicarious calibration campaign at Lunar lake playa, Nevada (USA), *Metrologia*, 35, 631-638, 1998.
- [28] Tsuchida, S. and A.Kamei, personal correspondence, 2009..

AUTHORS PROFILE

Kohei Arai, He received BS, MS and PhD degrees in 1972, 1974 and 1982, respectively. He was with The Institute for Industrial Science and Technology of the University of Tokyo from April 1974 to December 1978 also was with National Space Development Agency of Japan from January, 1979 to March, 1990. During from 1985 to 1987, he was with Canada Centre for Remote Sensing as a Post Doctoral Fellow of National Science and Engineering Research Council of Canada. He moved to Saga University as a Professor in Department of Information Science on April 1990. He was a councilor for the Aeronautics and Space related to the Technology Committee of the Ministry of Science and Technology during from 1998 to 2000. He was a councilor of Saga University for 2002 and 2003. He also was an executive councilor for the Remote Sensing Society of Japan for 2003 to 2005. He is an Adjunct Professor of University of Arizona, USA since 1998. He also is Vice Chairman of the Commission "A" of ICSU/COSPAR since 2008. He wrote 30 books and published 482 journal papers

Vital Sign and Location/Attitude Monitoring with Sensor Networks for the Proposed Rescue System for Disabled and Elderly Persons Who Need a Help in Evacuation from Disaster Areas

Kohei Arai¹

Graduate School of Science and Engineering
Saga University
Saga City, Japan

Abstract—Method and system for vital sign (Body temperature, blood pressure, bless, Heart beat pulse rate, and consciousness) and location/attitude monitoring with sensor network for the proposed rescue system for disabled and elderly persons who need a help in evacuation from disaster areas is proposed. Experimental results show that all of vital signs as well as location and attitude of the disabled and elderly persons are monitored with the proposed sensor networks.

Keyword—vital sign; heart beat puls rate; body temperature; blood pressure; blesses; consciousness; sensor network

I. INTRODUCTION

Handicapped, disabled, diseased, elderly persons as well as peoples who need help in their ordinary life are facing too dangerous situation in event of evacuation when disaster occurs. In order to mitigate victims, evacuation system has to be created. Authors proposed such evacuation system as a prototype system already [1]-[4]. The system needs information of victims' locations, physical and psychological status as well as their attitudes. Authors proposed sensor network system which consist GPS receiver, attitude sensor, physical health monitoring sensors which allows wearable body temperature, heart beat pulse rates; bless monitoring together with blood pressure monitoring [5]-[7]. Also the number of steps, calorie consumptions is available to monitor. Because it is difficult to monitor the blood pressure with wearable sensors, it is done by using the number of steps and body temperature. In addition to these, psychological status is highly required for vital sign monitoring (consciousness monitoring). By using EEG sensors, it is possible to monitor psychological status in the wearable sensor. These are components of the proposed physical health and psychological monitoring system.

Method and system for vital sign (Body temperature, blood pressure, bless, Heart beat pulse rate, and consciousness) and location/attitude monitoring with sensor network for the proposed rescue system for disabled and elderly persons who need a help in evacuation from disaster areas is proposed. Experimental results show that all of vital signs as well as location and attitude of the disabled and elderly persons are monitored with the proposed sensor networks.

Section 2 describes the proposed acceleration sensor system followed by experiment method and results. Then conclusion is described together with some discussions..

II. PROPOSED SENSOR NETWORK SYSTEM

A. System Configuration

Figure 1 shows the entire system configuration of the proposed physical and psychological health monitoring system. Patients have physical and psychological health sensors and send the acquired data through Bluetooth and Internet to the Health Data Collection Center: HDCC server. On the other hand, volunteers receive health data of the previously designated several patients together with traffic flow information and appropriate route information. When something wrong occurs on the designated patients, HDCC provides information which required for rescue to the designated volunteers then the volunteers rescue patients in an efficient and an effective manner.

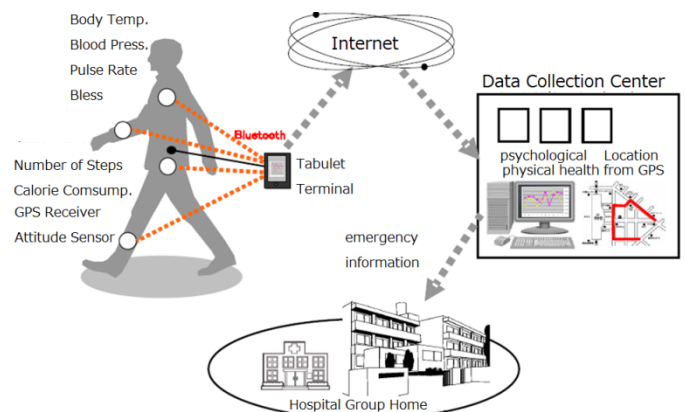


Fig. 1. Entire system configuration of the proposed wearable physical and psychological health monitoring system

B. Sensor and Communication System

In order for evacuation and rescue, victims' location and attitude is important. Therefore, GPS receiver and accelerometer are added to the aforementioned measuring

sensors for body temperature pulse rate, blood pressure, bress, and eeg, emg. All sensors should be wearable and can be attached to ones' tall forehead. Acquired data can be transmitted to mobile devices in ones' pockets. Through WiFi network or wireless LAN connection, acquired data can be collected in the designated information collection center. Then acquired data can be refereed from the designated volunteers who are responsible to help victims for evacuation and rescue.

III. EXPERIMENTS

A. Experimental Method

Four patients are participated to the experiments. The difference due to gender can be discussed through a comparison between patients A and C while the difference due to age can be discussed through a comparison between patients B and C. Meanwhile, the difference due to the degree of Alzheimer can be discussed through a comparison between patients B and D as shown in Table 1.

TABLE I. FOUR PATIENTS

Patient	Male/Female	Age	Remarks
1	Male	37	Good in Health
2	Female	47	Good in Health
3	Female	39	Good in Health
4	Female	91	Weak Alzheimer
5	Male	36	Good in Health
6	Male	39	Good in Health
7	Male	49	Good in Health
8	Female	29	Good in Health
9	Female	53	Good in Health
10	Female	56	Good in Health
11	Female	58	Good in Health

Experiments are conducted for eight hours a day for almost every working day (Monday to Friday) for six months starting from May 2012. Measuring time intervals are different by the measuring items. GPS location can be measured every two seconds while accelerometer data can be obtained every 10 seconds.

Meanwhile, body temperature, pulse rate can be measured every one minutes while blood pressure is measured every one hour together with EEG and EMG signals. The number of steps is measured when the walking event happened. At the end of day, four patients evaluate their physical and psychological conditions which are listed in Table 2.

The 20 items listed in the Table 2 are questionnaires for four patients. In the Table, Ai is questionnaire for physical health while Bi is questionnaire for psychological health. The patients respond to the questionnaire above with five levels range from 0 to 4 grades. Total Score is defined as sum of the aforementioned self evaluation of 20 items including physical and psychological health items.

TABLE II. SELF EVALUATION ITEMS

A1	Feel fever
B1	Loosing thinking capability
A2	Feel tiredness
B2	Could not sleep well
A3	Get tired after exercise
B3	Feel bad
A4	Muscle hurt
B4	Unconfident about health
A5	Feel depression
B5	Do not want to work
A6	Limper hurt
B6	Cannot remember something
A7	Head ach
B7	Loosing balance
A8	Cannot recover after sleep
B8	Cannot think deeply
A9	Throat hurt
B9	Loosing concentration
A10	Joint hurt
B10	Sleep for too long time

B. Experimental Results

Figure 2 shows physical and psychological stress for the patients. Physical and psychological stress is different each other participants as shown in Figure 2. There are patients who are sensitive to their stress such as Patient No.8. There are also patients who are not so sensitive to their stress such as patient No. 5.

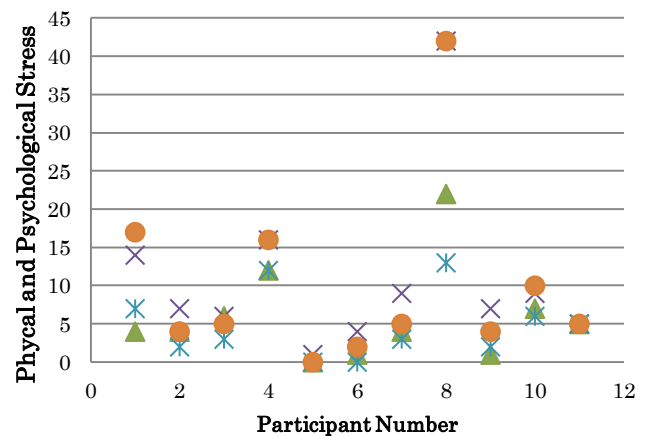


Fig. 2. Physical and psychological stress for the patients

Physical and psychological stress does not depend on male / female difference as shown in Figure 3. Also it is found that physical and psychological stress does not depend on age as shown in Figure 4 (a). Also Figure 4 (b) shows age dependency on physical conditions of body temperature, blood pressure, pulse rate, and the number of steps.

An example of relation between total score of stress (sum of physical and psychological stress) and measured physical conditions of body temperature, blood pressure, pulse rate, and the number of steps (for the patient with weak Alzheimer) is shown in Figure 5.

As shown in Figure 5, there is no relation between total score of stress (sum of physical and psychological stress) and measured physical conditions of body temperature, blood pressure, pulse rate, and the number of steps (for the patient with weak Alzheimer). This is same thing for the other patients. During the experiments, patients have to repeat the following cycle of “walk for 10 minutes and then take a rest for 10 minutes” for 10 times. Therefore, only the number of steps is proportional to the total score.

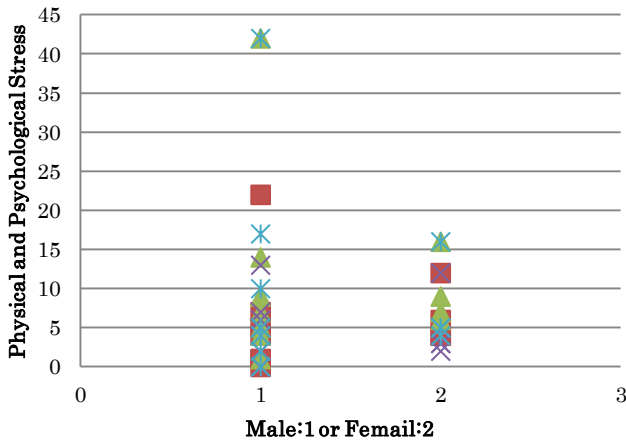
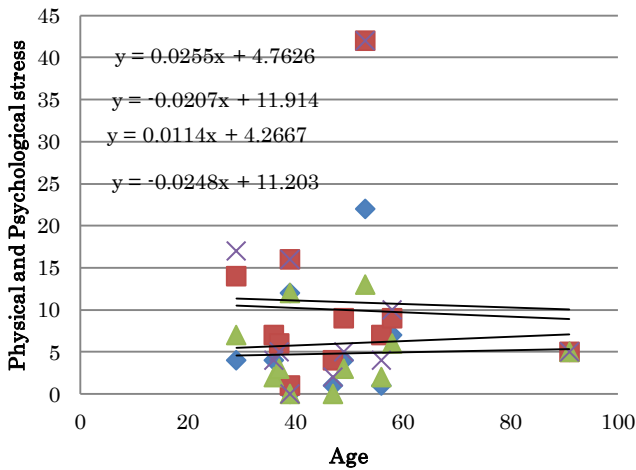
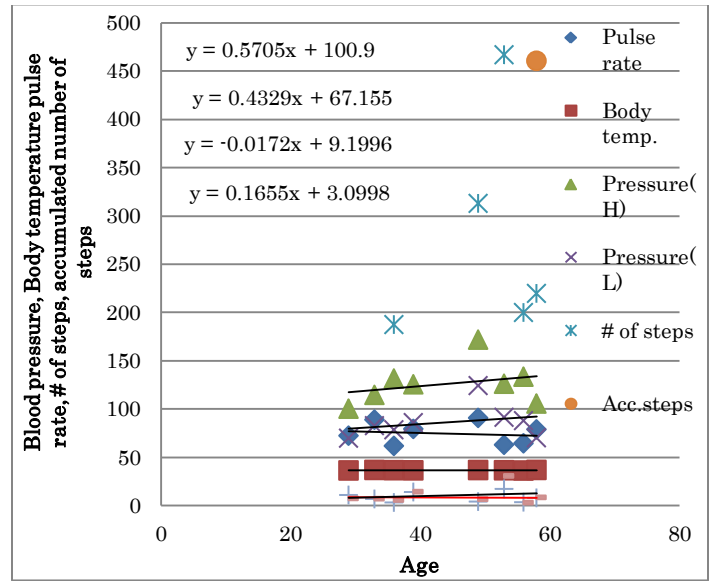


Fig. 3. Sex independency on physical and psychological stress



(a) Age independency on physical and psychological stress



(b) Relation between physical conditions and age

Fig. 4. Age independency on physical and psychological stress as well as age dependency on physical conditions

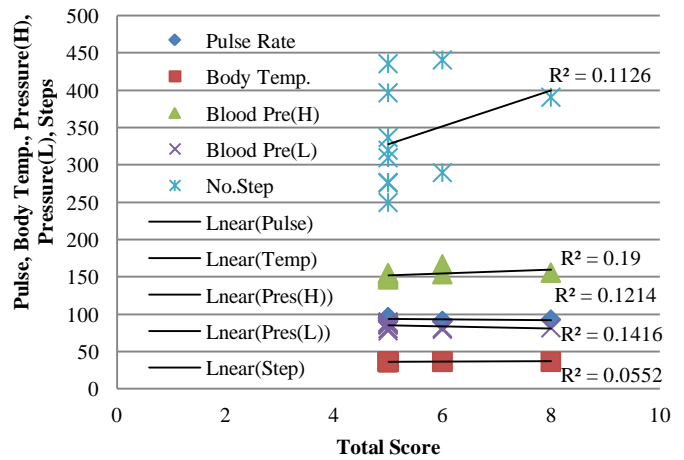
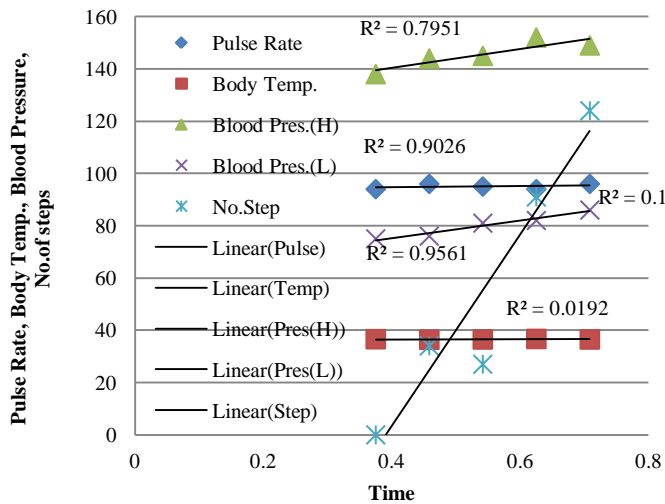
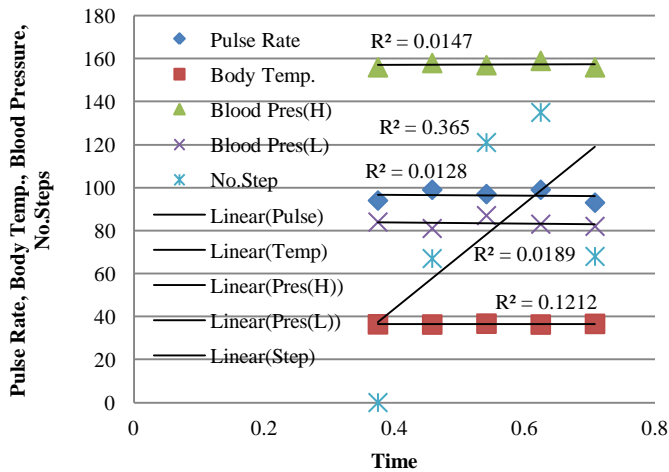


Fig. 5. An example of relation between total score of stress (sum of physical and psychological stress) and measured physical conditions of body temperature, blood pressure, pulse rate, and the number of steps (for the patient with weak Alzheimer)

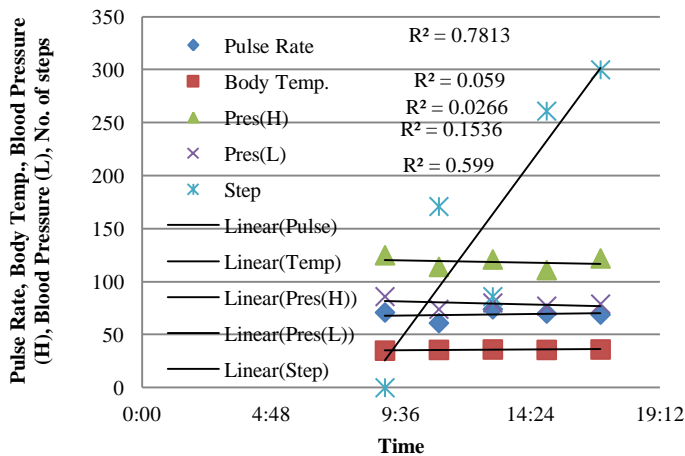
In accordance with increasing of time duration, the number of steps is increased obviously. In accordance with increasing of the number of steps, blood pressure (High) and blood pressure (Low) is increased usually. It, however, is not always that pulse rate is proportional to the number of steps as shown in Figure 6.



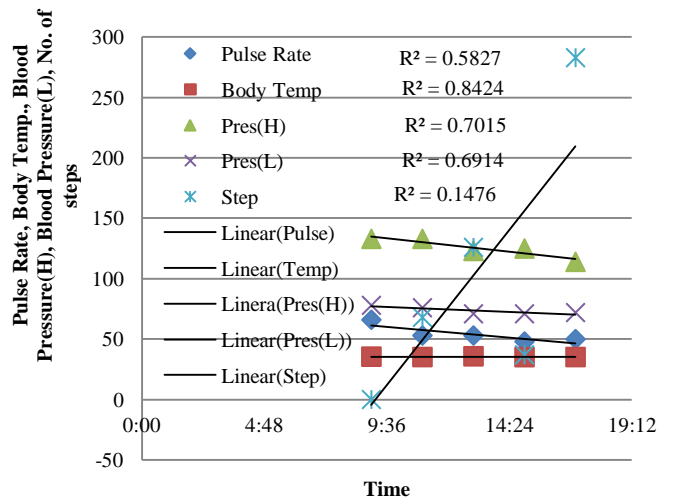
(a) Patient with weak Alzheimer (Minimum total score)



(b) Patient with weak Alzheimer (Maximum total score)



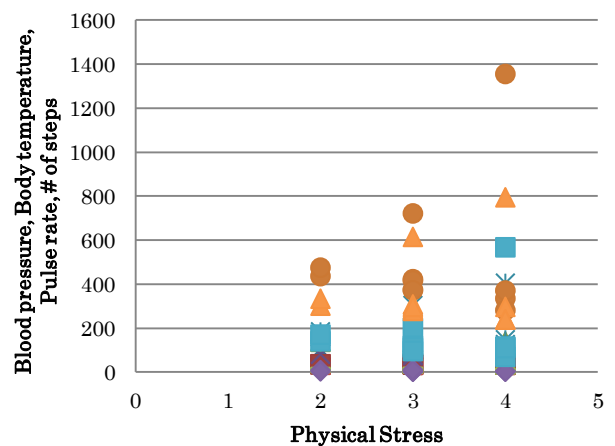
(c) Male patient whose age is 37 (Minimum total score)



(d) Male patient whose age is 37 (Maximum total score)

Fig. 6. Examples of relation between the number of steps (Time) and measured physical conditions, blood pressure, pulse rate, body temperature

In more detail, relation between physical stress as well as psychological stress and measured physical conditions of blood pressure, pulse rate, body temperature and the number of steps are shown in Figure 7 together with relation between standard deviation of measured physical conditions of blood pressure, pulse rate, body temperature and the number of steps and physical and psychological stress. Figure 8-13 shows relations between physical stress as well as psychological stress and measured physical conditions of blood pressure, pulse rate, body temperature and the number of steps together with relation between standard deviation of measured physical conditions of blood pressure, pulse rate, body temperature and the number of steps and physical and psychological stress for the male whose age is 49 years old, the female whose age is 58 years old, the female whose age is 56 years old, the male whose age is 39 years old, the female whose age is 53 years old, the female whose age is 29 years old, respectively.



(a) Mean of physical condition (Physical stress)

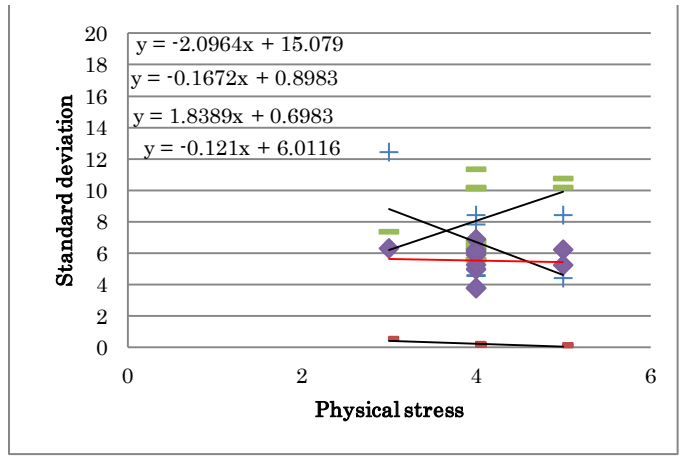
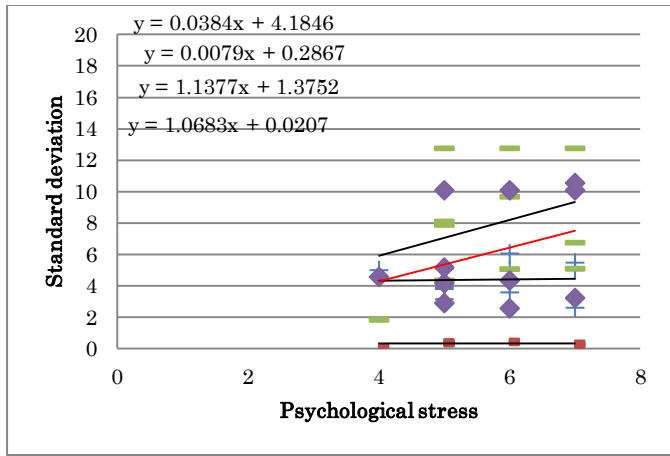
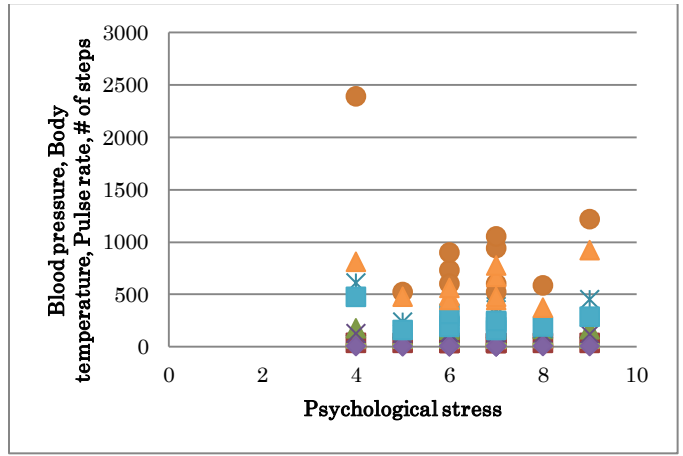
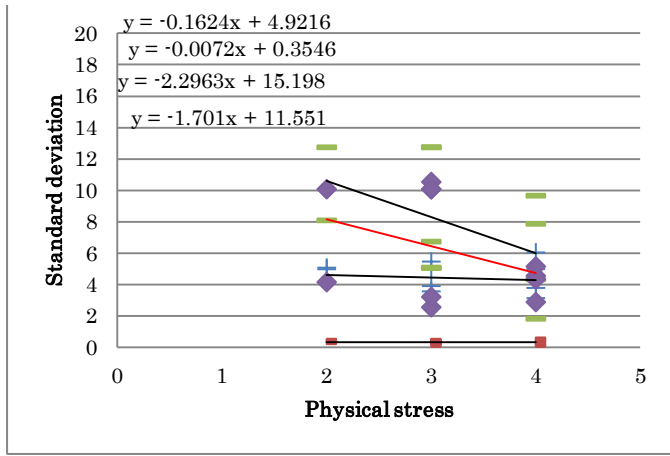
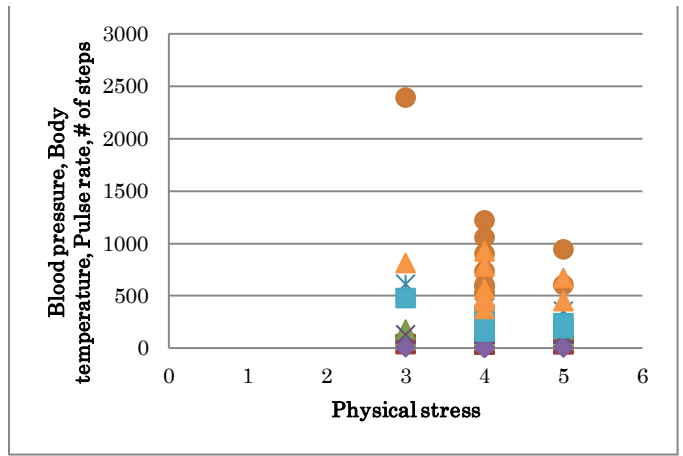
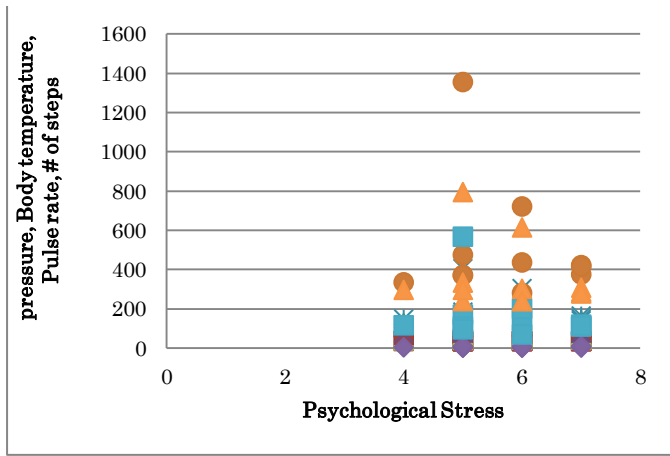
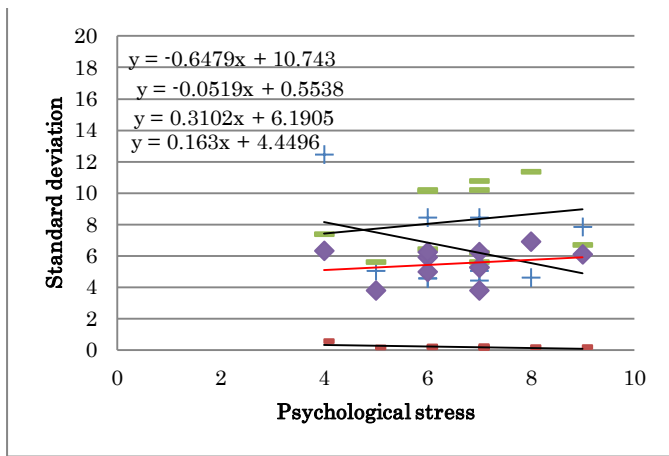
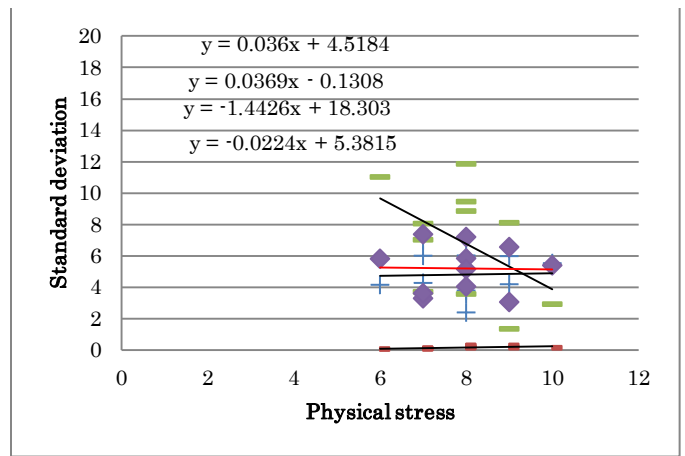


Fig. 7. Relation between physical stress as well as psychological stress and measured physical conditions of blood pressure, pulse rate, body temperature and the number of steps together with relation between standard deviation of measured physical conditions of blood pressure, pulse rate, body temperature and the number of steps and physical and psychological stress for the male whose age is 36 years old

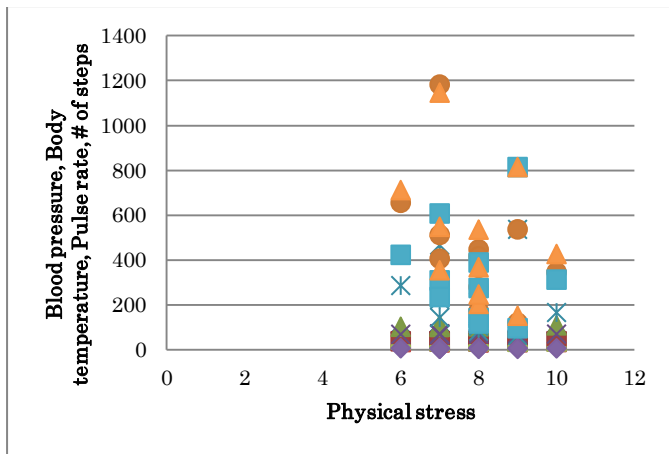


(d) Standard deviation of physical condition (Psychological stress)

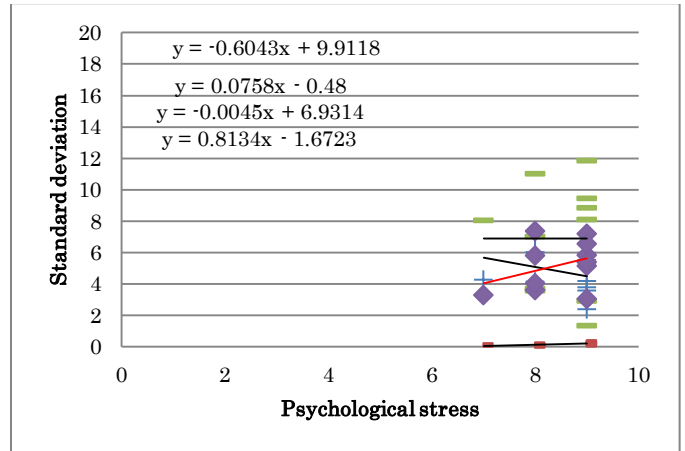


(c) Standard deviation of physical condition (Physical stress)

Fig. 8. Relation between physical stress as well as psychological stress and measured physical conditions of blood pressure, pulse rate, body temperature and the number of steps together with relation between standard deviation of measured physical conditions of blood pressure, pulse rate, body temperature and the number of steps and physical and psychological stress for the male whose age is 49 years old

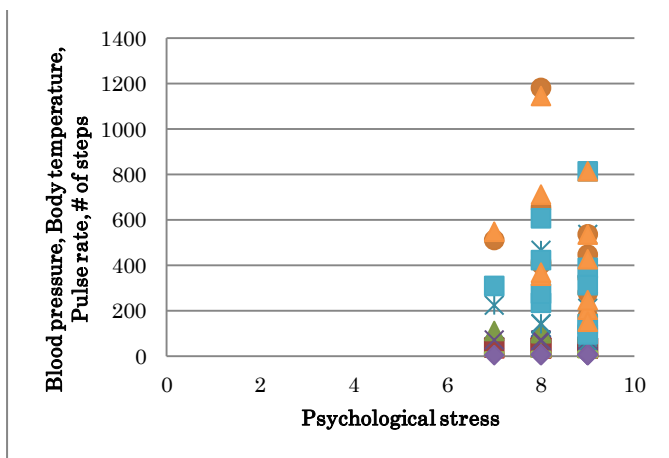


(a) Mean of physical condition (Physical stress)

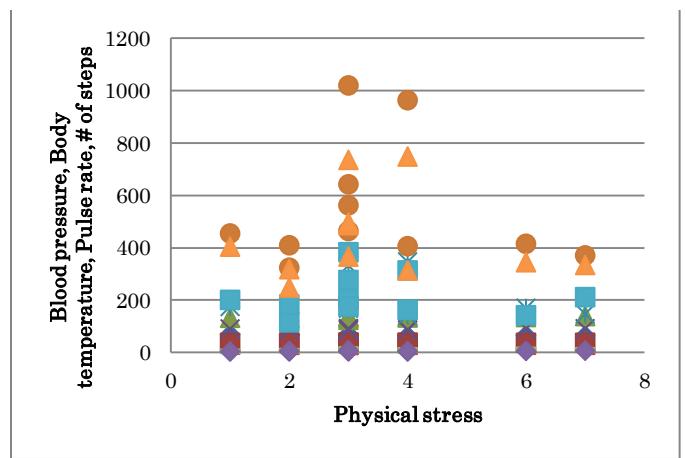


(d) Standard deviation of physical condition (Psychological stress)

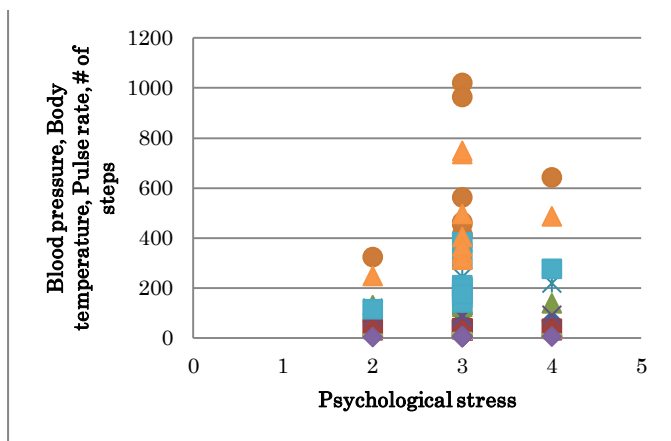
Fig. 9. Relation between physical stress as well as psychological stress and measured physical conditions of blood pressure, pulse rate, body temperature and the number of steps together with relation between standard deviation of measured physical conditions of blood pressure, pulse rate, body temperature and the number of steps and physical and psychological stress for the female whose age is 58 years old



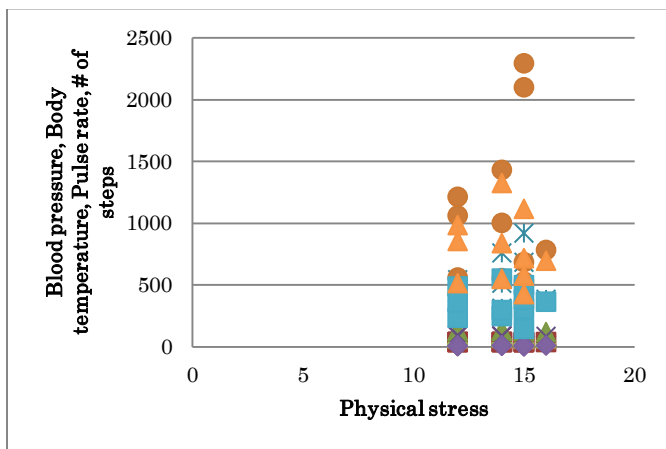
(b) Mean of physical condition (Psychological stress)



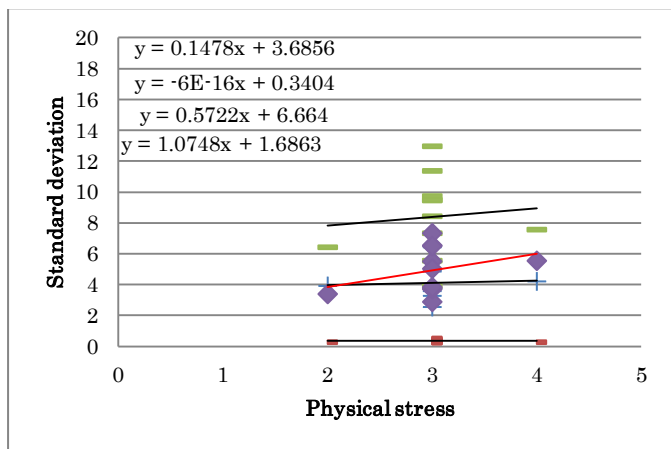
(a) Mean of physical condition (Physical stress)



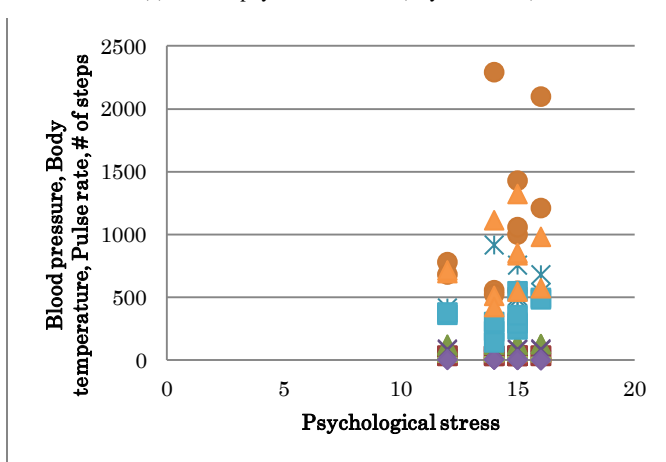
(b) Mean of physical condition (Psychological stress)



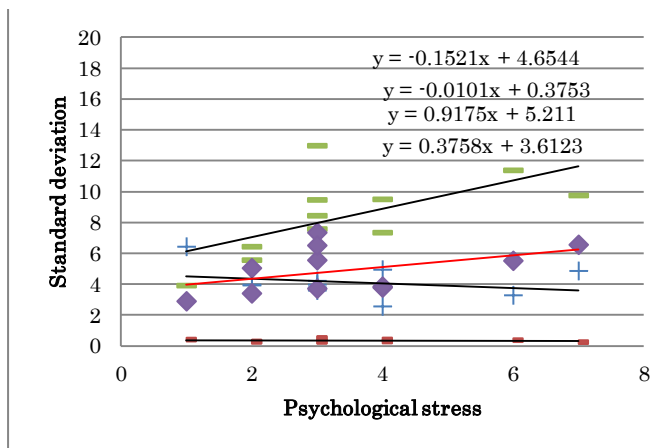
(a) Mean of physical condition (Physical stress)



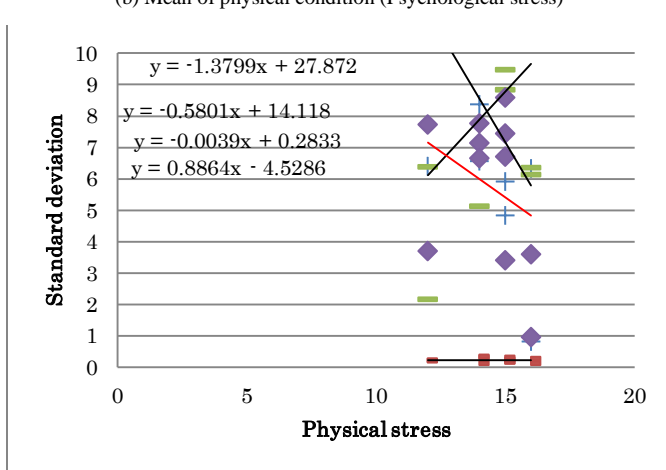
(c) Standard deviation of physical condition (Physical stress)



(b) Mean of physical condition (Psychological stress)

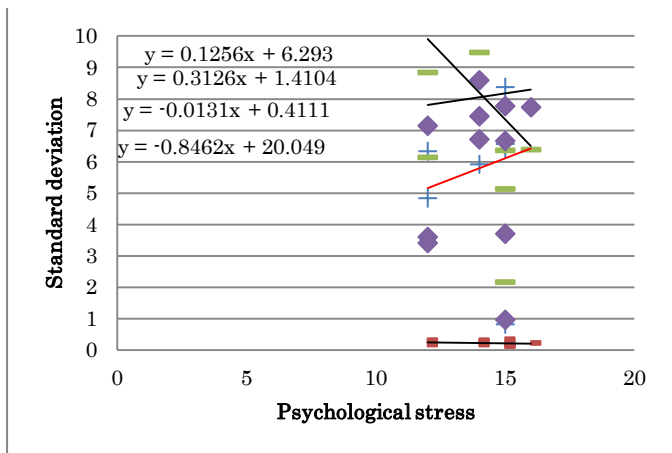


(d) Standard deviation of physical condition (Psychological stress)

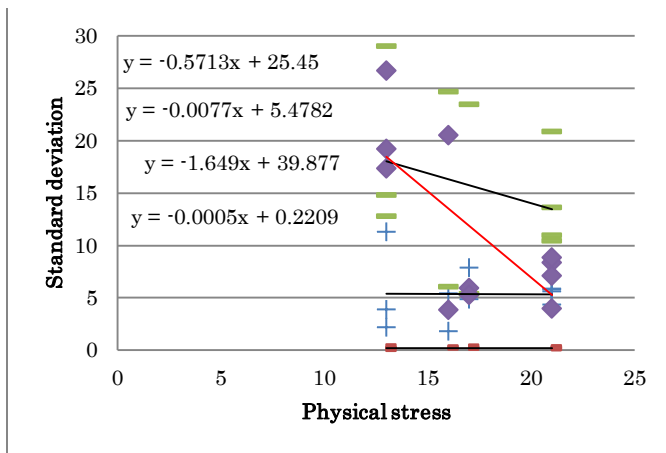


(c) Standard deviation of physical condition (Physical stress)

Fig. 10. Relation between physical stress as well as psychological stress and measured physical conditions of blood pressure, pulse rate, body temperature and the number of steps together with relation between standard deviation of measured physical conditions of blood pressure, pulse rate, body temperature and the number of steps and physical and psychological stress for the female whose age is 56 years old

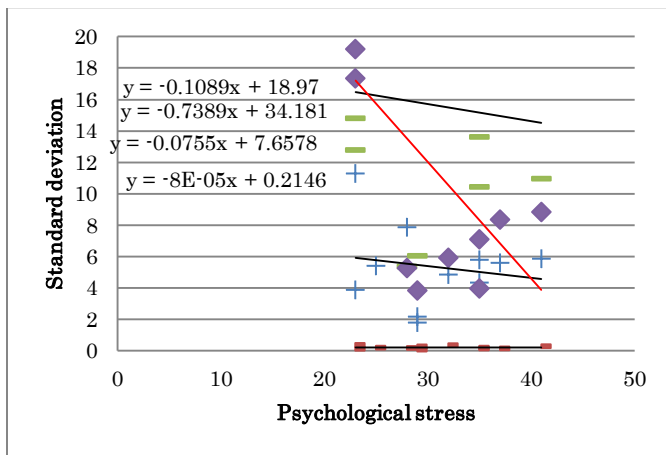


(d) Standard deviation of physical condition (Psychological stress)



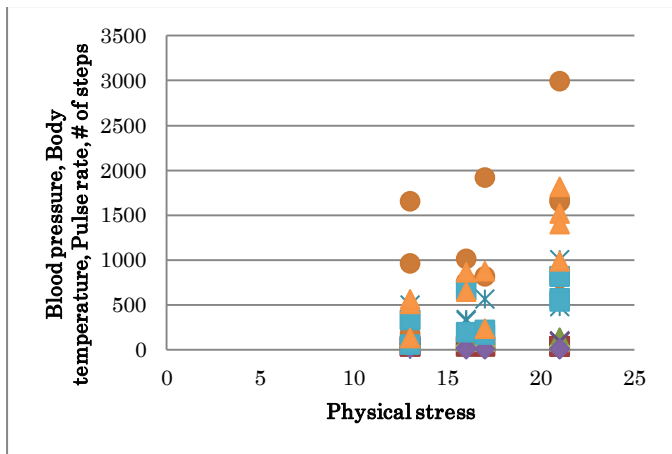
(c) Standard deviation of physical condition (Physical stress)

Fig. 11. Relation between physical stress as well as psychological stress and measured physical conditions of blood pressure, pulse rate, body temperature and the number of steps together with relation between standard deviation of measured physical conditions of blood pressure, pulse rate, body temperature and the number of steps and physical and psychological stress for the male whose age is 39 years old

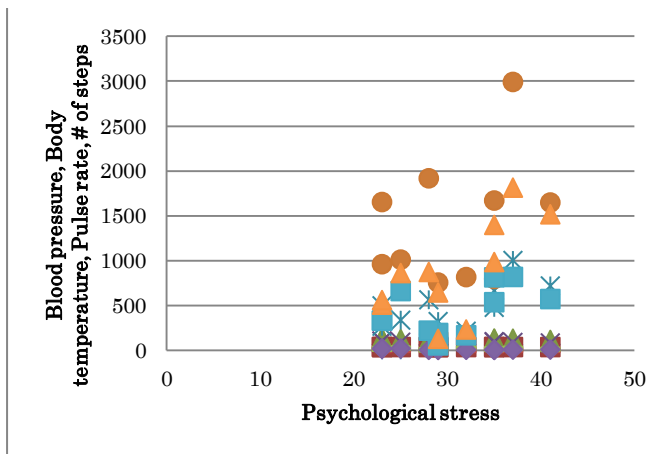


(d) Standard deviation of physical condition (Psychological stress)

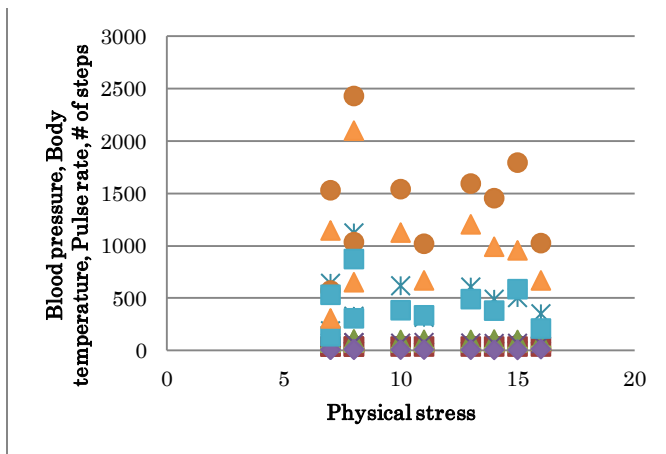
Fig. 12. Relation between physical stress as well as psychological stress and measured physical conditions of blood pressure, pulse rate, body temperature and the number of steps together with relation between standard deviation of measured physical conditions of blood pressure, pulse rate, body temperature and the number of steps and physical and psychological stress for the female whose age is 53 years old



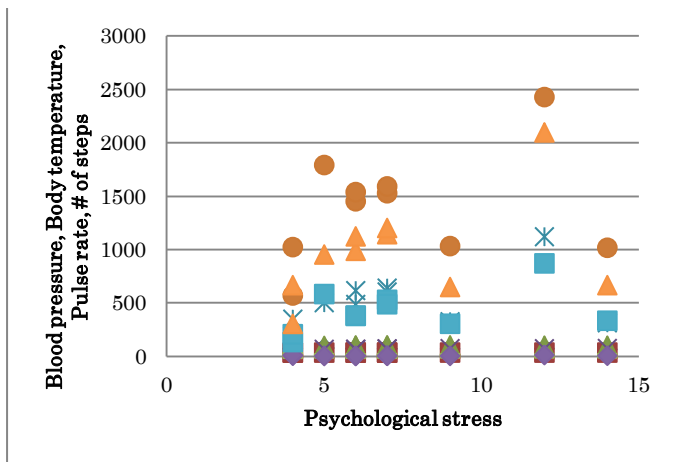
(a) Mean of physical condition (Physical stress)



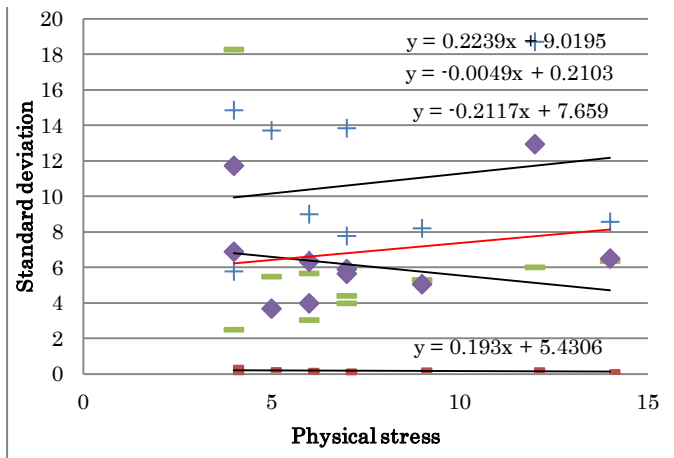
(b) Mean of physical condition (Psychological stress)



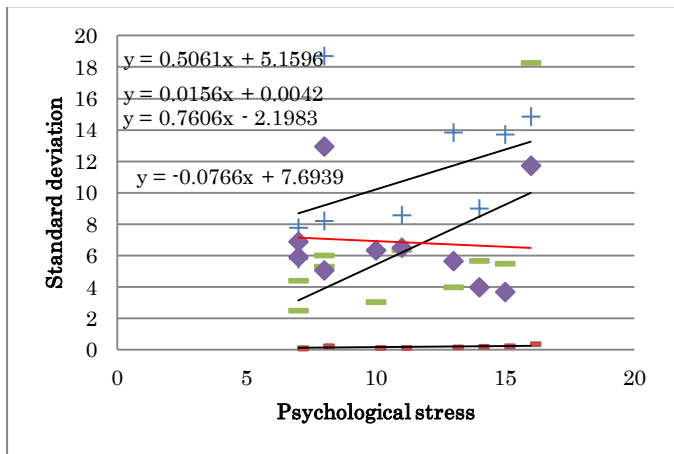
(a) Mean of physical condition (Physical stress)



(b) Mean of physical condition (Psychological stress)



(c) Standard deviation of physical condition (Physical stress)



(d) Standard deviation of physical condition (Psychological stress)

Fig. 13. Relation between physical stress as well as psychological stress and measured physical conditions of blood pressure, pulse rate, body temperature and the number of steps together with relation between standard deviation of measured physical conditions of blood pressure, pulse rate, body temperature and the number of steps and physical and psychological stress for the female whose age is 29 years old

Through these experiments, it is found that the followings,

- There is no difference between male and female on physical and psychological stress
- There is difference between the person in healthy condition and the patient with weak Alzheimer
- There are age dependencies on physical and psychological stress as well as blood pressure
- In accordance with increasing of the number of steps, physical stress is increased while psychological stress is decreased. This trend is observed from the relations between standard deviation of physical conditions, blood pressure, body temperature, pulse rate and physical and psychological stress. Also this trend is remarkable for young generation of patients.

Consciousness is measured with EEG sensor together with eye movement observation. Quick eye movements (Succored movements) are highly related to EEG sensor signals. This fact is verified with the following experiments.

By using EEG analyzer tools, we analyze the fatigue effect between the condition when user is looking at one point and condition when user is looking at four points. In order to analyze fatigue effect, we use Peak Alpha Frequency: PAF [8]-[11]. It is possible to measure psychological status by using PAF derived from EEG signal. Psychological health condition is measured with Bio Switch MCTOS of Brain Wave Measuring instrument (BM-Set1) manufactured by Technos Japan Co. Ltd. every one hour.

Figure 14 shows alpha and beta frequency components of EEG signals measured with the male patient whose age is 49. At the beginning of the experiment, he surprised so much that beta signal raised remarkably. At that time, his eye moved as quickly as shown in Figure 15. This situation is same for the other patients. Therefore, it is said that there is high relation between eye movement and psychological status.

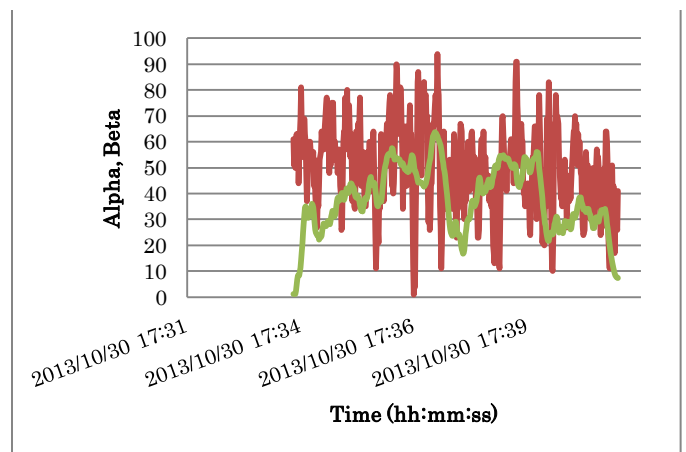


Fig. 14. alpha and beta frequency components of EEG signals measured with the male patient whose age is 49

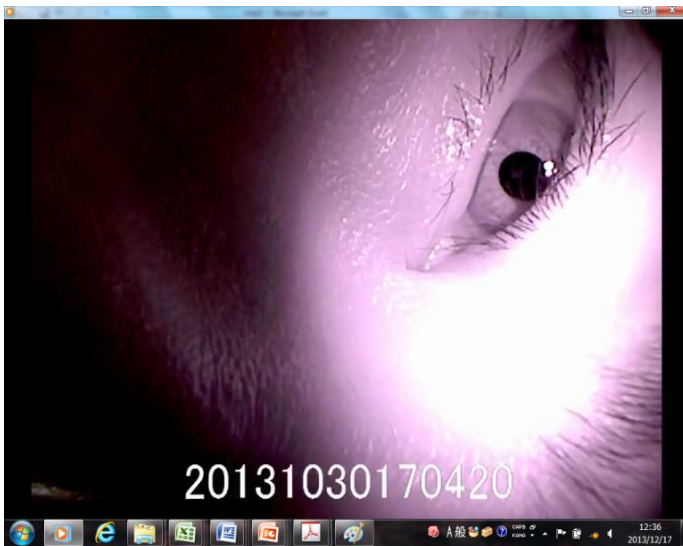


Fig. 15. Quick eye movements observed for the male patient whose age is 49

IV. CONCLUSION

Method and system for vital sign (Body temperature, blood pressure, blood sugar, Heart beat pulse rate, and consciousness) and location/attitude monitoring with sensor network for the proposed rescue system for disabled and elderly persons who need a help in evacuation from disaster areas is proposed. Experimental results show that all of vital signs as well as location and attitude of the disabled and elderly persons are monitored with the proposed sensor networks.

Through the experiments with 11 patients, it is found the followings,

- There is no relation between pulse rate and age
- Body temperature is stable for time duration through the experiments
- There is no age dependency on the number of steps (calorie consumption)
- Psychological status can be estimated with eye movements→There is relation between EEG signal and eye movements (psychological status)
- There is no difference between male and female on physical and psychological stress
- There is difference between the person in healthy condition and the patient with weak Alzheimer
- There are age dependencies on physical and psychological stress as well as blood pressure

- In accordance with increasing of the number of steps, physical stress is increased while psychological stress is decreased. This trend is observed from the relations between standard deviation of physical conditions, blood pressure, body temperature, pulse rate and physical and psychological stress. Also this trend is remarkable for young generation of patients.

ACKNOWLEDGMENT

The author would like to thank all the patients who are contributed to the experiments conducted. The author also would like to thank Professor Dr. Takao Hotokebuchi, President of Saga University for his support this research works.

REFERENCES

- [1] Kohei Arai, Tran Xuan Sang, Decision making and emergency communication system in rescue simulation for people with disabilities, International Journal of Advanced Research in Artificial Intelligence, 2, 3, 77-85, 2013.
- [2] K.Arai, T.X.Sang, N.T.Uyen, Task allocation model for rescue disabled persons in disaster area with help of volunteers, International Journal of Advanced Computer Science and Applications, 3, 7, 96-101, 2012.
- [3] K.Arai, T.X.Sang, Emergency rescue simulation for disabled persons with help from volunteers, International Journal of Research and Review on Computer Science, 3, 2, 1543-1547, 2012.
- [4] K. Arai, and T. X. Sang, "Fuzzy Genetic Algorithm for Prioritization Determination with Technique for Order Preference by Similarity to Ideal Solution", International Journal of Computer Science and Network Security, vol.11, no.5, 229-235, May 2011.
- [5] Arai K., R. Mardiyanto, Evaluation of Students' Impact for Using the Proposed Eye Based HCI with Moving and Fixed Keyboard by Using EEG Signals, International Journal of Review and Research on Computer Science(IJRCS), 2, 6, 1228-1234, 2011
- [6] K.Arai, Wearable healthy monitoring sensor network and its application to evacuation and rescue information server system for disabled and elderly person, International Journal of Research and Review on Computer Science, 3, 3, 1633-1639, 2012.
- [7] K.Arai, Wearable Physical and Psychological Health Monitoring System, Proceedings of the Science and Information Conference 2013 October 7-9, 2013 | London, UK

AUTHORS PROFILE

Kohei Arai, He received BS, MS and PhD degrees in 1972, 1974 and 1982, respectively. He was with The Institute for Industrial Science and Technology of the University of Tokyo from April 1974 to December 1978 also was with National Space Development Agency of Japan from January, 1979 to March, 1990. During from 1985 to 1987, he was with Canada Centre for Remote Sensing as a Post Doctoral Fellow of National Science and Engineering Research Council of Canada. He moved to Saga University as a Professor in Department of Information Science on April 1990. He was a councilor for the Aeronautics and Space related to the Technology Committee of the Ministry of Science and Technology during from 1998 to 2000. He was a councilor of Saga University for 2002 and 2003. He also was an executive councilor for the Remote Sensing Society of Japan for 2003 to 2005. He is an Adjunct Professor of University of Arizona, USA since 1998. He also is Vice Chairman of the Commission "A" of ICSU/COSPAR since 2008. He wrote 31 books and published 442 journal papers

Method and System for Human Action Detections with Acceleration Sensors for the Proposed Rescue System for Disabled and Elderly Persons Who Need a Help in Evacuation from Disaster Area

Kohei Arai¹

Graduate School of Science and Engineering
Saga University
Saga City, Japan

Abstract—Method and system for human action detections with acceleration sensors for the proposed rescue system for disabled and elderly persons who need a help in evacuation from disaster areas is proposed. Not only vital signs, blood pressure, heart beat pulse rate, body temperature, bless and consciousness, but also, the location and attitude of the persons have to be monitored for the proposed rescue system. The attitude can be measured with acceleration sensors. In particular, it is better to discriminate the attitudes, sitting, standing up, and lying down. Also, action speed has to be detected. Experimental results show that these attitude monitoring can be done with acceleration sensors.

Keywords—vital sign; heart beat puls ratee; body temperature; blood pressure; blesses, consciousness; seonsor network

I. INTRODUCTION

Handicapped, disabled, diseased, elderly persons as well as peoples who need help in their ordinary life are facing too dangerous situation in event of evacuation when disaster occurs. In order to mitigate victims, evacuation system has to be created. Authors proposed such evacuation system as a prototype system already [1]-[4].

The system needs information of victims' locations, physical and psychological status as well as their attitudes. Authors proposed sensor network system which consist GPS receiver, attitude sensor, physical health monitoring sensors which allows wearable body temperature, heart beat pulse rates; bless monitoring together with blood pressure monitoring [5]-[7]. Also the number of steps, calorie consumptions is available to monitor. Because it is difficult to monitor the blood pressure with wearable sensors, it is done by using the number of steps and body temperature. In addition to these, psychological status is highly required for vital sign monitoring (consciousness monitoring). By using EEG sensors, it is possible to monitor psychological status in the wearable sensor. These are components of the proposed physical health and psychological monitoring system.

Method and system for human action detections with

acceleration sensors for the proposed rescue system for disabled and elderly persons who need a help in evacuation from disaster area is proposed. Experimental results show that human actions can be estimated with acceleration sensors.

Section 2 describes the proposed acceleration sensor system followed by experiment method and results. Then conclusion is described together with some discussions..

II. PROPOSED SENSOR NETWORK SYSTEM

A. Acceleration Sensor Used

Figure 1 shows outlook of the acceleration sensor used in the proposed rescue system. It is the Small Sized Wireless Hybrid Sensor WAA-010

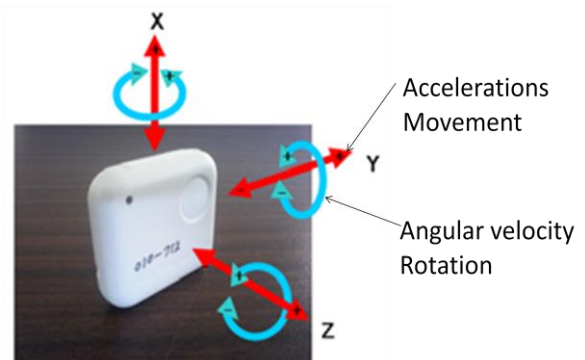


Fig. 1. Outlook of the Small Sized Wireless Hybrid Sensor WAA-010.

It allows measurements of movements in x, y, and z directions and roll, pitch and yaw rotations. WAA-010 is a multi sensor which allows measurements of attitude, angular velocity (gyro), Earth magnet in three axes. Also WAA-010 has communication capability to PC through Bluetooth communication links.

B. Acceleration Data Acquisition

Figure 2 (a) shows the toggle of the Bluetooth while Figure 2 (b) shows installation window of Bluetooth on PC display.



(a)Toggle of the Bluetooth



(b) Installation window of Bluetooth on PC display.

Fig. 2. Toggle of the Bluetooth and installation window of Bluetooth on PC display.

After the installation of acceleration sensor driver, communication port assignments, batteries of the three axis of acceleration, angular velocity as well as Earth magnet-meter can be monitored through PC screen which is shown in Figure 3.



(a)Port assignment



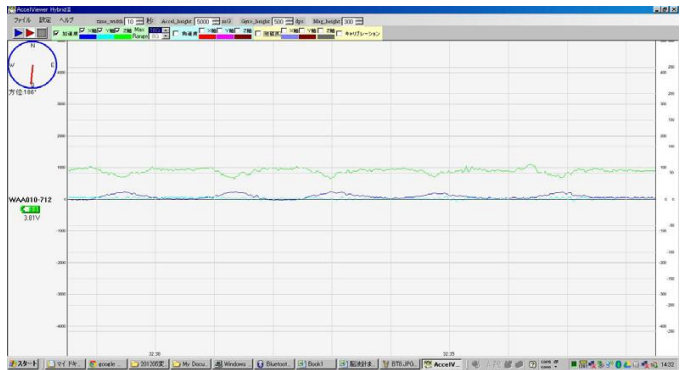
(b)Battery monitor

Fig. 3. Communication port assignment and battery monitor

III. EXPERIMENTS

A. Examples of Acceleration and Angular Velocity Data

Figure 4 (a) shows an example of acceleration sensor data with the maximum range of 5000mG while Figure 4 (b) shows an example of measured acceleration sensor data with the maximum range of 2000mG. As shown in Figure 4, the maximum range has to be adjusted for the acceleration of the target objects. Meanwhile, Figure 5 (a) and (b) shows an example of measured angular velocity with maximum of 500 dps and 200 dps, respectively. These examples are obtained through the experiments of which the acceleration sensor are held by hands. Therefore, these performances are just for the acceleration sensor only.



(a)5000mG



(b)2000mG

Fig. 4. Examples of acceleration sensor data



(a)500dps



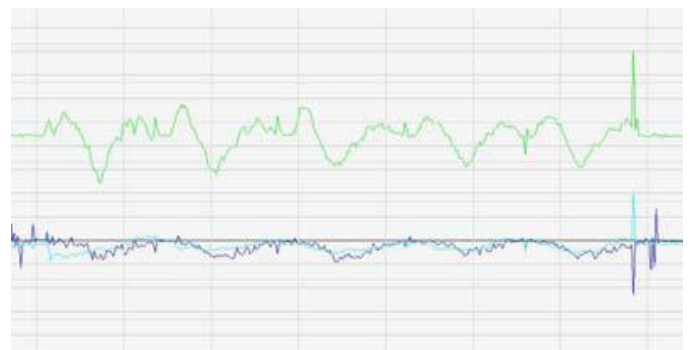
(b)200dps

Fig. 5. Examples of angular velocity measured

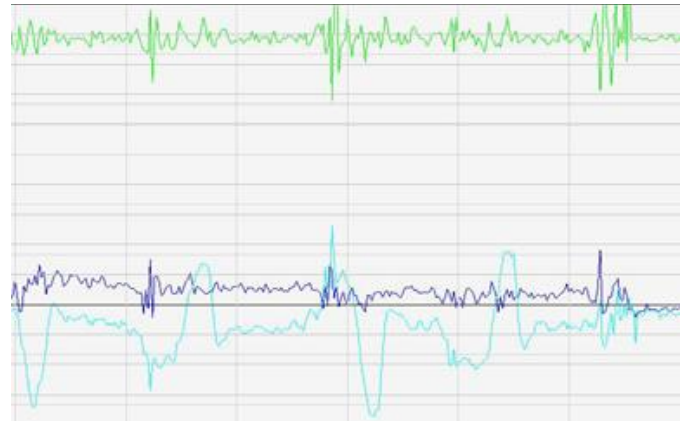
Meanwhile, example of acceleration sensor data (200mG of maximum range) for the motion in Z direction is shown in Figure 6 (a).

On the other hand, Figure 6 (b) and (c) shows examples of acceleration sensor data for the motion in Y and X directions, respectively.

Figure 7 (a), (b), and (c) shows examples of angular velocity data (500 dps of maximum range) for the rotations in Z, Y, X directions, roll, pitch and yaw angles, respectively.



(a)Z direction

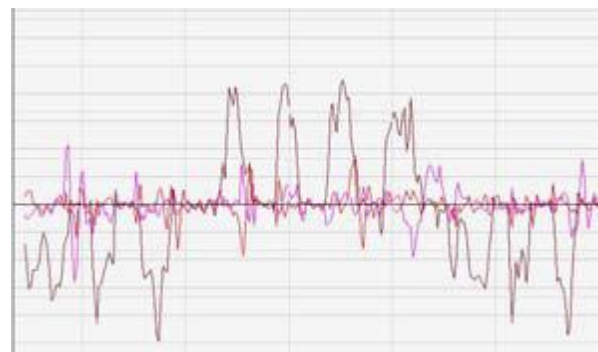


(b)Y direction

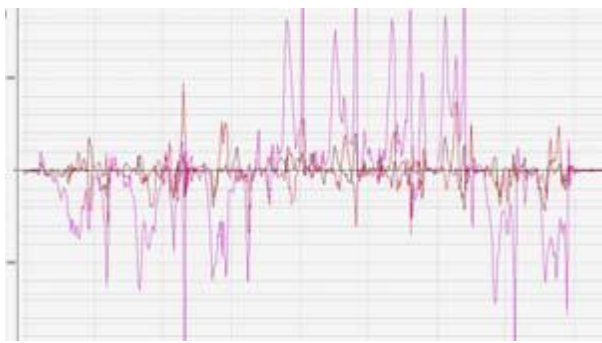


(c)X direction

Fig. 6. Examples of acceleration sensor data for the motions in X, Y, and Z directions



(a)Rotation in Z direction



(b)Rotation in Y direction



(c)Rotation in X direction

Fig. 7. Examples of angular velocity data

B. Examples of Acceleration and Angular Velocity Data Attached to the Wearing Glass End

Acceleration sensor is then attached to the wearing glass end as is shown in Figure 8. Not only the acceleration sensor but also body temperature, heart beat pulse rate sensors as well as EEG sensor head are attached to the glass end together with battery and Bluetooth communicator. At the forehead, EEG sensor head is attached with spring wire extended from the center of the glass. Therefore most of vital signs can be measured with the glass.

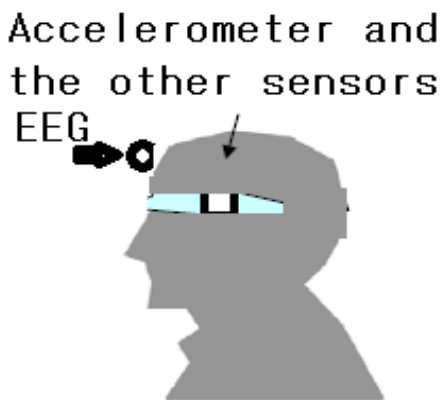
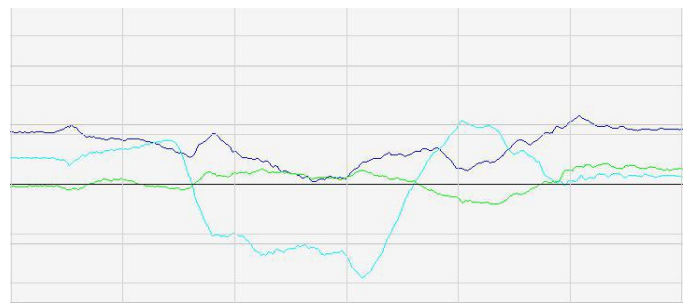
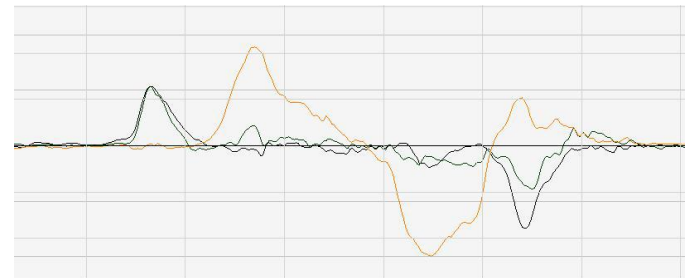


Fig. 8. Location of the acceleration sensor (at the glass end)

Figure 9 shows examples of acceleration sensor and angular velocity data when the user lie down and stand up slowly. Meanwhile, Figure 10 shows examples of those when the user sit down on a chair slowly.

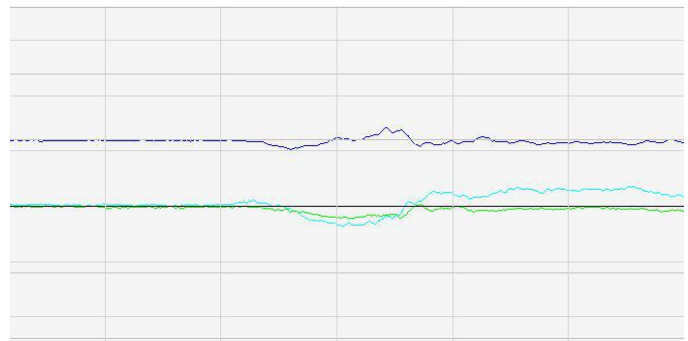


(a)Acceleration (X: Dark Blue, Y: Blue (Effective), Z: Green)

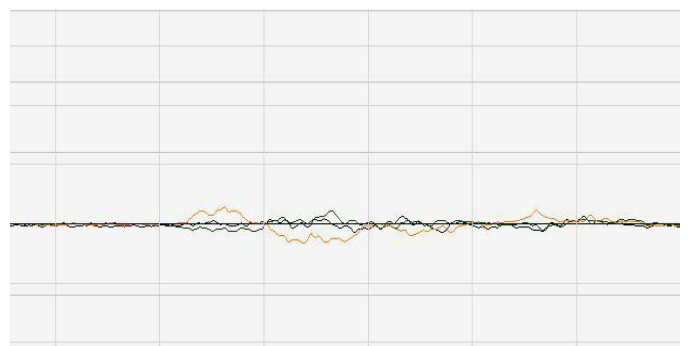


(b)Angular velocity (X: Black, Y: Green, Z: Red (Effective))

Fig. 9. Examples of acceleration sensor and angular velocity data when the user laid down and stand up slowly.



(a)Acceleration (X: Dark Blue, Y: Blue (Effective), Z: Green)

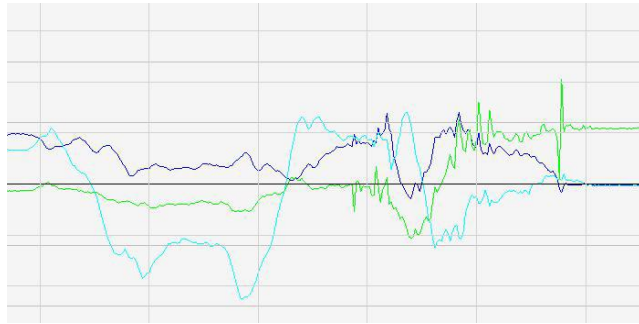


(b)Angular velocity (X: Black, Y: Green, Z: Red (Effective))

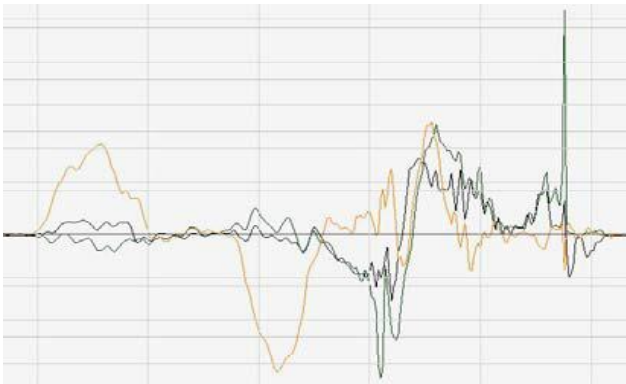
Fig. 10. Examples of acceleration sensor and angular velocity data when the user sit down on chair slowly.

Figure 11 shows examples of acceleration sensor and angular velocity data when the user lie down and stand up quickly. Meanwhile, Figure 12 shows examples of those when the user sit down on a chair quickly. On the other hand, Figure 13 (a) shows Y axis data when the user lies down and stand up

slowly while Figure 13 (b) shows X axis data when the user sit down on the chair slowly .

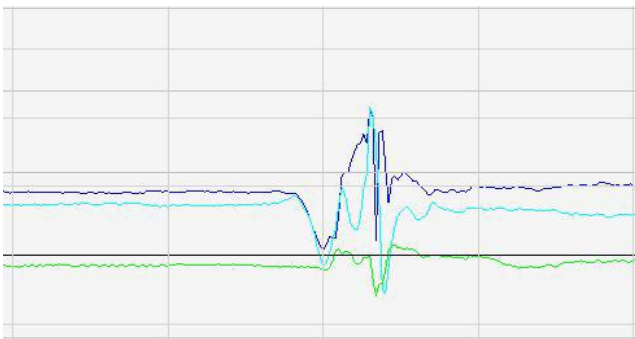


(a)Acceleration (X: Dark Blue, Y: Blue (Effective), Z: Green)



(b)Angular velocity (X: Black, Y: Green, Z: Red (Effective))

Fig. 11. Examples of acceleration sensor and angular velocity data when the user lie down and the stand up quickly.



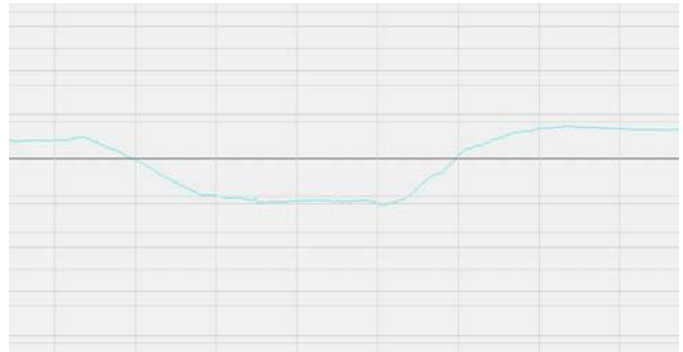
(a)Acceleration (X: Dark Blue, Y: Blue (Effective), Z: Green)



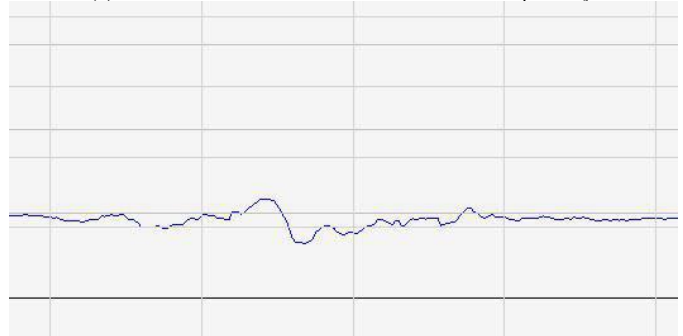
(b)Angular velocity (X: Black, Y: Green, Z: Red (Effective))

Fig. 12. Examples of acceleration sensor and angular velocity data when the user sit down on chair quickly.

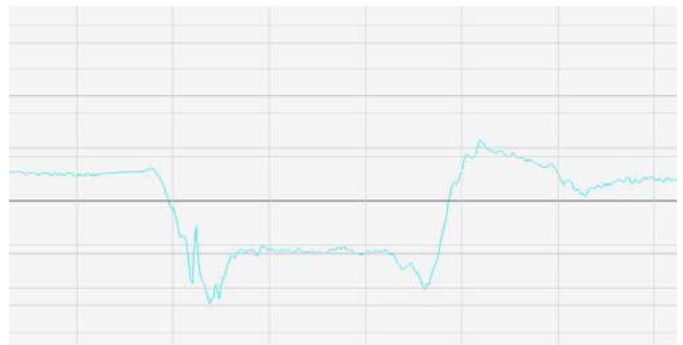
Furthermore, Figure 13 (c) shows Y axis data when the user lies down and the stand up quickly while Figure 13 (d) shows X axis data when the user sit on the chair quickly.



(a) Y axis data when the user lies down and stand up slowly



(b) X axis data when the user sit down on the chair slowly



(c) Y axis data when the user lies down and the stand up quickly

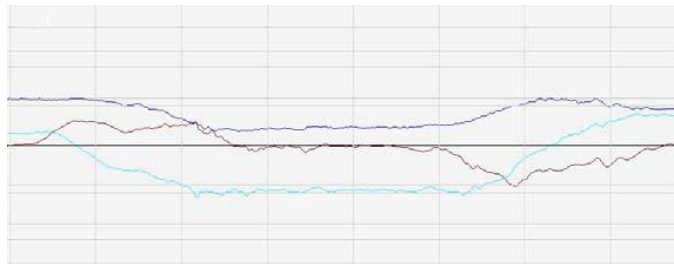


(d) X axis data when the user sit on the chair quickly

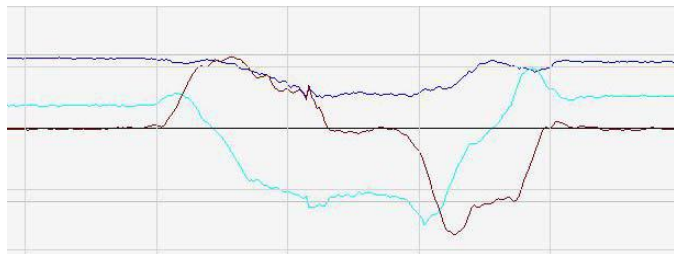
Fig. 13. Specific axis data for the action of lie down and then stand up as well as sit down on the chair, slowly and quickly

C. Validation of Acceleration and Angular Velocity Data

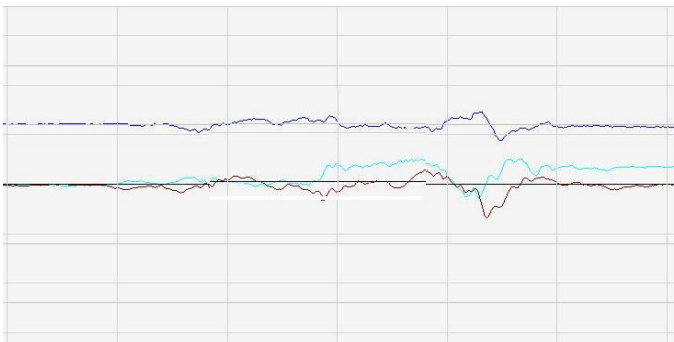
Three axes of acceleration sensor and angular velocity sensor data are validated for the actions “Lie down and then stand up slowly”, “Sit down on the chair slowly”, “Lie down and then stand up quickly”, “Sit down on the chair quickly”. The results are shown in Figure 14. Through these validations, it is found that the most effective signal for detection of lie down and then stand up is acceleration in Y axis while that for detecting of sit down action is angular velocity sensor data in Z axis as are shown in Table 1.



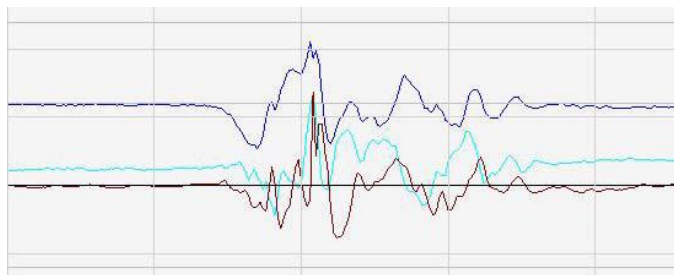
(a) “Lie down and then stand up slowly”



(b) “Lie down and then stand up quickly”



(c) “Sit down on the chair slowly”



(d) “Sit down on the chair quickly”

Fig. 14. Validation of three axes of acceleration sensor and angular velocity sensor data (X: Dark Blue, Y: Blue, Z: Green for acceleration sensor, and X: Black, Y: Green, Z: Red for angular velocity sensor)

TABLE I. SUMMARY OF VALIDATION RESULTS FOR DETECTION OF USERS’ ACTIONS OF “LIE DOWN AND THEN STAND UP” AND “SIT DOWN ON THE CHAIR”

	Action	Slow action		Quick action		
		Lie and up	down stand	Sit on chair	Lie and up	down stand
On	Accelerations X	0	2	2	3	
On	Accelerations Y	3	1	3	2	
Off	Accelerations Z	0	1	2	1	
Off	Angular Velocity X	2	0	2	1	
Off	Angular Velocity Y	1	0	2	1	
On	Angular Velocity Z	3	1	3	2	

IV. CONCLUSION

Method and system for human action detections with acceleration sensors for the proposed rescue system for disabled and elderly persons who need a help in evacuation from disaster areas is proposed. Not only vital signs, blood pressure, heart beat pulse rate, body temperature, bless and consciousness, but also, the location and attitude of the persons have to be monitored for the proposed rescue system. The attitude can be measured with acceleration sensors.

In particular, it is better to discriminate the attitudes, sitting, standing up, and lying down. Also, action speed has to be detected. Experimental results show that these attitude monitoring can be done with acceleration sensors.

Through these validations, it is found that the most effective signal for detection of lie down and then stand up is acceleration in Y axis while that for detecting of sit down action is angular velocity sensor data in Z axis. Namely, validation results for detection of users’ actions of “Lie down and then stand up” and “Sit down on the chair”

ACKNOWLEDGMENT

The author would like to thank all the patients who are contributed to the experiments conducted. The author also would like to thank Professor Dr. Takao Hotokebuchi, President of Saga University for his support this research works.

REFERENCES

[1] Kohei Arai, Tran Xuan Sang, Decision making and emergency communication system in rescue simulation for people with disabilities, International Journal of Advanced Research in Artificial Intelligence, 2, 3, 77-85, 2013.

- [2] K.Arai, T.X.Sang, N.T.Uyen, Task allocation model for rescue disable persons in disaster area with help of volunteers, International Journal of Advanced Computer Science and Applications, 3, 7, 96-101, 2012.
- [3] K.Arai, T.X.Sang, Emergency rescue simulation for disabled persons with help from volunteers, International Journal of Research and Review on Computer Science, 3, 2, 1543-1547, 2012.
- [4] K. Arai, and T. X. Sang, "Fuzzy Genetic Algorithm for Prioritization Determination with Technique for Order Preference by Similarity to Ideal Solution", International Journal of Computer Science and Network Security, vol.11, no.5, 229-235, May 2011.
- [5] Arai K., R. Mardiyanto, Evaluation of Students' Impact for Using the Proposed Eye Based HCI with Moving and Fixed Keyboard by Using EEG Signals, International Journal of Review and Research on Computer Science(IJRRCS), 2, 6, 1228-1234, 2011
- [6] K.Arai, Wearable healthy monitoring sensor network and its application to evacuation and rescue information server system for disabled and elderly person, International Journal of Research and Review on Computer Science, 3, 3, 1633-1639, 2012.
- [7] K.Arai, Wearable Physical and Psychological Health Monitoring System, Proceedings of the Science and Information Conference 2013 October 7-9, 2013 | London, UK

AUTHORS PROFILE

Kohei Arai, He received BS, MS and PhD degrees in 1972, 1974 and 1982, respectively. He was with The Institute for Industrial Science and Technology of the University of Tokyo from April 1974 to December 1978 also was with National Space Development Agency of Japan from January, 1979 to March, 1990. During from 1985 to 1987, he was with Canada Centre for Remote Sensing as a Post Doctoral Fellow of National Science and Engineering Research Council of Canada. He moved to Saga University as a Professor in Department of Information Science on April 1990. He was a councilor for the Aeronautics and Space related to the Technology Committee of the Ministry of Science and Technology during from 1998 to 2000. He was a councilor of Saga University for 2002 and 2003. He also was an executive councilor for the Remote Sensing Society of Japan for 2003 to 2005. He is an Adjunct Professor of University of Arizona, USA since 1998. He also is Vice Chairman of the Commission "A" of ICSU/COSPAR since 2008. He wrote 31 books and published 442 journal papers

A New Trust Evaluation for Trust-based RS

Sajjawat Charoenrien
Department of Mathematics
Chulalongkorn University
Bangkok, Thailand

Saranya Maneeroj
Department of Mathematics
Chulalongkorn University
Bangkok, Thailand

Abstract—Trust-based recommender systems provide the recommendations on the most suitable items for the individual users by using the trust values from their trusted friends. Usually, the trust values are obtained directly from the users, or by calculated using the similarity values between the pair of users. However, the current trust value evaluation can cause the following three problems. First, it is difficult to identify the co-rated items for calculating the similarity values between the users. Second, the current trust value evaluation still has symmetry property which makes the same trust value on both directions (trustor and trustee). Finally, the current trust value evaluation does not focus on how to adjust the trust values for the remote user. To eliminate all of these problems, our purposed method consists of three new factors. First, the similarity values between the users are calculated using a latent factor model instead of the co-rated items. Second, in order to identify the trustworthiness for every user in trust network, the degrees of reliability are calculated. Finally, we use the number of hops for adjusting the trust value for the remote users who are expected to be low trust as shown in the real-world application concept. This trust evaluation leads to better predicted rating and getting more predictable ratings. Consequently, from our experiment, the more efficiency trust-based recommender system is obtained, comparing with the classical method on both accuracy and coverage.

Keywords—trust-based recommender systems; trust values; similarity values

I. INTRODUCTION

Recommender systems (RS) act as the tools that help selecting the most relevant items to the target users. First, the users' preference ratings on items are collected. After that, the similarities between users are calculated by using the ratings on their co-rated items. These similarities are then applied to select the nearest neighbors for each user. Finally, recommender systems predict the ratings for a target user by using the ratings from his neighbors. However, usually most users tend to provide the small fraction of all possible ratings. This leads to a sparsity problem which the system cannot provide the accurate prediction and, for some items, unpredictable.

In order to solve this problem, Trust-Aware Recommender systems (TARS) [3] have been implemented. The system uses not only the users' ratings data, but also the trust information for prediction. These trust values are usually collect directly from users or calculated as the same way as similarity values. However, calculating trust values this way has cause many problems. First, the similarity value has symmetry property which makes the trust value on both directions of the pair of users to be the same.

Actually, the trust value between two persons might not be the same. For example, user A might trust user B but user B might not trust user A. Therefore, the trust between these two should not be the same. Second, the systems may not be able to effectively find the trust values due to the sparsity problem. For the last, it cannot use the transitive property of graph to calculate the trust value between the friends of friends for a user. TidalTrust [1][4] and MoleTrust [5] were proposed to solve this problem. Both of them use the propagation technique to propagate the trust values for the raters (who rated score on the target item). The propagated trust values are calculated every time when the friends of friends of the target users are visited. However, finding the propagation in a very large trust network is time consuming. Thus, another model has been proposed by Y. Guo. [9] This model tries to find the trust factor of the raters toward the ratings.

The trust factor is used to calculate the trust value as the important factor. The trust factor calculates from the number of friends and number of evaluated items belonging to that rater and the experience of rater on the past rated item, with the rater. That means the trust values are calculated from the relations between the raters and target users. However, this method does not concern the number of the hops, which might reduce the trust values of the remoteness users. While exploring the trust network, a target user has to visit the friends of his friends until he retrieves the wanted rating. Every time of the visiting, the number of hops is increased. If the number of hops is large, the two users are far from each other and they are less related. Therefore, the number of hops should be included in the model to suit the real world applications.

In this work, a new trust evaluation method is proposed. This method has three factors for calculating the trust value of each rater, e.g. similarity value between a pair of user, trustworthiness and number of hops. By using the latent feature model for calculating similarity value for each pair of users, the sparsity and symmetry problems can be solved. The second factor, trust worthiness is the extended idea from Y. GUO, which tries to find the degree of reliability of each rater in the trust.

Finally, the number of hops is used to adjust the trust values of the raters based on the distance from the target users in the trust network. These three factors are combined in this work to make a new trust value calculation. After that, the new trust value is used in rating prediction. It improves the quality of the prediction than the classical trust-based recommender systems on both accuracy and coverage as shown in the experiment in the fourth section of this paper.

II. RELATED WORKS

Recommender system involves three major steps. First, the system collects rating data representing the user's preference towards the different items. Second, it generates the user's pattern based on his past experience towards those items. Finally, RS makes the prediction for the new items based on the user's preference pattern. However, usually, the numbers of ratings are not large enough to give an effective prediction. This problem is called sparsity problem, which leads to inaccurate rating prediction or unpredictable for some items. After that, the study of Swearingen & Sinha [7] on the usability of three book RS and three movie RS has found that, by integrating trust information into the RS, the prediction is improved. Moreover, Ziegler & Golbeck [8] investigated the correlations between trust and similarity definition. They found that the trust values between each pair of user in the RS were calculated by using their similarity values on the co-rated items (the overlap items that have been rated from both users). However, it still leads to two problems. First, the trust value from similarity value is symmetry on the both side of the users, such as $A \rightarrow B$ equals to $B \rightarrow A$. In fact, two users who trust each other might not have the same trust value because it opposes to the fact which two persons not necessary to trust each other. One person can trust the other by one side. Another problem is that sometimes, the system cannot calculate the similarity values for some pairs of users because they do not have the co-rated items. To solve this, J. O' Donovan [6] proposed the work called Trust in Recommender Systems. In their work, the trust values can be found from the reliabilities of the raters which are indicated the amount of corrected ratings they have made. The trust value is the ratio between the number of correctly predicted ratings and the whole number of the predicted ratings as (1).

$$Trust^p = \frac{|CorrectSet(p)|}{|RecSet(p)|} \quad (1)$$

Where p is rater, $CorrectSet(p)$ is the set of correctly predicted items, and $RecSet(p)$ is the set of all predicted items. Although the trust values calculated by J. O' Donovan can solved the symmetry problem, it did not use information in trust network which contains the relationships among the users to make more accurate prediction. Trust network can be represented as a graph that consists of nodes (as the user) and edges (as the relationship between the users).

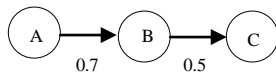


Fig. 1. The sample of Trust network

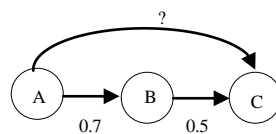


Fig. 2. Example of a figure caption. (figure caption)

The weight on each edge shows the trust value from source user to destination users in as Fig. 1. Sometimes, when the

friends of the target user cannot provide the prediction for him, the system might use the opinions of the friends of that user's friends instead. The opinions from the target user's friends of friends can be transitively obtained from their directed friends. However, the target user might not have directed trust to these friends of friends. The example of this is shown in Fig. 2, if user A is a friend with user B and user B is a friend with user C, then how much user A trusts user C? Messa [3] proposed TAR architecture to provide trust value calculation for friends of friends.

From the TAR architecture, the predicted ratings are generated by rating predictor module using output from both User Similarity and Estimated Trust modules. The User Similarity is the process which calculates the similarity value between a pair of users.

While the Estimated Trust finds the trust values on friends of friends, which can solve the previous problem. TidalTrust and MoleTrust are the traditional methods that used to find the trust values from friends of friends for the target users. Both of them use transitive property of the graph to propagate the trust value from friends to friends. They use depth first search to propagate trust value from the target user to the rater. In the propagation process, the trust values are calculated by using the trust values of the previous friends as shown in (2).

$$trust(u) = \frac{\sum_{i \in predecessors} (trust(i) * trust_edge(i,u))}{\sum_{i \in predecessors} (trust(i))} \quad (2)$$

Where u is target user, i is the user whom the target user trusted, $trust(i)$ is the trust value of user i , $trust_edge(i,u)$ is the trust between user i and user u and predecessors are the previous friends of the user.

The different between their methods is that, in MoleTrust the cycle from the trust network is removed to reduce the distance of the trust propagation, in order to improve the performance. In contrast, TidalTrust propagates to every node in the trust network that is connected.

On the very large trust network, the propagation technique is not good because the exploration on every node on the graph takes a large amount of time, depending on the complexity of that the trust network.

Y. Guo [9] proposed trust value calculation without propagation. This method finds the trust factor which is the main factor of the trust factor. It calculates from the combination of the number of friends and number of evaluated items. If a user has the number of friends more than the others, he is more reliable.

$$T_i = \frac{2(1-1/\ln f_i) * (1-1/\ln (q_i+3))}{2-1/\ln f_i - 1/\ln (q_i+3)} \quad (3)$$

Where i is the user whom the target user trusted, T_i is the trust factor of user i , f_i is the number of user i 's evaluation on each item and q_i is the number of recommendations user i has made for the others.

In the real world application, when considering the transitive property, a friend who is far away from target user should have lesser trust value than close friend. While exploring the trust network, the target user will visit the friend of friend until retrieve the rating. Every time of the visiting, the number of hops is increased every time. If the number of hops is large, the two users are far from each other and they are less related. Therefore, the number of hops should be included into the model to suit the real world applications.

In this work, a new trust value calculation that solves the problems mentioned above is proposed. First, this method uses the latent features of users for finding similarity instead of using co-rated items. Second, the symmetry problem is eliminated by exploiting the degree of reliability of each user. And, finally, this method considers the distance among friends by using the number of hops.

Therefore, we can summarize pros and cons of related trust methods comparing with our proposed method on three attributes: symmetry or asymmetry of initial trust value, transitive opinion from the directed friends to the friend of the directed friends and concerning the number of hops of remoteness users as shown in the following Table I.

TABLE I. PROS AND CONS COMPARISON OF EACH METHOD

Method	Initial Trust Value	Transitive Opinion	Concern the number of hops
J. O'Donovan's Method	Asymmetry	No	No
TidalTrust	Symmetry	Yes	No
MoleTrust	Symmetry	Yes	No
Y Guo's Method	Asymmetry	Yes	No
Proposed Method	Asymmetry	Yes	Yes

III. PROPOSE METHOD

The new trust value calculation proposed in this work consists of three main steps. First, the similarity values for all pairs of users are calculated. Then, then reliability concept is combined into trust value calculation in order to get rid of symmetry problem. Finally, the number of hops is included in the calculation to reduce the trust of remote friends.

To guarantee that the trust values can be calculated for every pair of users, the singular value decomposition (SVD) [2] is applied in this work instead of relying on the co-rated items. First, the latent features of the user are extracted by the following.

$$R=USV^t \tag{4}$$

Where R is the user-rating matrix, U is the user matrix, S is the reduced matrix and V^t is the transpose matrix of the item matrix. From matrix U , each row is represented as the user feature vector. Each feature vector of user contains the latent features representing the user's characteristic. The cosine similarity is then applied on these feature vectors to find the similarity for every pair of users by the following.

$$sim_{A,B} = \frac{\sum_{i=1}^n A_i \times B_i}{\sqrt{\sum_{i=1}^n (A_i)^2} \times \sqrt{\sum_{i=1}^n (B_i)^2}} \tag{5}$$

Where A_i is the i^{th} latent feature of user A (target user), B_i is the i^{th} latent feature of user B and n is the number of latent features.

To prevent the symmetry problem of the trust values on both directions of the pair of users, the system uses not only the similarity value between a pair of users ($sim(A,B)$) but also concerns the reliability of rater(B) in the network. That is, reliability concept by Y. Guo [9] is applied in this work by using the number of in-degree which is represented the number of friends who trust rater (B).

$$trustworthiness_B = \frac{\ln(n_{in,B}+e)}{\ln(\max(\{n_{in,C} | C \in \{user\ in\ Trust\ Network\}\})+e)} \tag{6}$$

Where e is a natural number, $n_{in,B}$ is the number of the in-degree edges of the user B and

$\max(\{n_{in,C} | C \in \{user\ in\ Trust\ Network\}\})$ is the maximum number of the in-degree edge of the user in the trust network. Also, the confidence of B towards A is calculated by merging $sim(A,B)$ and $trustworthiness_B$ using harmonic mean as shown in (7).

$$confidence_B = \frac{2 \times trustworthiness_B \times sim_{A,B}}{trustworthiness_B + sim_{A,B}} \tag{7}$$

Moreover, to make the method suitable for the real world situation, the confidence level of user who is far from target user should be adjusted by using number of hops as shown in (8).

$$trust_{A \rightarrow B} = confidence_B \times \frac{1}{d_B} \tag{8}$$

Where d is the number of hops from user A to B

After gathering the trust values of all raters from previous steps, the predicted rating can be calculated by using trust values of target user to all the raters who have rated the target item as weights.

$$predict\ rating_t = \frac{\sum_{i \in Rater} rating(i) * trust_{t \rightarrow i}}{\sum_{i \in Rater} trust_{t \rightarrow i}} \tag{9}$$

Where t is target user, $rating(i)$ is an actual rating of rater(i) on the target item and $trust_{t \rightarrow i}$ is trust value of target user(t) toward rater (i).

IV. EXPERIMENT

In order to evaluate the performance of our proposed method, we compares our work with 2 classical trusted based RS methods: TidalTrust and MoleTrust

A. Dataset

The Epinions dataset is used in this work. This dataset consists of user-rating data containing 664,824 reviews from 49,290 users on 139,738 items, and also the trust network data containing 487,181 issued trust statements.

B. Evaluation Metric

To evaluate the model, we use two measurements: RMSE and coverage.

1) *RMSE (Root Mean Square Error)*: It represents the accuracy of the prediction. The lower the value means the method is more accurate than the method with higher RMSE. This value can be calculated by the following

$$RMSE = \sqrt{\frac{\sum_{(u,i) \in R_{u,i}} (r_{u,i} - \hat{r}_{u,i})^2}{|\{(u,i) \in R_{u,i}\}|}} \quad (10)$$

Where $r_{u,i}$ is an actual rating of user(u) on target item(i), $\hat{r}_{u,i}$ is a predicted rating of user(u) on target item(i) and $\{(u,i) \in R_{u,i}\}$ is the set of user who rated on item(i).

2) *Prediction Coverage*: This value indicates the fraction of the ratings that can be predicted from all of the rating available.

$$coverage = \frac{|\{(u,i) \in \hat{R}_{u,i}\}|}{|\{(u,i) \in R_{u,i}\}|} \quad (11)$$

Where $|\{(u,i) \in \hat{R}_{u,i}\}|$ is the number of ratings that can be predictable and $|\{(u,i) \in R_{u,i}\}|$ is number of all ratings. The higher coverage means the system provides more predictable rating.

C. Experimental Results

In the experiment, we compare TidalTrust and MoleTrust with the proposed method by using the dataset mentioned above. To predict the rating for the target item, we use the leave one out technique (hide only the actual rating on the target item of the target user in the dataset, and uses the rest for prediction) . Instead of using all ratings in the dataset, we randomly select one target item per target user and only the first 5,000 users are use as the test set. To avoid the bias, we use the same random data on TidalTrust, MoleTrust and proposed methods. The results of the experiment are shown as Fig. 3.

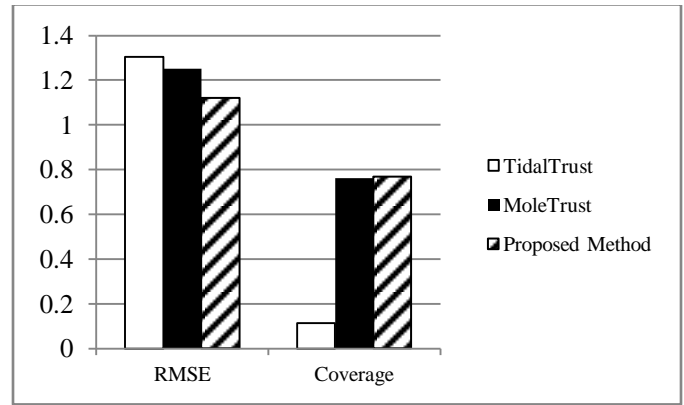


Fig. 3. Comparison of RMSE and Coverage between the proposed method and others

From the results shown above, RMSE of our proposed method is lower than TidalTrust and MoleTrust. It can be concluded that proposed method provides better accuracy. In the aspect of prediction coverage, our proposed method provides higher coverage values than both TidalTrust and MoleTrust. It can be concluded that proposed method provides more predictable items.

V. DISCUSSION

A. Accuracy

The reasons that proposed method has better accuracy than both TidalTrust and MoleTrust are following by this:

Both current trust-based RSs calculate the trust values by using the co-rated items which is hard to be identified because of the sparsity problem. The small number of co-rated items leads to the low quality neighbor which causes the low accuracy in prediction. On the other hand, the purpose method uses latent features of user instead of co-rated items. About 5,000 user features are extracted from user-rating matrix, so, it can represent user characteristic more correctly.

The current trust-based RSs do not consider the degree of reliability for each user in trust network. In the proposed method, the ratio between the numbers of friends on each specified user to the maximum number of friends from all users in the trust network is used to determine the reliability.

The current trust based RSs do not concern the remoteness of the friends of the target users. This type of friends should have the lesser trust value comparing to the close friends. The proposed method deals with this by adjusting the trust values using the number of hops.

B. Coverage

The reason that proposed method can provide more prediction coverage than the other two methods is that the proposed uses the latent features of user for calculating the similarity values without using co-rated items. Therefore, it can calculate similarity values for all pairs of users. However, it cannot provide 100% coverage because the target item obtains the rating only from the target user, not from other users. Therefore, there is no rating from rater for the prediction step. However, this case occurs not only in our proposed method, but also in current trust based RS such as MoleTrust and TidalTrust as well.

VI. CONCLUSION

A new trust evaluation calculation is proposed in this work. It consists of three new factors. First, the similarity values between the users are calculated using a latent factor model instead of the co-rated items. Second, in order to identify the trustworthiness for every user in trust network, the degrees of reliability are calculated. Finally, we use the number of hops for adjusting the trust value for the remote users who are expected to be low trust as shown in the real-world application concept. From the experiment results, our proposed method is more efficiency than the classical trust based RS (MoleTrust and TidalTrust) on both accuracy and coverage.

VII. FUTURE WORK

Usually, Recommender System calculates a prediction by using opinion of the directed friends who rated the target item. However, in the trust-based recommender system, the rater

who rated the target item may not be the directed friend of the target user. Therefore, there should be the way to translate the rater's opinion into directed friend's opinion. This is an objective of our near-future work.

REFERENCES

- [1] J. Golbeck, "Computing and Applying Trust in Web-based Social Networks", PhD thesis, University of Maryland College Park, 2005.
- [2] B. M. Sarwar, G. Karypis, J. A. Konstan, and J. Riedl, "Application of Dimensionality Reduction in Recommender Systems: a Case Study", ACM WebKDD 2000 Workshop, 2000.
- [3] P. Massa and P. Avesani, "Trust-aware recommender systems", In ACM Recommender Systems Conference (RecSys), USA, 2007.
- [4] J. Golbeck, "Personalizing Applications through Integration of Inferred Trust Values in Semantic Web-Based Social Networks", Proceedings of Semantic Network Analysis Workshop, Galway, Ireland, 2005.
- [5] P. Massa and P. Avesani, "Trust metrics on controversial users: balancing between tyranny of the majority and echo chambers", International Journal on Semantic Web and Information Systems (IJSWIS), 3(1), 2007.
- [6] J. O'Donovan, B. Smyth, "Trust in recommender systems", Proceedings of the 10th international conference on Intelligent user interfaces, San Diego, California, USA, January 10-13, 2005.
- [7] R. Sinha and K. Swearingen, "Comparing recommendations made by online systems and friends.", In Proceedings of the DELOS-NSF Workshop on Personalization and Recommender Systems in Digital Libraries. Dublin, Ireland, 2001
- [8] C. Ziegler and J. Golbeck, "Investigating interactions of trust and interest similarity", Decision Support Systems, v.43 n.2, p.460-475, March, 2007
- [9] Y. Guo, X. Cheng, D. Dong and C. L. Rishuang Wang, "An Improved Collaborative Filtering Algorithm Based on Trust in E-Commerce Recommendation Systems," research supported by a grant from the Chinese National Science Foundation Key Project, IEEE 2010, pp 1-4

Human Lips-Contour Recognition and Tracing

Md. Hasan Tareque¹
Department of Computer Science and Engineering
IBAIS University
Dhaka, Bangladesh

Ahmed Shoeb Al Hasan²
Department of Computer Science and Engineering
Bangladesh University of Business & Technology
Dhaka, Bangladesh

Abstract—Human-lip detection is an important criterion for many automated modern system in present day. Like computerized speech reading, face recognition etc. system can work more precisely if human-lip can detect accurately. There are many processes for detecting human-lip. In this paper an approach is developed so that the region of a human-lip can be detected, we called it lip contour. For this a region-based Active Contour Model (ACM) is introduced with watershed segmentation. In this model we used global energy terms instead of local energy terms because, global energy gives better convergence rate for malicious environment. At the time of ACM initialization by using H^∞ based on Lyapunov stability theory, the system gives more accurate and stable result.

Keywords—Watershed Model; Active contour models (ACM); H^∞ filter Contour model; Lyapunov stability theory

I. INTRODUCTION

Automatic lips contour detection and tracking is always a crucial prerequisite process for various kinds of applications. It has been extensively utilized in the state-of-the art of audio-visual speech recognition. [1]

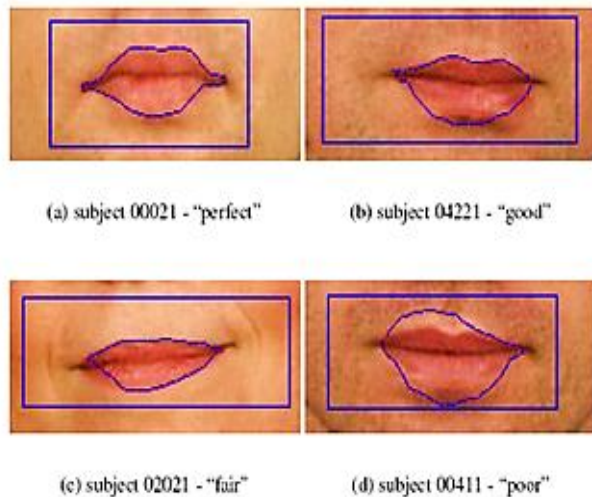


Fig. 1. Different shape of lips contour

There are several uses of lips contour detection like Audio-visual speech authentication [3], intelligent human-computer interaction Human expression recognition [2] etc. Automatic Speech Recognition (ASR) [4] systems use only Acoustic Information, for this system show poor performance in noisy environment. Bimodal Audio-Visual Systems signal often contains information that is complementary to audio

information. Again visual information is not affected by acoustic noise. For this overall performance of the combined system is better [5]-[7].

Moreover, when working with the video sequence, an automatic and precise initial contour placement for the ACM is a crucial issue. Therefore, lips tracking algorithm is adopted into the system to keep track on the lips feature points at the subsequent incoming video frame as the initialization of the ACM lips contour process. In this paper, the conventional H^∞ filtering is modified according to the LST as to assure that the system is always at the stable condition. Additionally, by properly selecting the Lyapunov function $V(k)$, during the system design, as the time approaches to infinity, the tracking error of the proposed H^∞ filtering would asymptotically converge to zero. This is because the Lyapunov function [11] selected for the proposed system,

$$V(k) = e^{2k}$$

This consists of a unique global minimum point at the system origin. From the simulation results demonstrated, the modified H^∞ shows an appreciable improvement in terms of reducing the lips feature points tracking error compared to the conventional H^∞ approach

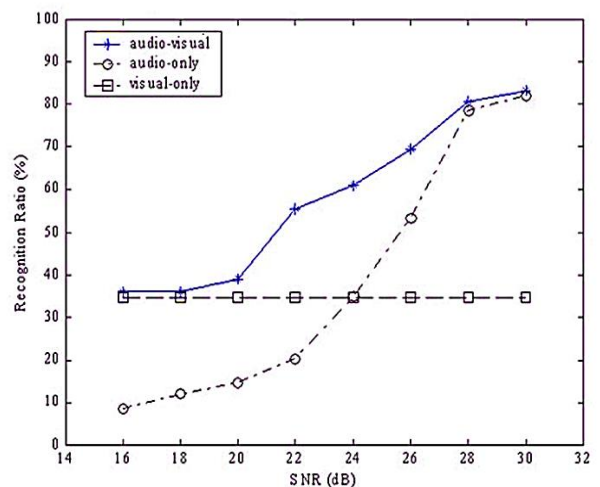


Fig. 2. SNR ratio of different system

In this paper some of the terminology will be discussed like

A. Contour:

A contour line of a function of two variables is a curve along which the function has a constant value. Minimal Cost

Path: The optimal path from every pixel in the image to the seed point is determined by using Dijkstra's algorithm.[9]

B. Active contour model:

Active contour model, also called snakes, is a framework for delineating an object outline from a possibly noisy 2D image. This framework attempts to minimize an energy associated to the current contour as a sum of an internal and external energy.[12]

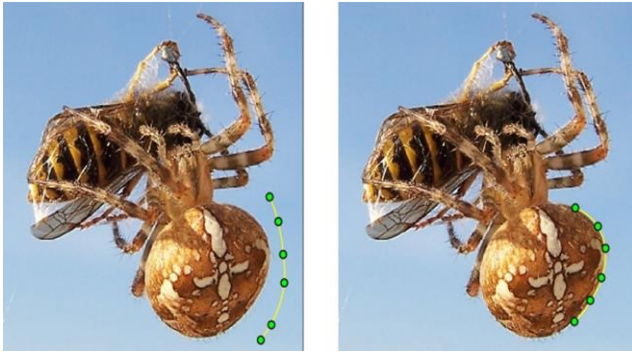


Fig. 3. Active contour model.

C. H^∞ filter:

After a decade or so of reappraising the nature and role of Kalman filters, engineers realized they needed a new filter that could handle system modelling errors and noise uncertainty. State estimators that can tolerate such uncertainty are called robust. The H^∞ filter [8] was designed for robustness.

D. Lyapunov stability theory:

The most important type is that concerning the stability of solutions near to a point of equilibrium. If all solutions of the dynamical system that start out near an equilibrium point x_e stay near x_e forever, then x_e is Lyapunov stable. [12]

II. LIPS CONTOUR DETECTION & TRACKING

In this paper, instead of utilizing the global region model, the active contour energy with the local information interpretation corresponds to the watershed segmentation is proposed. This gives better performance on the contour detection compared to the global energies calculation, particularly when the inner and outer region shares the similar image statistic. Performs is better compared to the localized ACM algorithm.

Compared to the aforementioned approach, the integration of ACM and watershed segmentation presented in this paper not only provides high deformability but is also better in handling the unclear boundary between lips and facial skin.

For video sequence, an automatic and precise initial contour placement for the ACM is a crucial issue. Keep track on the lips feature points at the subsequent incoming video frame as the initialization of the ACM [6] lips contour process.

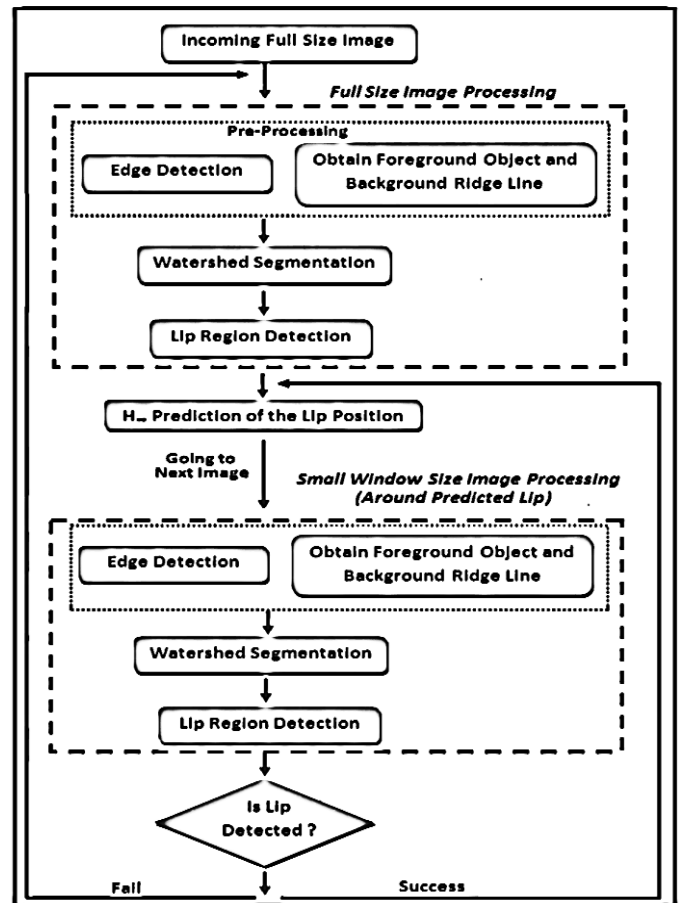


Fig. 4. Follow chart of the system.

H^∞ filtering is modified according to the LST as to assure that the system is always at the stable condition. By properly selecting the Lyapunov function, $V(k)$, as the time approaches to infinity, the tracking error of the proposed H^∞ filtering would asymptotically converge to zero. This is because the Lyapunov function selected for the proposed system,

$$V(k) = e^{2k}$$

The overall process of the proposed lips contour detection and tracking is demonstrated in Figure 5. The input image is first sent to the lips localization to roughly obtain the lips location. Subsequently, the watershed region segmentation and at the same time, also the ACM initialization are working on the lips image. The output from the watershed and the ACM initial contour position are then passed to the localized region-based ACM for further lips contour detection. Once the lips contour is successfully detected, the feature points from the detected contour are extracted and used by the modified H^∞ lips tracking process to keep track on the initial contour position of the succeeding image. The lips localization is triggered only once per 20 rounds of the overall lips detection process.

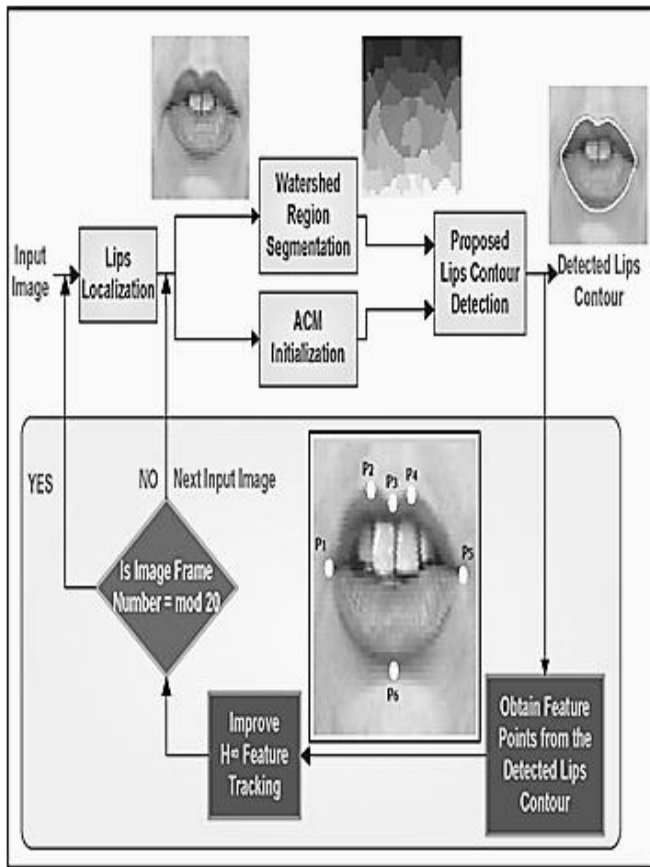


Fig. 5. Overview of the overall system.

III. LIPS CONTOUR DETECTION WITH LOCALIZED WATERSHED-BASED ACTIVE CONTOUR MODEL

Each pixel is situated at a certain altitude levels. Where the white pixel (intensity value = 255) is referred to as the maximum altitude while black pixel (intensity value = 0) is known as the minimum altitude.

The watershed algorithm which applied in this paper is based on the rain-flow simulation. By employing the falling rain concept, the raindrop falls from the highest altitude to the lowest (known as catchment basin) according to the steepest descent order.

The coloured watershed regions are known as the local mask region M , for a particular point within the narrow band. The local exterior region is illustrated in orange colour while the red region is known as the local interior region.

The local mask region can be mathematically construed:

$$M(x, y) = \begin{cases} 1, & \text{if } \|x - y\| < w \\ 0, & \text{if otherwise} \end{cases}$$

Where w is known as the segmented watershed region situated at the local point to be analyzed, and including the segmented watershed regions located at the points of north, east, south and west from the local point. The energy function,

F of an image, $i(x, y)$ could be mathematically written as follows:

$$F(C, u, v) = \alpha \cdot \text{Length}(C) + \lambda \int_{in} |i(x, y) - u|^2 dx dy + \lambda \int_{out} |i(x, y) - v|^2 dx dy$$

Where $\alpha \geq 0$, $\lambda > 0$, u and v are the average intensities levels inside and outside of the curve C , respectively.

By applying the level set approach onto the variation of the ACM, the unknown C is substituted with the unknown value ϕ , $\phi(x, y)$ is taken as the signed distance function, where $\phi(x, y) > 0$ inside the curve, $\phi(x, y) < 0$ outside the curve, and $\phi(x, y) = 0$ on the curve.

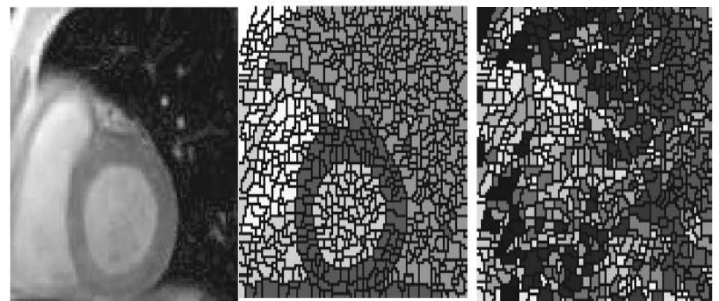


Fig. 6. a) Original image (b) expected watershed segmentation (c) over-segmentation.

So by applying Sobel filtering & watershed segmentation the system can gain expected segmentation.

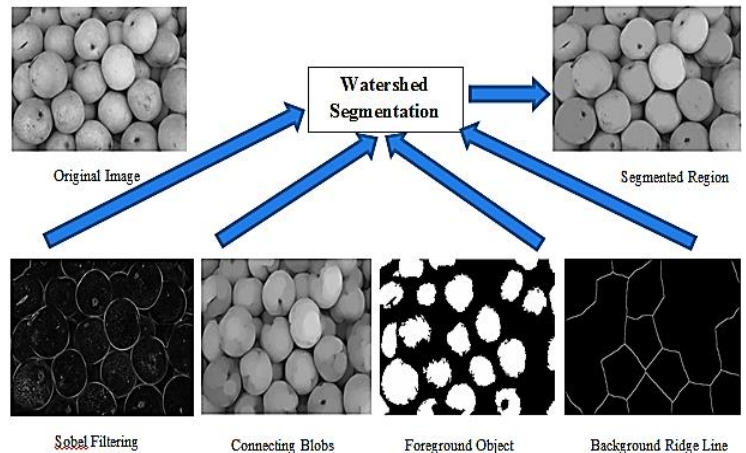


Fig. 7. The outcomes of the pre-processing procedures.

IV. MODIFIED H^∞ BASED ON LYAPUNOV STABILITY THEORY FOR LIPS TRACKING SYSTEM

An active shape model sample grey level perpendicular to the lip contour and centered at the model points.

After obtaining the lips contour from the proposed localized ACM system as discussed in the previous section, six feature

points from the detected lips region is tracked using the modified H^∞ filtering. [9]

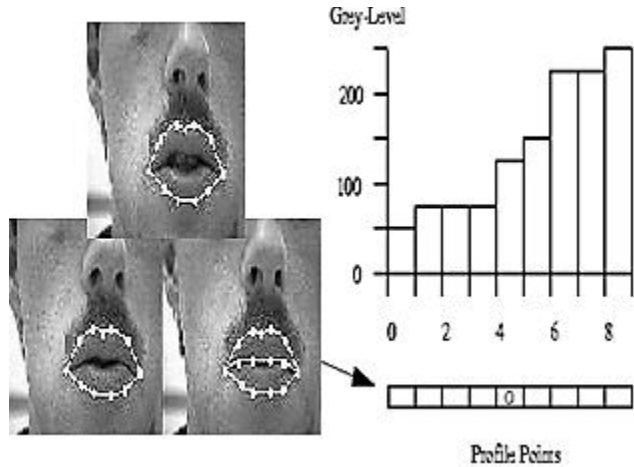


Fig. 8. Profile points & grey-level.

After obtaining the lips contour from the proposed localized ACM system as discussed in the previous section, six feature points from the detected lips region are tracked using the modified H^∞ filtering which is elaborated in this section. The feature points include the right and left lip corners, the lower central point, and three points of the Cupidon's bow as depicted in Fig. 1. The six feature points ($P_1 - P_6$) have to be first extracted from the detected contour. P_1 and P_5 are, respectively, obtained from the right and left most of the contour. Whereas P_6 situated at the bottom of the lips contour while P_3 at the upper contour that has the similar vertical coordination as P_6 . P_2 , which is the left Cupidon's bow is obtained by calculating the maximum altitude between P_1 and P_3 , while P_4 (the right Cupidon's bow) is the maximum altitude between P_5 and P_3 .

H^∞ filtering is mathematically represented according to the state-space concept. State equation:

$$X_k = AX_{k-1} + w_k$$

Where $X_k = [x_{k-p+1}^T x_{k-p+2}^T \dots x_k^T]^T$, A is known as the $P \times P$ dimensional state transition matrix, which bring forward the state value, X_k from time k to $k + 1$, w_k is the P -dimensional model error that analogous covariance matrix is known as $Q_k = E [w_k w_k^T]$.

Observation equation: $y_k = CX_{k-1} + v_k$

Where y_k is known as the N -dimensional sequential observation vector, C is the $N \times P$ dimensional observation function, v_k is the observation error that analogous covariance matrix is known as $R_k = E [v_k v_k^T]$.

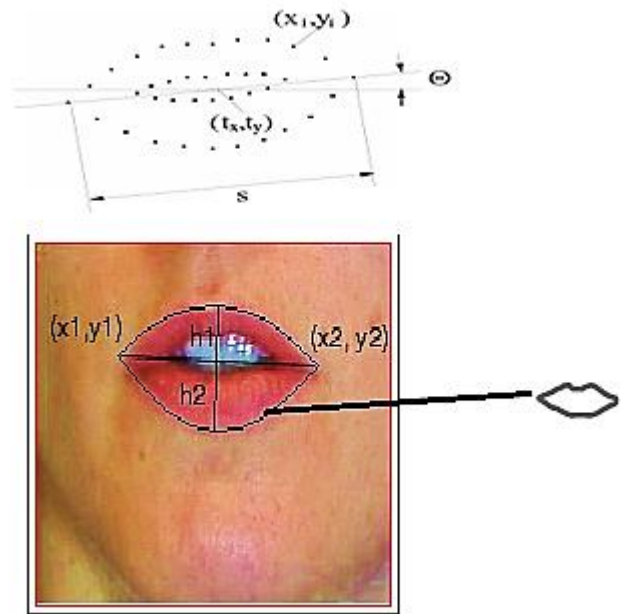


Fig. 9. Lip feature extraction and tracking.

In this paper a new gain for the H^∞ filtering parameter updating rules is proposed.

The modified H^∞ is interpreted as follows.

Theorem: With the given linear parameter vector, H_k and desired output, d_k , the state vector, x_k is updated as follows:

$$x_k = x_{k-1} + g_k \alpha_k$$

The modified H^∞ adaptation gain that fulfills the condition of $\Delta v < 0$ is proposed as follows:

$$g_k = \left[I - \frac{F_k P_{k-1} L_k F_k^T e_{k-1} - P_k}{\alpha_k} e_{k-1} \right] \frac{H_k}{\|H_k\|^2}$$

where

$$L_k = I - \gamma Q P_k + H_k^T V^{-1} H_k P_k$$

$$P_k = F P_k L_k F^T + W.$$

Where γ is known as the user-defined performance bound, Q , W and V are the respective weighting matrices for the estimation error, process noise, and measurement noise. The priori estimation error, α_k , is denoted as follows:

$$\alpha_k = d_k - x_{k-1}^T H_k.$$

When the time, k , approaches infinity, the tracking error, e_k , would be asymptotically converged to the value of zero.

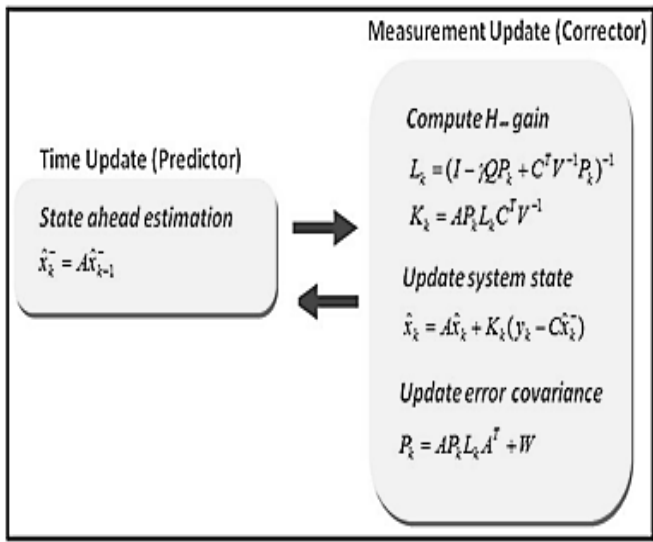


Fig. 10. The process flow of the H^∞ filter algorithm

V. FUTURE WORK

This method can be applied in 3-D system by some modification. Face recognition, emotion detection, speech recognition from a video etc. area can achieve a high percentage of accuracy by applying lips detection method.

VI. CONCLUSION

It is well known that visual information from lip shapes and movements helps improve the accuracy and robustness of a speech recognition system. Hence, the development of an accurate and robust algorithm for extracting lip features relevant to speech information becomes vital. Watershed-based active contour model and modified H^∞ filtering is illustrated in this paper. Compared to the global region-based ACM, the performance of the proposed localized ACM is successfully improved. The modified H^∞ tracking approach validates improved lips feature points tracking compared to the conventional H^∞ algorithm [11].

By applying Shape Constraint factor this method could be more robust. Given an image, the region of the lip may be located by using Shape Models. The overall system would be implemented into the audio-visual speech recognition for further research in the future. This system can be used to identify face or face recognition system.

But the system has High time complexity. Tracking through large number of frames point P1-P6 sometimes difficult to identify in robust situation. Sometime the skin & lip color are too similar that hard to distinguish. As a result contour detection might be tuff. For different expression like smiley, sad etc. finding accurate contour of the lip is a challenge.

VII. ACKNOWLEDGMENT

A special thanks to Prof. Dr. Mohammad Mahfuzul Islam for giving us a chance to work with this topic. Also a superior thanks goes to Siew Wen Chin, Kah Phooi Seng, Li-Minn Ang, King Hann Lim, there works really was very helpful.

REFERENCES

- [1] B. J. Borgstrom and A. Alwan, "A low-complexity parabolic lip contour model with speaker normalization for high-level feature extraction in noise-robust audiovisual speech recognition," *IEEE Trans. Syst. Man Cybern. Part A: Syst. Hum.*, vol. 38, no. 6, pp. 1273–1280, Nov. 2008.
- [2] Y. Zhang, Q.-J. Liu, Y.-H. Li, and Z. Li, "Intelligent wheelchair multi-modal human-machine interfaces in lip contour extraction based on PMM," in *Proc. IEEE Int. Conf. ROBIO*, Dec. 2009, pp. 2108–2113.
- [3] M.-I. Faraj and J. Bigun, "Audio-visual person authentication using lip-motion from orientation maps," *Pattern Recognit. Lett.*, vol. 28, no. 11, pp. 1368–1382, Aug. 2007.
- [4] J. A. Dargham, A. Chekima, and S. Omatu, "Lip detection by the use of neural networks," *Artif. Life Robot.*, vol. 12, nos. 1–2, pp. 301–306, 2008.
- [5] K. S. Jang, "Lip contour extraction based on active shape model and snakes," *Int. J. Comp. Sci. Network Security*, vol. 7, no. 10, pp. 148–153, Oct. 2007.
- [6] T. F. Chan and L. A. Vese, "Active contours without edges," *IEEE Trans. Image Process.*, vol. 10, no. 2, pp. 266–277, Feb. 2001.
- [7] S. Lankton and A. Tannenbaum, "Localizing region-based active contours," *IEEE Trans. Image Process.*, vol. 17, no. 11, pp. 2029–2039, Nov. 2008.
- [8] N. Eveno, A. Caplier, and P.-Y. Coulon, "Accurate and quasi-automatic lip tracking," *IEEE Trans. Circuits Syst. Video Technol.*, vol. 14, no. 5, pp. 706–715, May 2004.
- [9] C. S. Wen et al., "Lips detection for audio-visual speech recognition system," in *Proc. Int. Symp. ISPADS*, 2009, pp. 1–4.
- [10] W.-Y. Chang, C.-S. Chen, and Y.-D. Jian, "Visual tracking in highdimensional state space by appearance-guided particle filtering," *IEEE Trans. Image Process.*, vol. 17, no. 7, pp. 1154–1167, Jul. 2008.
- [11] Siew Wen Chin, Kah Phooi Seng, and Li-Minn Ang, "Lips Contour Detection and Tracking Using Watershed Region-Based Active Contour Model and Modified H^∞ ," *IEEE Transactions On Circuits And Systems For Video Technology*, Vol. 22, No. 6, June 2012.
- [12] N. Widynski, S. Dubuisson, and I. Bloch, "Integration of fuzzy spatial information in tracking based on particle filtering," *IEEE Trans. Syst. Man Cybern. Part B: Cybern.*, vol. 41, no. 3, pp. 635–649, Jun. 2011.

New concepts of fuzzy planar graphs

Sovan Samanta

Anita Pal

Madhumangal Pal

Department of Applied
Mathematics with Oceanology
and Computer Programming,
Vidyasagar University,
Midnapore - 721 102, India.
email: ssamantavu@gmail.com

Department of Mathematics,
National Institute of
Technology Durgapur,
Durgapur-713209, India.
e-mail: anita.buie@gmail.com

Department of Applied
Mathematics with Oceanology
and Computer Programming,
Vidyasagar University,
Midnapore - 721 102, India.
email: mmpalvu@gmail.com

Abstract—Fuzzy planar graph is an important subclass of fuzzy graph. Fuzzy planar graphs and its several properties are presented. A very close association of fuzzy planar graph is fuzzy dual graph. This is also defined and several properties of it are studied. Isomorphism on fuzzy graphs are well defined in literature. Isomorphic relation between fuzzy planar graph and its dual graph are established.

Keywords: Fuzzy graphs, fuzzy planar graphs, fuzzy dual graphs, isomorphism.

I. INTRODUCTION

Graph theory has vast applications in data mining, image segmentation, clustering, image capturing, networking, communication, planning, scheduling. For example, a data structure can be designed in the form of a tree which utilizes vertices and edges. Similarly, modeling of network topologies can be done using the concept of graph. In the same way, the most important concept of graph colouring is utilized in resource allocation, scheduling, etc. Also, paths, walks and circuits are used to solve many problems, viz. travelling salesman, database design, resource networking. This leads to the development of new algorithms and new theories that can be used in various applications.

There are many practical applications with a graph structure in which crossing between edges is a nuisance such as design problems for circuits, subways, utility lines, etc. Crossing of two connections normally means that the communication lines must be run at different heights. This is not a big issue for electrical wires, but it creates extra expenses for some types of lines, e.g. burying one subway tunnel under another. Circuits, in particular, are easier to manufacture if their connections can be constructed in fewer layers. These applications are designed by the concept of planar graphs. Circuits where crossing of lines is necessary, can not be represented by planar graphs. Numerous computational challenges including image segmentation or shape matching can be solved by means of cuts of planar graph.

After development of fuzzy graph theory by Rosenfeld [23], the fuzzy graph theory is increased with a large number of branches. McAllister [17] characterised the fuzzy intersection graphs. In this paper, fuzzy intersection graphs have been defined from the concept of intersection of fuzzy sets.

Samanta and Pal [25] introduced fuzzy tolerance graphs as the generalisation of fuzzy intersection graphs. They also defined fuzzy threshold graphs [26]. Fuzzy competition graphs [24] are another kind of fuzzy graphs which are the intersection of the fuzzy neighbourhoods of vertices of a fuzzy graph. Many works have been done on fuzzy sets as well as on fuzzy graphs [2], [3], [4], [5], [7], [8], [10], [11], [12], [13], [14], [15], [19]. Abdul-jabbar et al. [1] introduced the concept of fuzzy planar graph. In this paper, the crisp planar graph is considered and the membership values are assigned on vertices and edges. They also defined fuzzy dual graph as a straight forward way as crisp dual graph. Again, Nirmala and Dhanabal [22] defined special fuzzy planar graphs. The work presented in this paper is similar to the work presented in [1]. In these papers, the crossing of edges in fuzzy planar graph is not allowed. But, in our work, we define fuzzy planar graph in such a way that the crossing of edges is allowed. Also, we define the fuzzy planarity value which measures the amount of planarity of a fuzzy planar graph. These two concepts are new and no work has been done with these ideas. It is also shown that an image can be represented by a fuzzy planar graph and contraction of such image can be made with the help of fuzzy planar graph. The fuzzy multigraphs, fuzzy planar graphs and fuzzy dual graphs are illustrated by examples. Also, lot of results are presented for these graphs. These results have certain applications in subway tunnels, routes, oil/gas pipelines representation, etc.

II. PRELIMINARIES

A finite graph is a graph $G = (V, E)$ such that V and E are finite sets. An infinite graph is one with an infinite set of vertices or edges or both. Most commonly in graph theory, it is implied that the graphs discussed are finite. A *multigraph* [6] is a graph that may contain multiple edges between any two vertices, but it does not contain any self loops. A graph can be drawn in many different ways. A graph may or may not be drawn on a plane without crossing of edges.

A drawing of a geometric representation of a graph on any surface such that no edges intersect is called embedding [6]. A graph G is *planar* if it can be drawn in the plane with its edges only intersecting at vertices of G . So the graph is non-planar

if it can not be drawn without crossing. A planar graph with cycles divides the plane into a set of regions, also called *faces*. The length of a face in a plane graph G is the total length of the closed walk(s) in G bounding the face. The portion of the plane lying outside a graph embedded in a plane is infinite region.

In graph theory, the dual graph of a given planar graph G is a graph which has a vertex corresponding to each plane region of G , and the graph has an edge joining two neighboring regions for each edge in G , for a certain embedding of G .

A *fuzzy set* A on an universal set X is characterized by a mapping $m : X \rightarrow [0, 1]$, which is called the membership function. A fuzzy set is denoted by $A = (X, m)$.

A *fuzzy graph* [23] $\xi = (V, \sigma, \mu)$ is a non-empty set V together with a pair of functions $\sigma : V \rightarrow [0, 1]$ and $\mu : V \times V \rightarrow [0, 1]$ such that for all $x, y \in V$, $\mu(x, y) \leq \min\{\sigma(x), \sigma(y)\}$, where $\sigma(x)$ and $\mu(x, y)$ represent the membership values of the vertex x and of the edge (x, y) in ξ respectively. A loop at a vertex x in a fuzzy graph is represented by $\mu(x, x) \neq 0$. An edge is non-trivial if $\mu(x, y) \neq 0$.

A fuzzy graph $\xi = (V, \sigma, \mu)$ is complete if $\mu(u, v) = \min\{\sigma(u), \sigma(v)\}$ for all $u, v \in V$, where (u, v) denotes the edge between the vertices u and v .

Several definitions of strong edge are available in literature. Among them the definition of [9] is more suitable for our purpose. The definition is given below. For the fuzzy graph $\xi = (V, \sigma, \mu)$, an edge (x, y) is called *strong* [9] if $\frac{1}{2} \min\{\sigma(x), \sigma(y)\} \leq \mu(x, y)$ and weak otherwise. The strength of the fuzzy edge (x, y) is represented by the value $\frac{\mu(x, y)}{\min\{\sigma(x), \sigma(y)\}}$.

If an edge (x, y) of a fuzzy graph satisfies the condition $\mu(x, y) = \min\{\sigma(x), \sigma(y)\}$, then this edge is called effective edge [21]. Two vertices are said to be effective adjacent if they are the end vertices of the same effective edge. Then the effective incident degree of a fuzzy graph is defined as number of effective incident edges on a vertex v . If all the edges of a fuzzy graph are effective, then the fuzzy graph becomes complete fuzzy graph. A pendent vertex in a fuzzy graph is defined as a vertex of an effective incident degree one. A fuzzy edge is called a fuzzy *pendant edge* [24], if one end vertex is fuzzy pendant vertex. The membership value of the pendant edge is the minimum among the membership values of the end vertices.

A *homomorphism* [20] between fuzzy graphs ξ and ξ' is a map $h : S \rightarrow S'$ which satisfies $\sigma(x) \leq \sigma'(h(x))$ for all $x \in S$ and $\mu(x, y) \leq \mu'(h(x), h(y))$ for all $x, y \in S$ where S is set of vertices of ξ and S' is that of ξ' .

A *weak isomorphism* [20] between fuzzy graphs is a bijective homomorphism $h : S \rightarrow S'$ which satisfies $\sigma(x) = \sigma'(h(x))$ for all $x \in S$.

A *co-weak isomorphism* [20] between fuzzy graphs is a bijective homomorphism $h : S \rightarrow S'$ which satisfies $\mu(x, y) = \mu'(h(x), h(y))$ for all $x, y \in S$.

An *isomorphism* [20] between fuzzy graphs is a bijective homomorphism $h : S \rightarrow S'$ which satisfies $\sigma(x) = \sigma'(h(x))$ for all $x \in S$ and $\mu(x, y) = \mu'(h(x), h(y))$ for all $x, y \in S$.

The *underlying crisp graph* of the fuzzy graph $\xi = (V, \sigma, \mu)$ is denoted as $\xi^* = (V, \sigma^*, \mu^*)$ where $\sigma^* = \{u \in V | \sigma(u) > 0\}$ and $\mu^* = \{(u, v) \in V \times V | \mu(u, v) > 0\}$.

A (crisp) *multiset* over a non-empty set V is simply a mapping $d : V \rightarrow N$, where N is the set of natural numbers. Yager [31] first discussed fuzzy multisets, although he used the term “fuzzy bag”. An element of nonempty set V may occur more than once with possibly the same or different membership values. A natural generalization of this interpretation of multiset leads to the notion of *fuzzy multiset*, or *fuzzy bag*, over a non-empty set V as a mapping $\tilde{C} : V \times [0, 1] \rightarrow N$. The membership values of $v \in V$ are denoted as $v_{\mu^j}, j = 1, 2, \dots, p$ where $p = \max\{j : v_{\mu^j} \neq 0\}$. So the fuzzy multiset can be denoted as $M = \{(v, v_{\mu^j}), j = 1, 2, \dots, p | v \in V\}$.

To define fuzzy planar graph, fuzzy multigraph is essential as planar graphs contain multi-edges. In the next section, fuzzy multigraph is defined.

III. FUZZY MULTIGRAPH

In this section, the fuzzy multigraph is defined.

Definition 1: Let V be a non-empty set and $\sigma : V \rightarrow [0, 1]$ be a mapping. Also let $E = \{(x, y), (x, y)_{\mu^j}, j = 1, 2, \dots, p_{xy} | (x, y) \in V \times V\}$ be a fuzzy multiset of $V \times V$ such that $(x, y)_{\mu^j} \leq \min\{\sigma(x), \sigma(y)\}$ for all $j = 1, 2, \dots, p_{xy}$, where $p_{xy} = \max\{j | (x, y)_{\mu^j} \neq 0\}$. Then $\psi = (V, \sigma, E)$ is denoted as fuzzy multigraph where $\sigma(x)$ and $(x, y)_{\mu^j}$ represent the membership value of the vertex x and the membership value of the edge (x, y) in ψ respectively.

It may be noted that there may be more than one edge between the vertices x and y . $(x, y)_{\mu^j}$ denotes the membership value of the j -th edge between the vertices x and y . Note that p_{xy} represents the number of edges between the vertices x and y .

IV. FUZZY PLANAR GRAPHS

Planarity is important in connecting the wire lines, gas lines, water lines, printed circuit design, etc. But, some times little crossing may be accepted to these design of such lines/circuits. So fuzzy planar graph is an important topic for these connections.

A crisp graph is called non-planar graph if there is at least one crossing between the edges for all possible geometrical representations of the graph. Let a crisp graph G has a crossing for a certain geometrical representation between two edges (a, b) and (c, d) . In fuzzy concept, we say that this two edges have membership values 1. If we remove the edge (c, d) , the graph becomes planar. In fuzzy sense, we say that the edges (a, b) and (c, d) have membership values 1 and 0 respectively.

Let $\xi = (V, \sigma, \mu)$ be a fuzzy graph and for a certain geometric representation, the graph has only one crossing between two fuzzy edges $((w, x), \mu(w, x))$ and $((y, z), \mu(y, z))$. If $\mu(w, x) = 1$ and $\mu(y, z) = 0$, then we say that the fuzzy graph has no crossing. Similarly, if $\mu(w, x)$ has value near to 1 and $\mu(y, z)$ has value near to 0, the crossing will not be important for the planarity. If $\mu(w, x)$ has value near to 1 and

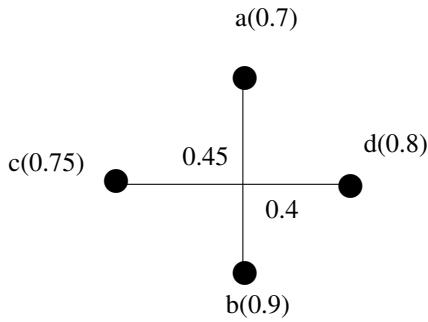


Fig. 1. Intersecting value between two intersecting edges.

$\mu(w, x)$ has value near to 1, then the crossing becomes very important for the planarity.

Before going to the main definition, some co-related terms are discussed below.

A. Intersecting value in fuzzy multigraph

In fuzzy multigraph, when two edges intersect at a point, a value is assigned to that point in the following way. Let in a fuzzy multigraph $\psi = (V, \sigma, E)$, E contains two edges $((a, b), (a, b)_{\mu^k})$ and $((c, d), (c, d)_{\mu^l})$ which are intersected at a point P , where k and l are fixed integers.

Strength of the fuzzy edge (a, b) can be measured by the value $I_{(a,b)} = \frac{(a,b)_{\mu^k}}{\min\{\sigma(a), \sigma(b)\}}$. If $I_{(a,b)} \geq 0.5$, then the fuzzy edge is called strong otherwise weak.

We define the intersecting value at the point P by $\mathcal{I}_P = \frac{I_{(a,b)} + I_{(c,d)}}{2}$. If the number of point of intersections in a fuzzy multigraph increases, planarity decreases. So for fuzzy multigraph, \mathcal{I}_P is inversely proportional to the planarity. Based on this concept, a new terminology is introduced below for a fuzzy planar graph.

Definition 2: Let ψ be a fuzzy multigraph and for a certain geometrical representation P_1, P_2, \dots, P_z be the points of intersections between the edges. ψ is said to be fuzzy planar graph with fuzzy planarity value f , where

$$f = \frac{1}{1 + \{\mathcal{I}_{P_1} + \mathcal{I}_{P_2} + \dots + \mathcal{I}_{P_z}\}}.$$

It is obvious that f is bounded and the range of f is $0 < f \leq 1$.

If there is no point of intersection for a certain geometrical representation of a fuzzy planar graph, then its fuzzy planarity value is 1. In this case, the underlying crisp graph of this fuzzy graph is the crisp planar graph. If f decreases, then the number of points of intersection between the edges increases and obviously the nature of planarity decreases. From this analogy, one can say that every fuzzy graph is a fuzzy planar graph with certain fuzzy planarity value.

Example 1: Here an example is given to calculate the intersecting value at the intersecting point between two edges. Two edges (a, b) and (c, d) are intersected where $\sigma(a) = 0.7, \sigma(b) = 0.9, \sigma(c) = 0.75, \sigma(d) = 0.8, \mu(a, b) = 0.4, \mu(c, d) = 0.45$ (see Fig. 1). Strength of the edge (a, b) is $\frac{0.4}{0.7} = 0.57$ and that of (c, d) is $\frac{0.45}{0.75} = 0.6$. Thus the intersecting value at the point is $\frac{0.57+0.6}{2} = 0.585$.

Fuzzy planarity value for a fuzzy multigraph is calculated from the following theorem.

Theorem 1: Let ψ be a fuzzy multigraph such that edge membership value of each intersecting edge is equal to the minimum of membership values of its end vertices. The fuzzy planarity value f of ψ is given by $f = \frac{1}{1+N_p}$, where N_p is the number of point of intersections between the edges in ψ .

Proof. Let $\psi = (V, \sigma, E)$ be a fuzzy multigraph such that edge membership values of each intersecting edge is equal to minimum of its vertex membership values. For the fuzzy multigraph, $(x, y)_{\mu^j} = \min\{\sigma(x), \sigma(y)\}$ for each intersecting edge (x, y) and $j = 1, 2, \dots, p_{xy}$.

Let P_1, P_2, \dots, P_k , be the point of intersections between the edges in ψ , k being an integer. For any intersecting edge (a, b) in ψ , $I_{(a,b)} = \frac{(a,b)_{\mu^j}}{\min\{\sigma(a), \sigma(b)\}} = 1$. Therefore, for P_1 , the point of intersection between the edges (a, b) and (c, d) , \mathcal{I}_{P_1} is equals to $\frac{1+1}{2} = 1$. Hence $\mathcal{I}_{P_i} = 1$ for $i = 1, 2, \dots, k$.

Now, $f = \frac{1}{1+\mathcal{I}_{P_1}+\mathcal{I}_{P_2}+\dots+\mathcal{I}_{P_k}} = \frac{1}{1+(1+1+\dots+1)} = \frac{1}{1+N_p}$, where N_p is the number of point of intersections between the edges in ψ . \square

Definition 3: A fuzzy planar graph ψ is called strong fuzzy planar graph if the fuzzy planarity value of the graph is greater than 0.5.

The fuzzy planar graph of Example 5 is not strong fuzzy planar graph as its fuzzy planarity value is less than 0.5.

Thus, depending on the fuzzy planarity value, the fuzzy planar graphs are divided into two groups namely, strong and weak fuzzy planar graphs.

Theorem 2: Let ψ be a strong fuzzy planar graph. The number of point of intersections between strong edges in ψ is at most one.

Proof. Let $\psi = (V, \sigma, E)$ be a strong fuzzy planar graph. Let, if possible, ψ has at least two point of intersections P_1 and P_2 between two strong edges in ψ .

For any strong edge $((a, b), (a, b)_{\mu^j})$, $(a, b)_{\mu^j} \geq \frac{1}{2} \min\{\sigma(a), \sigma(b)\}$. So $I_{(a,b)} \geq 0.5$.

Thus for two intersecting strong edges $((a, b), (a, b)_{\mu^j})$ and $((c, d), (c, d)_{\mu^i})$, $\frac{I_{(a,b)} + I_{(c,d)}}{2} \geq 0.5$, that is, $\mathcal{I}_{P_1} \geq 0.5$. Similarly, $\mathcal{I}_{P_2} \geq 0.5$. Then $1 + \mathcal{I}_{P_1} + \mathcal{I}_{P_2} \geq 2$. Therefore, $f = \frac{1}{1+\mathcal{I}_{P_1}+\mathcal{I}_{P_2}} \leq 0.5$. It contradicts the fact that the fuzzy graph is a strong fuzzy planar graph.

So number of point of intersections between strong edges can not be two. It is clear that if the number of point of intersections of strong fuzzy edges increases, the fuzzy planarity value decreases. Similarly, if the number of point of intersection of strong edges is one, then the fuzzy planarity value $f > 0.5$. Any fuzzy planar graph without any crossing between edges is a strong fuzzy planar graph. Thus, we conclude that the maximum number of point of intersections between the strong edges in ψ is one. \square

Face of a planar graph is an important feature. We now introduce the fuzzy face of a fuzzy planar graph.

Fuzzy face in a fuzzy graph is a region bounded by fuzzy edges. Every fuzzy face is characterized by fuzzy edges in its boundary. If all the edges in the boundary of a fuzzy face

have membership value 1, it becomes crisp face. If one of such edges is removed or has membership value 0, the fuzzy face does not exist. So the existence of a fuzzy face depends on the minimum value of strength of fuzzy edges in its boundary. A fuzzy face and its membership value are defined below.

Definition 4: Let $\psi = (V, \sigma, E)$ be a fuzzy planar graph and

$E = \{((x, y), (x, y)_{\mu^j}), j = 1, 2, \dots, p_{xy} | (x, y) \in V \times V\}$ and $p_{xy} = \max\{j | (x, y)_{\mu^j} \neq 0\}$. A fuzzy face of ψ is a region, bounded by the set of fuzzy edges $E' \subset E$, of a geometric representation of ψ . The membership value of the fuzzy face is

$$\min \left\{ \frac{(x, y)_{\mu^j}}{\min\{\sigma(x), \sigma(y)\}}, j = 1, 2, \dots, p_{xy} | (x, y) \in E' \right\}.$$

A fuzzy face is called strong fuzzy face if its membership value is greater than 0.5, and weak face otherwise. Every fuzzy planar graph has an infinite region which is called outer fuzzy face. Other faces are called inner fuzzy faces.

Example 2: In Fig. 2, F_1, F_2 and F_3 are three fuzzy faces. F_1 is bounded by the edges $((v_1, v_2), 0.5), ((v_2, v_3), 0.6), ((v_1, v_3), 0.55)$ with membership value 0.833. Similarly, F_2 is a fuzzy bounded face. F_3 is the outer fuzzy face with membership value 0.33. So F_1 is a strong fuzzy face and F_2, F_3 are weak fuzzy faces.

Every strong fuzzy face has membership value greater than 0.5. So every edge of a strong fuzzy face is a strong fuzzy edge.

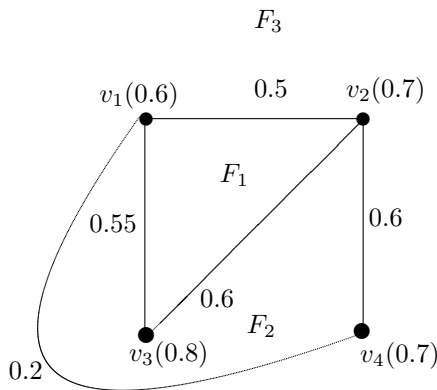


Fig. 2. Example of faces in fuzzy planar graph.

Theorem 3: If the fuzzy planarity value of a fuzzy planar graph is greater than 0.67, then the graph does not contain any point of intersection between two strong edges.

Proof. Let $\psi = (V, \sigma, E)$ be a fuzzy planar graph with fuzzy planarity value f , where $f \geq 0.67$. Let, if possible, P be a point of intersection between two strong fuzzy edges $((a, b), (a, b)_{\mu^j})$ and $((c, d), (c, d)_{\mu^j})$.

For any strong edge $((a, b), (a, b)_{\mu^j})$, $(a, b)_{\mu^j} \geq \frac{1}{2} \min\{\sigma(a), \sigma(b)\}$. Therefore, $I_{(a,b)} \geq 0.5$. For the minimum value of $I_{(a,b)}$ and $I_{(c,d)}$, $\mathcal{I}_P = 0.5$ and $f = \frac{1}{1+0.5} < 0.67$. A

contradiction arises. Hence, ψ does not contain any point of intersection between strong edges. \square

Motivated from this theorem, we introduce a special type of fuzzy planar graph called 0.67-fuzzy planar graph whose fuzzy planarity value is more than or equal to 0.67. As in mentioned earlier, if the fuzzy planarity value is 1, then the geometrical representation of fuzzy planar graph is similar to the crisp planar graph. It is shown in Theorem 7, if fuzzy planarity value is 0.67, then there is no crossing between strong edges. For this case, if there is any point of intersection between edges, that is the crossing between the weak edge and any other edge. Again, the significance of weak edge is less compared to strong edges. Thus, 0.67-fuzzy planar graph is more significant. If fuzzy planarity value increases, then the geometrical structure of planar graph tends to crisp planar graph.

Any fuzzy planar graph without any point of intersection of fuzzy edges is a fuzzy planar graph with fuzzy planarity value 1. Therefore, it is a 0.67-fuzzy planar graph.

V. FUZZY DUAL GRAPH

We now introduce dual of 0.67-fuzzy planar graph. In fuzzy dual graph, vertices are corresponding to the strong fuzzy faces of the 0.67-fuzzy planar graph and each fuzzy edge between two vertices is corresponding to each edge in the boundary between two faces of 0.67-fuzzy planar graph. The formal definition is given below.

Definition 5: Let $\psi = (V, \sigma, E)$ be a 0.67-fuzzy planar graph and $E = \{((x, y), (x, y)_{\mu^j}), j = 1, 2, \dots, p_{xy} | (x, y) \in V \times V\}$. Again, let F_1, F_2, \dots, F_k be the strong fuzzy faces of ψ . The fuzzy dual graph of ψ is a fuzzy planar graph $\psi' = (V', \sigma', E')$, where $V' = \{x_i, i = 1, 2, \dots, k\}$, and the vertex x_i of ψ' is considered for the face F_i of ψ .

The membership values of vertices are given by the mapping $\sigma' : V' \rightarrow [0, 1]$ such that $\sigma'(x_i) = \max\{(u, v)_{\mu^j}, j = 1, 2, \dots, p_{uv} | (u, v)$ is an edge of the boundary of the strong fuzzy face $F_i\}$.

Between two faces F_i and F_j of ψ , there may exist more than one common edge. Thus, between two vertices x_i and x_j in fuzzy dual graph ψ' , there may be more than one edge. We denote $(x_i, x_j)_{\nu^l}$ be the membership value of the l -th edge between x_i and x_j . The membership values of the fuzzy edges of the fuzzy dual graph are given by $(x_i, x_j)_{\nu^l} = (u, v)_{\mu^j}^l$ where $(u, v)^l$ is an edge in the boundary between two strong fuzzy faces F_i and F_j and $l = 1, 2, \dots, s$, where s is the number of common edges in the boundary between F_i and F_j or the number of edges between x_i and x_j .

If there be any strong pendant edge in the 0.67-fuzzy planar graph, then there will be a self loop in ψ' corresponding to this pendant edge. The edge membership value of the self loop is equal to the membership value of the pendant edge.

Fuzzy dual graph of 0.67-fuzzy planar graph does not contain point of intersection of edges for a certain representation, so it is 0.67-fuzzy planar graph with planarity value 1. Thus the fuzzy face of fuzzy dual graph can be similarly described as in 0.67-fuzzy planar graphs.

Example 3: In Fig. 3, a 0.67-fuzzy planar graph $\psi = (V, \sigma, E)$ where $V = \{a, b, c, d\}$ is given. For this graph let $\sigma(a) = 0.6, \sigma(b) = 0.7, \sigma(c) = 0.8, \sigma(d) = 0.9$.

and $E = \{((a, b), 0.5), ((a, c), 0.4), ((a, d), 0.55), ((b, c), 0.45), ((c, d), 0.7)\}$.

Thus, the 0.67-fuzzy planar graph has the following fuzzy faces

F_1 (bounded by $((a, b), 0.5), ((a, c), 0.4), ((b, c), 0.45)$),

F_2 (bounded by $((a, d), 0.55), ((c, d), 0.7), ((a, c), 0.4)$),

and outer fuzzy face

F_3 (surrounded by $((a, b), 0.5), ((b, c), 0.45), ((c, d), 0.7), ((a, d), 0.55)$).

The fuzzy dual graph is constructed as follows. Here all the fuzzy faces are strong fuzzy faces. For each strong fuzzy face, we consider a vertex for the fuzzy dual graph. Thus the vertex set $V' = \{x_1, x_2, x_3, x_4\}$ where the vertex x_i is taken corresponding to the strong fuzzy face F_i , $i = 1, 2, 3, 4$. So $\sigma'(x_1) = \max\{0.5, 0.4, 0.45\} = 0.5$, $\sigma'(x_2) = \max\{0.55, 0.7, 0.4\} = 0.7$, $\sigma'(x_3) = \max\{0.5, 0.45, 0.7, 0.55\} = 0.7$.

There are two common edges (a, d) and (c, d) between the faces F_2 and F_3 in ψ . Hence between the vertices x_2 and x_3 , two edges exist in the fuzzy dual graph of ψ . Here membership values of these edges are given by $(x_2, x_4)_{\nu^1} = (c, d)_{\mu^1} = 0.7$, $(x_2, x_4)_{\nu^2} = (a, d)_{\mu^1} = 0.55$.

The membership values of other edges of the fuzzy dual graph are calculated as $(x_1, x_2)_{\nu^1} = (a, c)_{\mu^1} = 0.4$, $(x_1, x_3)_{\nu^1} = (a, b)_{\mu^1} = 0.5$, $(x_1, x_3)_{\nu^2} = (b, c)_{\mu^1} = 0.45$.

Thus the edge set of fuzzy dual graph is $E' = \{((x_1, x_2), 0.4), ((x_1, x_3), 0.5), ((x_1, x_3), 0.45), ((x_2, x_3), 0.7), ((x_2, x_3), 0.55)\}$.

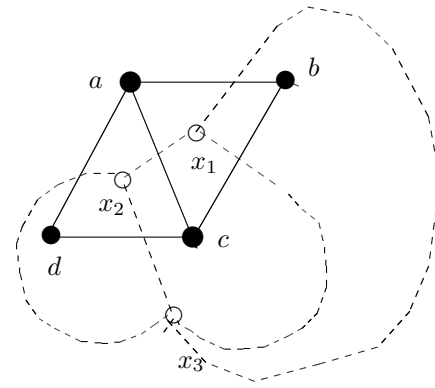
In Fig. 3, the fuzzy dual graph $\psi' = (V', \sigma', E')$ of ψ is drawn by dotted line.

Theorem 4: Let ψ be a 0.67-fuzzy planar graph without weak edges. The number of vertices, number of fuzzy edges and number of strong faces of ψ are denoted by n, p, m respectively. Also let ψ' be the fuzzy dual graph of ψ . Then
(i) the number of vertices of ψ' is equal to m ,
(ii) number of edges of ψ' is equal to p ,
(iii) number of fuzzy faces of ψ' is equal to n .

Proof. Proof of (i), (ii) and (iii) are obvious from the definition of fuzzy dual graph. \square

Theorem 5: Let ψ' be a fuzzy dual graph of a 0.67-fuzzy planar graph ψ . The number of strong fuzzy faces in ψ' is less than or equal to the number of vertices of ψ .

Proof. Here ψ' is a fuzzy dual graph of a 0.67-fuzzy planar graph ψ . Let ψ has n vertices and ψ' has m strong fuzzy faces. Now, ψ may have weak edges and strong edges. To construct fuzzy dual graph, weak edges are to eliminate. Thus if ψ has some weak edges, some vertices may have all its adjacent edges as weak edges. Let the number of such vertices be t . These vertices are not bounding any strong fuzzy faces. If we remove these vertices and adjacent edges, then the number of vertices is $n - t$. Again, from Theorem 4, $m = n - t$. Hence, in general $m \leq n$. This concludes that the number of strong fuzzy faces in ψ' is less than or equal to the number of vertices of ψ . \square



$\sigma(a) = 0.6$	$(a, b)_{\mu^1} = 0.5$
$\sigma(b) = 0.7$	$(a, c)_{\mu^1} = 0.4$
$\sigma(c) = 0.8$	$(a, d)_{\mu^1} = 0.55$
$\sigma(d) = 0.9$	$(b, c)_{\mu^1} = 0.45$
<hr/>	
$\sigma'(x_1) = 0.5$	$(x_1, x_2)_{\nu^1} = 0.4$
$\sigma'(x_3) = 0.6$	$(x_1, x_3)_{\nu^1} = 0.5$
$\sigma'(x_2) = 0.7$	$(x_1, x_3)_{\nu^2} = 0.45$
	$(x_2, x_3)_{\nu^1} = 0.5$
	$(x_2, x_3)_{\nu^2} = 0.7$

Fig. 3. Example of fuzzy dual graph.

An example is considered to illustrate the statement. Let $\psi = (V, \sigma, E)$ be a 0.67-fuzzy planar graph where $V = \{a, b, c, d\}$. $\sigma(a) = 0.8, \sigma(b) = 0.7, \sigma(c) = 0.9, \sigma(d) = 0.3$. $E = \{((a, b), 0.7), ((b, c), 0.7), ((c, d), 0.2), ((b, d), 0.2), ((a, d), 0.2)\}$. The corresponding fuzzy dual graph is $\psi' = (V', \sigma', E')$ where $V' = \{x_1, x_2, x_3\}$. $\sigma'(x_1) = 0.7, \sigma'(x_2) = 0.7, \sigma'(x_3) = 0.7$. $E' = \{((x_1, x_2), 0.2), ((x_1, x_3), 0.2), ((x_1, x_3), 0.7), ((x_2, x_3), 0.2), ((x_2, x_3), 0.7)\}$. Here number of strong fuzzy face is one while number of fuzzy face is three (see Fig. 4).

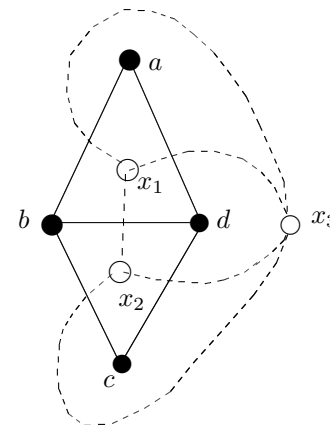


Fig. 4. Example of a fuzzy dual graph with strong face.

Theorem 6: Let $\psi = (V, \sigma, E)$ be a 0.67-fuzzy planar graph without weak edges and the fuzzy dual graph of ψ be $\psi' = (V', \sigma', E')$. The membership values of fuzzy edges of

ψ' are equal to membership values of the fuzzy edges of ψ .
Proof. Let $\psi = (V, \sigma, E)$ be a 0.67-fuzzy planar graph without weak edges. The fuzzy dual graph of ψ is $\psi' = (V', \sigma', E')$ which is a 0.67-fuzzy planar graph as there is no point of intersection between any edges. Let $\{F_1, F_2, \dots, F_k\}$ be the set of strong fuzzy faces of ψ .

From the definition of fuzzy dual graph we know that $(x_i, x_j)_{\mu^l} = (u, v)_{\mu^l}$ where $(u, v)^l$ is an edge in the boundary between two strong fuzzy faces F_i and F_j and $l = 1, 2, \dots, s$, where s is the number of common edges in the boundary between F_i and F_j .

The numbers of fuzzy edges of two fuzzy graphs ψ and ψ' are same as ψ has no weak edges. For each fuzzy edge of ψ there is a fuzzy edge in ψ' with same membership value. \square

VI. ISOMORPHISM ON FUZZY PLANAR GRAPHS

Isomorphism between fuzzy graphs is an equivalence relation. But, if there is an isomorphism between two fuzzy graph and one is fuzzy planar graph, then the other will be fuzzy planar graph. This result is proved in the following theorem.

Theorem 7: Let ψ be a fuzzy planar graph. If there exists an isomorphism $h : \psi \rightarrow \xi$ where ξ is a fuzzy graph, ξ can be drawn as fuzzy planar graph with same planarity value of ψ .

Proof. Let ψ be a fuzzy planar graph and there exists an isomorphism $h : \psi \rightarrow \xi$ where ξ is a fuzzy graph. Now, isomorphism preserves edge and vertex weights. Also the order and size of fuzzy graphs are preserved in isomorphic fuzzy graphs [20]. So, the order and size of ξ will be equal to ψ . Then, ξ can be drawn similarly as ψ . Hence, the number of intersection between edges and fuzzy planarity value of ξ will be same as ψ . This concludes that ξ can be drawn as fuzzy planar graph with same fuzzy planarity value. \square

In crisp graph theory, dual of dual graph of a planar graph is planar graph itself. In fuzzy graph concept, fuzzy dual graph of a fuzzy dual graph is not isomorphic to fuzzy planar graph. The membership values of vertices of fuzzy dual graph are the maximum membership values of its bounding edges of the corresponding fuzzy faces in fuzzy planar graph. Thus vertex weight is not preserved in fuzzy dual graph. But edge weight is preserved in fuzzy dual graph. This result is established in following theorem.

Theorem 8: Let ψ_2 be the fuzzy dual graph of fuzzy dual graph of a 0.67-fuzzy planar graph ψ without weak edges. Then there exists a co-weak isomorphism between ψ and ψ_2 .

Proof. Let ψ be a 0.67-fuzzy planar graph which has no weak edges. Also let, ψ_1 be the fuzzy dual graph of ψ and ψ_2 be the fuzzy dual graph of ψ_1 . Now we have to establish a co-weak isomorphism between ψ_2 and ψ . As the number of vertices of ψ_2 is equal to that of strong fuzzy faces of ψ_1 . Again the number of strong fuzzy faces is equal to the number of vertices of ψ . Thus, the number of vertices of ψ_2 and ψ are same. Also, the numbers of edges of a fuzzy planar graph and its dual graph are same. By the definition of fuzzy dual graph, the edge membership value of an edge in fuzzy dual graph is equal to the edge membership value of an edge in fuzzy

planar graph. Thus we can construct a co-weak isomorphism from ψ_2 to ψ . Hence the result is true. \square

The Theorem 8 can be explained by the following example. Here a 0.67-fuzzy planar graph ψ is constructed (See Fig. 5(a)). Then its fuzzy dual graph ψ_1 is drawn in Fig. 5(b). Also the fuzzy dual graph ψ_2 of ψ_1 is drawn in Fig. 5(c). Now, we construct a bijective mapping from vertices of ψ_2 to vertices of ψ as $a_1 \rightarrow a, b_1 \rightarrow b, c_1 \rightarrow c, d_1 \rightarrow d$. Similarly, we can extend the mapping from edge set of ψ_2 to the edge set of ψ . It is observed that the vertex membership values of ψ_2 is less than or equal to the vertex membership values of ψ under the mapping and edge membership values are equal under the mapping. Thus the mapping is said to satisfy the co-weak isomorphism property.

Two fuzzy planar graphs with same number of vertices may be isomorphic. But, the relations between fuzzy planarity values of two fuzzy planar graphs may have the following relations.

Theorem 9: Let ξ_1 and ξ_2 be two isomorphic fuzzy graphs with fuzzy planarity values f_1 and f_2 respectively. Then $f_1 = f_2$.

The proof of the theorem is the immediate consequence of Theorem 7.

Theorem 10: Let ξ_1 and ξ_2 be two weak isomorphic fuzzy graphs with fuzzy planarity values f_1 and f_2 respectively. $f_1 = f_2$ if the edge membership values of corresponding intersecting edges are same.

Proof. Here $\xi_1 = (V, \sigma_1, \mu_1)$ and $\xi_2 = (V, \sigma_2, \mu_2)$ are two weak isomorphic fuzzy graphs with fuzzy planarity values f_1 and f_2 respectively. As two fuzzy graphs are weak isomorphic, $\sigma_1(x) = \sigma_2(y)$ for some x in ξ_1 and y in ξ_2 . Let the graphs have one point of intersection. Let two intersecting edges be (a_1, b_1) and (c_1, d_1) in ξ_1 . Also two corresponding edges in ξ_2 be (a_2, b_2) and (c_2, d_2) . Then, intersecting value of the point is given by $\frac{\mu(a_1, b_1) + \mu(c_1, d_1)}{\sigma(a_1) \wedge \sigma(b_1) + \sigma(c_1) \wedge \sigma(d_1)}$. The intersecting value of the corresponding point in ξ_2 is given as $\frac{\mu(a_2, b_2) + \mu(c_2, d_2)}{\sigma(a_2) \wedge \sigma(b_2) + \sigma(c_2) \wedge \sigma(d_2)}$. Now, $f_1 = f_2$, if $\mu(a_1, b_1) = \mu(a_2, b_2)$. The number of point of intersections may increase. But, if the sum of the intersecting value of ξ_1 is equal to that of ξ_2 , fuzzy planarity values of the graphs must be equal. Thus, for equality of f_1 and f_2 , the edge membership values of intersecting edges of ξ are equal to the edge membership values of the corresponding edges in ξ_2 . \square

Theorem 11: Let ξ_1 and ξ_2 be two co-weak isomorphic fuzzy graphs with fuzzy planarity values f_1 and f_2 respectively. $f_1 = f_2$ if the minimum of membership values of the end vertices of corresponding intersecting edges are same.

Proof. Here $\xi_1 = (V, \sigma_1, \mu_1)$ and $\xi_2 = (V, \sigma_2, \mu_2)$ are two co-weak isomorphic fuzzy graphs with fuzzy planarity values f_1 and f_2 respectively. As two fuzzy graphs are co-weak isomorphic, $\mu_1(x, y) = \mu_2(z, t)$ for some edge (x, y) in ξ_1 and (z, t) in ξ_2 . Let the graphs have one point of intersection. Let two intersecting edges be (a_1, b_1) and (c_1, d_1) in ξ_1 . Also, two corresponding edges in ξ_2 be (a_2, b_2) and (c_2, d_2) . Then, inter-

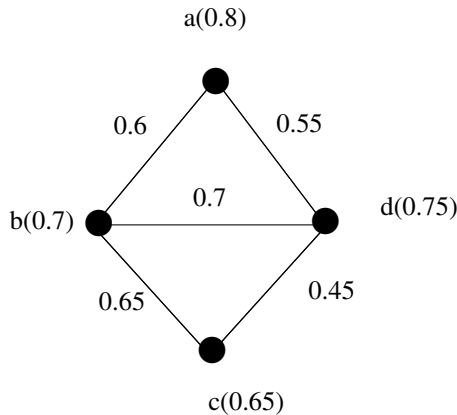
secting value of the point is given by $\frac{\mu(a_1, b_1) + \mu(c_1, d_1)}{\sigma(a_1) \wedge \sigma(b_1) + \sigma(c_1) \wedge \sigma(d_1)}$. The intersecting value of the corresponding point in ξ_2 is given as $\frac{\mu(a_2, b_2) + \mu(c_2, d_2)}{\sigma(a_2) \wedge \sigma(b_2) + \sigma(c_2) \wedge \sigma(d_2)}$. Now, the fuzzy planarity values $f_1 = f_2$, if $\sigma_1(a_1) \wedge \sigma_1(b_1) = \sigma_2(a_2) \wedge \sigma_2(b_2)$. The number of point of intersections of ξ_1 is equal to that of ξ_2 , fuzzy planarity values of the graphs must be equal. Thus, for equality of f_1 and f_2 , the minimum membership value of end vertices of an edge in ξ_1 is equal to that of a corresponding edge in ξ_2 . \square

VII. CONCLUSION

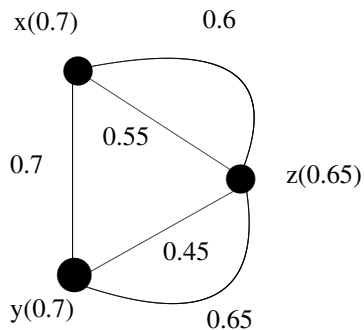
This study describes the fuzzy multigraphs, fuzzy planar graphs, and a very important consequence of fuzzy planar graph known as fuzzy dual graphs. In crisp planar graph, no edge intersects other. In fuzzy graph, an edge may be weak or strong. Using the concept of weak edge, we define fuzzy planar graph in such a way that an edge can intersect other edge. But, this facility violates the definition of planarity of graph. Since the role of weak edge is insignificant, the intersection between a weak edge and an other edge is less important. Motivating from this idea, we allow the intersection of edges in fuzzy planar graph. It is well known that if the membership values of all edges become one, the graph becomes crisp graph. Keeping this idea in mind, we define a new term called fuzzy planarity value of a fuzzy graph. If the fuzzy planarity value of a fuzzy graph is one, then no edge crosses other edge. This leads to the crisp planar graph. Thus, the fuzzy planarity value measures the amount of planarity of a fuzzy graph. This is a very interesting concept of fuzzy graph theory. Strong fuzzy planar graphs and a distinguishable subclass of strong fuzzy planar graph namely 0.67-fuzzy planar graphs have been exemplified. From the definitions, it is concluded that 0.67-fuzzy planar graph \subset strong fuzzy planar graph \subset fuzzy planar graph. Another important term of planar graph is "face" which is redefined in fuzzy planar graph. A particular type of fuzzy face called strong fuzzy face is incorporated. Besides, isomorphism properties of fuzzy planar graphs are investigated. It is shown that dual of dual fuzzy graphs are co-weak isomorphism to fuzzy planar graph. Several properties of isomorphism on fuzzy planar graphs are explained. It may be noted that, in this article, fuzzy dual graph is defined for the 0.67-fuzzy planar graph. But, if the planarity value is less than 0.67, then some modification is required to define dual graph. This is to be investigated in near future.

REFERENCES

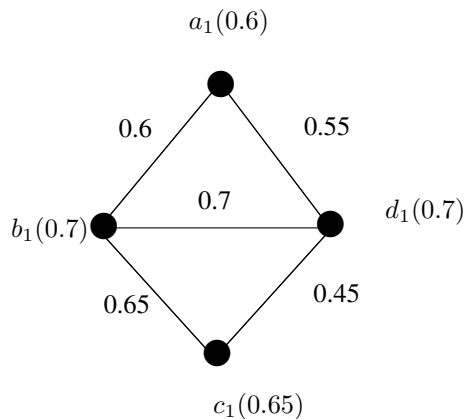
- [1] N. Abdul-jabbar, J. H. Naom and, E. H. Ouda, Fuzzy dual graph, *Journal Of Al-Nahrain University*, 12(4), 168-171, 2009.
- [2] M. Akram, Bipolar fuzzy graphs, *Information Science*, 181, 5548-5564, 2011.
- [3] M. Akram, Interval-valued fuzzy line graphs, *Neural Computing & Applications*, 21, 145-150, 2012.
- [4] M. Akram and W. A. Dudek, Intuitionistic fuzzy hypergraphs with applications, *Information Sciences*, 218, 182-193, 2013.
- [5] M. Akram, Bipolar fuzzy graphs with applications, *Knowledge Based Systems*, 39, 1-8, 2013.
- [6] V. K. Balakrishnan, *Graph Theory*, McGraw-Hill, 1997.
- [7] K. R. Bhutani and A. Battou, On M-strong fuzzy graphs, *Information Sciences*, 155(12), 103-109, 2003.



(a): A 0.67-fuzzy planar graph ψ



(b): Fuzzy dual graph ψ_1 of ψ



(c): Fuzzy dual graph ψ_2 of ψ_1

Fig. 5. Dual of dual is co-weak isomorphic to planar graph in fuzzy graph theory.

- [8] K. R. Bhutani and A. Rosenfeld, Strong arcs in fuzzy graphs, *Information Sciences*, 152, 319-322, 2003.
- [9] C. Eslahchi and B. N. Onaghe, Vertex strength of fuzzy graphs, *International Journal of Mathematics and Mathematical Sciences*, Volume 2006, Article ID 43614, Pages 1-9, DOI 10.1155/IJMMS/2006/43614.
- [10] M. Fazzolari and H. Ishibuchi, A review of the application of multiobjective evolutionary fuzzy systems: current status and further directions, *IEEE Transaction on Fuzzy Systems*, 21(1), 45-65, 2013.
- [11] P. Ghosh, K. Kundu and D. Sarkar, Fuzzy graph representation of a fuzzy concept lattice, *Fuzzy Sets and Systems*, 161(12), 1669-1675, 2010.
- [12] L. T. Koczy, Fuzzy graphs in the evaluation and optimization of networks, *Fuzzy Sets and Systems*, 46, 307-319, 1992.
- [13] Q. Liang and J. M. Mendel, MPEG VBR video traffic modelling and classification using fuzzy technique, *IEEE Transaction on Fuzzy Systems*, 9(1), 183-193, 2001.
- [14] K. -C. Lin and M. -S. Chern, The fuzzy shortest path problem and its most vital arcs, *Fuzzy Sets and Systems*, 58, 343-353, 1993.
- [15] S. Mathew and M.S. Sunitha, Types of arcs in a fuzzy graph, *Information Sciences*, 179, 1760-1768, 2009.
- [16] S. Mathew and M.S. Sunitha, Strongest strong cycles and theta fuzzy graphs, *IEEE Transactions on Fuzzy Systems*, 2013.
- [17] M. L. N. McAllister, Fuzzy intersection graphs, *Comput. Math. Applic.*, 15 (10) , 871-886, 1988.
- [18] J. N. Mordeson and P. S. Nair, Fuzzy Graphs and Hypergraphs, Physica Verlag, 2000.
- [19] S. Munoz, M. T. Ortuno, J. Ramirez and J. Yanez, Coloring fuzzy graphs, *Omega*, 33(3), 211-221, 2005.
- [20] A. Nagoorgani and J. Malarvizhi, Isomorphism on fuzzy graphs, *World Academy of Science, Engineering and Technology*, 23, 505-511, 2008.
- [21] A. Nagoorgani and R. J. Hussain, Fuzzy effective distance K -dominating sets and their applications, *International Journal of Algorithms, Computing and Mathematics*, 2(3), 25-36, 2009.
- [22] G. Nirmala and K. Dhanabal, Special planar fuzzy graph configurations, *International Journal of Scientific and Research Publications*, 2(7), 1-4, 2012.
- [23] A. Rosenfeld, Fuzzy graphs, in: L.A. Zadeh, K.S. Fu, M. Shimura (Eds.), *Fuzzy Sets and Their Applications*, Academic Press, New York, 77-95, 1975.
- [24] S. Samanta and M. Pal, Fuzzy k -competition graphs and p -competition fuzzy graphs, *Fuzzy Engineering and Information*, 5(2), 191-204, 2013.
- [25] S. Samanta and M. Pal, Fuzzy tolerance graphs, *International Journal of Latest Trends in Mathematics*, 1(2), 57-67, 2011.
- [26] S. Samanta and M. Pal, Fuzzy threshold graphs, *CIIT International Journal of Fuzzy Systems*, 3(12), 360-364, 2011.
- [27] S. Samanta and M. Pal, Irregular bipolar fuzzy graphs, *International Journal of Applications of Fuzzy Sets*, 2, 91-102, 2012.
- [28] S. samanta and M. Pal, Bipolar fuzzy hypergraphs, *International Journal of Fuzzy Logic Systems*, 2(1), 17 – 28, 2012.
- [29] S. Samanta, M. Pal and A. Pal, Some more results on bipolar fuzzy sets and bipolar fuzzy intersection graphs, To appear in *The Journal of Fuzzy Mathematics*.
- [30] S. Samanta and M. Pal, A new approach to social networks based on fuzzy graphs, To appear in *Journal of Mass Communication and Journalism*.
- [31] R. R. Yager, On the theory of bags, *Int. J. General Systems*, 13, 23-37, 1986.

Some more results on fuzzy k -competition graphs

Sovan Samanta

Department of Applied
Mathematics with Oceanology
and Computer Programming,
Vidyasagar University,
Midnapore - 721 102, India.
email: ssamantavu@gmail.com

Madhumangal Pal

Department of Applied
Mathematics with Oceanology
and Computer Programming,
Vidyasagar University,
Midnapore - 721 102, India.
email: mmpalvu@gmail.com

Anita Pal

Department of Mathematics,
National Institute of
Technology Durgapur,
Durgapur-713209, India.
e-mail: anita.buie@gmail.com

Abstract—Fuzzy competition graph as the generalization of competition graph is introduced here. Fuzzy k -competition graph as a special type of fuzzy competition graph is defined here along with fuzzy isolated vertices. The fuzzy competition number is also introduced and investigated several properties. Isomorphism properties on fuzzy competition graphs are discussed.

Keywords: Fuzzy graphs, fuzzy competition graphs, fuzzy k -competition graphs, fuzzy competition number.

I. INTRODUCTION

The concept of fuzzy graph was introduced by Rosenfeld [36] in 1975. Fuzzy graph theory has a vast area of applications. It is used in evaluation of human cardiac function, fuzzy neural networks, etc. Fuzzy graphs can be used to solve traffic light problem, time table scheduling, etc. In fuzzy set theory, there are different types of fuzzy graphs which may be a graph with crisp vertex set and fuzzy edge set or fuzzy vertex set and crisp edge set or fuzzy vertex set and fuzzy edge set or crisp vertices and edges with fuzzy connectivity, etc. A lot of works have been done on fuzzy graphs [5], [6], [14], [20], [22], [26].

In 1968, Cohen [12] introduced the notion of competition graphs in connection with a problem in ecology. Let $\vec{D} = (V, \vec{E})$ be a digraph, which corresponds to a food web. A vertex $x \in V(\vec{D})$ represents a species in the food web and an arc $(x, s) \in \vec{E}(\vec{D})$ means that x preys on the species s . If two species x and y have a common prey s , they will compete for the prey s . Based on this analogy, Cohen defined a graph which represents the relations of competition among the species in the food web. The competition graph $C(\vec{D})$ of a digraph $\vec{D} = (V, \vec{E})$ is an undirected graph $G = (V, E)$ which has the same vertex set V and has an edge between two distinct vertices $x, y \in V$ if there exists a vertex $s \in V$ and arcs $(x, s), (y, s) \in \vec{E}(\vec{D})$. The competition graph is also applicable in channel assignment, coding, modelling of complex economic and energy systems, etc. [35].

A lot of works have been done on competition graphs and its variations. In all these works, it is assumed that the vertices and edges of the graphs are precisely defined. But, in reality we observe that sometimes the vertices and edges of a graph can not be defined precisely. For example, in ecology, species

may be of different types like vegetarian, non-vegetarian, strong, weak, etc. Similarly in ecology, preys may be tasty, digestive, harmful, etc. The terms tasty, digestive, harmful, etc. have no precise meanings. They are fuzzy in nature and hence the species and preys may be assumed as fuzzy sets and inter-relationship between the species and preys can be designed by a fuzzy graph. This motivates the necessity of fuzzy competition graphs.

The competition graphs and fuzzy graphs are well known topics. In this article, fuzzy competition graphs are defined as motivated from fuzzy food web. Also, the generalization of it, the fuzzy k -competition graphs is introduced. Fuzzy neighbourhood graphs and their properties are investigated. Fuzzy competition number and fuzzy isolated vertex are exemplified. Isomorphism of fuzzy competition graphs is discussed.

A. Review of literature

In 1968, Cohen [12] presented a nice technique for food webs to find minimum number of dimensions of niche spaces and defined competition graphs. After Cohen's introduction of competition graph, several variations of it are found in literature. These are p -competition graphs of a digraph [16], [19], tolerance competition graphs [9], m -step competition graphs of a digraph [11], competition hypergraphs [46], common enemy graph of a digraph [21], competition-common enemy graph of a digraph [45], etc. Surveys of the large literature related to competition graphs can be found in [10], [15], [43]. All these representations are crisp in sense and do not include all real field competitions. The competition graphs describe about the common prey and related species, but they do not measure the strength of competitions. These graphs do not show that how much the species depend on a common prey compared to other species. On the other hand fuzzy graph theory, after Rosenfeld [36], is increased with a large number of branches [2], [3], [4], [27], [28], [29], [30], [32], [34], [37], [38].

To include the representations of all real world competitions, fuzzy competition graphs are introduced. The relations among neighbourhoods of any species are described in fuzzy neighbourhood graphs. Sometimes the preys are so valuable that the species (competitors) compete strongly. Different level

of competitions can shown by “fuzzy k -competition graphs”, a generalization of fuzzy competition graph which is introduced here.

II. PRELIMINARIES

A. Competition graphs

A directed graph (digraph) \vec{G} is a graph which consists of non-empty finite set $V(\vec{G})$ of elements called vertices and a finite set $\vec{E}(\vec{G})$ of ordered pairs of distinct vertices called arcs. We will often write $\vec{G} = (V, \vec{E})$. For an arc $\overrightarrow{(u, v)}$, u is the tail and v is the head. The order (size) of \vec{G} is the number of vertices (arcs) in \vec{G} . The out-neighbourhood [17] of a vertex v is the set $N^+(v) = \{u \in V - v : (v, u) \in \vec{E}\}$. Similarly, the in-neighbourhood [17] $N^-(v)$ of a vertex v is the set $\{w \in V - v : (w, v) \in \vec{E}\}$. The open neighbourhood of a vertex is the union of out-neighbourhood and in-neighbourhood of the vertex. A walk in \vec{G} is an alternating sequence $W = x_1 \vec{e}_1 x_2 \vec{e}_2 \dots x_{k-1} \vec{e}_{k-1} x_k$ of vertices x_i and arcs \vec{e}_i of \vec{G} such that tail of \vec{e}_i is x_i and head is x_{i+1} for every $i = 1, 2, \dots, k-1$. A walk is closed if $x_1 = x_k$. A trail is a walk in which all arcs are distinct. A path is a walk in which all vertices are distinct. A path x_1, x_2, \dots, x_k with $k \geq 3$ is a cycle if $x_1 = x_k$.

For an undirected graph, open-neighbourhood [1] $N(x)$ of the vertex x is the set of all vertices adjacent to x in the graph. Open neighbourhood graph [1] $N(G)$ of G is a graph whose vertex set is same as G and has an edge between two vertices x and y in $N(G)$ if and only if $N(x) \cap N(y) \neq \phi$ in G . Closed neighbourhood $N[x]$ of x is the set $N(x) \cup \{x\}$. Closed neighbourhood graph $N[G]$ of a graph G is similarly defined, except has an edge in $N[G]$ if and only if $N[x] \cap N[y] \neq \phi$ in G . (p)-neighbourhood graph (read as open p -neighbourhood graph) [8], $N_p(G)$ of a graph G is a graph whose vertex set is same as G and has an edge between two vertices x and y if and only if $|N(x) \cap N(y)| \geq p$ (note that $|X|$ is the number of elements in the crisp set X) in G . Similarly [p]-neighbourhood graph (closed p -neighbourhood graph) $N_p[G]$ [8] is defined similar in $N_p(G)$ except there is an edge between x and y if and only if $|N[x] \cap N[y]| \geq p$ in G .

Definition 1: [12] The competition graph $C(\vec{G})$ of a digraph $\vec{G} = (V, \vec{E})$ is an undirected graph $G = (V, E)$ which has the same vertex set V and has an edge between distinct two vertices $x, y \in V$ if there exist a vertex $a \in V$ and arcs $\overrightarrow{(x, a)}, \overrightarrow{(y, a)} \in \vec{E}$ in \vec{G} . We say that a graph G is a competition graph if there exists a digraph \vec{G} such that $C(\vec{G}) = G$.

Many variations of competition graph have been available in literature [9], [11], [16], [19], [46]. One of the important graphs, known as p -competition graphs, is defined below.

Definition 2: [19] If p is a positive integer, the p -competition graph $C_p(\vec{G})$ corresponding to the digraph \vec{G} is defined to have a vertex set V with an edge between x and y in V if and only if, for some distinct vertices a_1, a_2, \dots, a_p in

$V, \overrightarrow{(x, a_1)}, \overrightarrow{(y, a_1)}, \overrightarrow{(x, a_2)}, \overrightarrow{(y, a_2)}, \dots, \overrightarrow{(x, a_p)}, \overrightarrow{(y, a_p)}$ are arcs in \vec{G} .

If \vec{G} is thought of as a food web whose vertices are the species in some ecosystem, (x, y) is an edge of $C_p(\vec{G})$ if and only if x and y have at least p common preys. So $C_1(\vec{G})$ is the competition graph.

B. Fuzzy graphs

A fuzzy set A on a set X is characterized by a mapping $m : X \rightarrow [0, 1]$, which is called the membership function. A fuzzy set is denoted by $A = (X, m)$. The support of A is $\text{supp } A = \{x \in X \mid m(x) \neq 0\}$. The core of A is the crisp set of all members whose membership values are 1. A is non trivial if $\text{supp } A$ is non-empty. The height of A is $h(A) = \max\{m(x) \mid x \in X\}$. A is normal if $h(A) = 1$. The membership function of the intersection of two fuzzy sets A and B with membership functions m_A and m_B respectively is defined as the minimum of the two individual membership functions. $m_{A \cap B} = \min\{m_A, m_B\}$. We write $A = (X, m) \leq B = (X, m')$ (fuzzy subset) if $m(x) \leq m'(x)$ for all $x \in X$. The family of all fuzzy subsets is denoted by $\mathcal{F}(X)$. The cardinality of a fuzzy set $A = (X, m)$ is a positive real number $c(A)$ or $|A|$ is the sum of membership values of the elements of X [?]. Now the fuzzy graph is defined below.

Definition 3: [36] A fuzzy graph $\xi = (V, \sigma, \mu)$ is a non-empty set V together with a pair of functions $\sigma : V \rightarrow [0, 1]$ and $\mu : V \times V \rightarrow [0, 1]$ such that for all $x, y \in V$, $\mu(x, y) \leq \sigma(x) \wedge \sigma(y)$ and μ is a symmetric fuzzy relation on σ . Here $\sigma(x)$ and $\mu(x, y)$ represent the membership values of the vertex x and of the edge (x, y) in ξ .

Since μ is well defined, a fuzzy graph has no multiple edges. A loop at a vertex x in a fuzzy graph is represented by $\mu(x, x) \neq 0$. The fuzzy set (V, σ) is called fuzzy vertex set of ξ and the elements of the fuzzy set are called fuzzy vertices. $(V \times V, \mu)$ is called the fuzzy edge set of ξ and the elements of the fuzzy set are called fuzzy edge. An edge is non-trivial if $\mu(x, y) \neq 0$. The fuzzy graph $\xi' = (V', \tau, \nu)$ is called a fuzzy subgraph [24] of ξ if $\tau(x) \leq \sigma(x)$ for all $x \in V'$ and $\nu(x, y) \leq \mu(x, y)$ for all $x, y \in V'$ where $V' \subset V$.

For the fuzzy graph $\xi = (V, \sigma, \mu)$, an edge $(x, y), x, y \in V$ is called strong [13] if $\frac{1}{2} \min\{\sigma(x), \sigma(y)\} \leq \mu(x, y)$ and it is called weak otherwise.

Like crisp digraphs there is fuzzy digraphs which are defined below.

Definition 4: [25] Directed fuzzy graph (fuzzy digraph) $\vec{\xi} = (V, \sigma, \vec{\mu})$ is a non-empty set V together with a pair of functions $\sigma : V \rightarrow [0, 1]$ and $\vec{\mu} : V \times V \rightarrow [0, 1]$ such that for all $x, y \in V$, $\vec{\mu}(x, y) \leq \sigma(x) \wedge \sigma(y)$.

Since $\vec{\mu}$ is well defined, a fuzzy digraph has at most two directed edges (which must have opposite directions) between any two vertices. Here $\vec{\mu}(u, v)$ is denoted by the membership value of the edge $\overrightarrow{(u, v)}$. The loop at a vertex x is represented by $\vec{\mu}(x, x) \neq 0$. Here $\vec{\mu}$ need not be symmetric as $\vec{\mu}(x, y)$ and $\vec{\mu}(y, x)$ may have different values. The underlying crisp graph of directed fuzzy graph is the graph similarly obtained except the directed arcs are replaced by undirected edges.

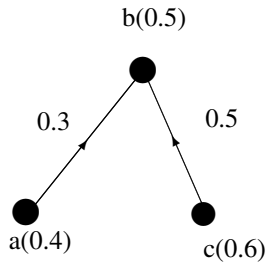


Fig. 1. Example of fuzzy out-neighbourhood and in-neighbourhood of a vertex

A homomorphism [27] between fuzzy graphs ξ and ξ' is a map $h : S \rightarrow S'$ which satisfies $\sigma(x) \leq \sigma'(h(x))$ for all $x \in S$ and $\mu(x, y) \leq \mu'(h(x), h(y))$ for all $x, y \in S$ where S is set of vertices of ξ and S' is that of ξ' .

A weak isomorphism [27] between fuzzy graphs is a bijective homomorphism $h : S \rightarrow S'$ which satisfies $\sigma(x) = \sigma'(h(x))$ for all $x \in S$.

A co-weak isomorphism [27] between fuzzy graphs is a bijective homomorphism $h : S \rightarrow S'$ which satisfies $\mu(x, y) = \mu'(h(x), h(y))$ for all $x, y \in S$.

An isomorphism [27] between fuzzy graphs is a bijective homomorphism $h : S \rightarrow S'$ which satisfies $\sigma(x) = \sigma'(h(x))$ for all $x \in S$ and $\mu(x, y) = \mu'(h(x), h(y))$ for all $x, y \in S$.

III. FUZZY COMPETITION GRAPHS

Now, we come to our main objective of the paper, the fuzzy competition graph. Like crisp graph, fuzzy out-neighbourhood and fuzzy in-neighbourhood of a vertex in directed fuzzy graph are defined below.

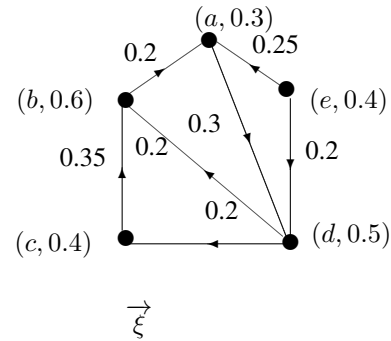
Definition 5: Fuzzy out-neighbourhood of a vertex v of a directed fuzzy graph $\vec{\xi} = (V, \sigma, \vec{\mu})$ is the fuzzy set $\mathcal{N}^+(v) = (X_v^+, m_v^+)$ where $X_v^+ = \{u | \vec{\mu}(v, u) > 0\}$ and $m_v^+ : X_v^+ \rightarrow [0, 1]$ defined by $m_v^+(u) = \vec{\mu}(v, u)$. Similarly, fuzzy in-neighbourhood of a vertex v of a directed fuzzy graph $\vec{\xi} = (V, \sigma, \vec{\mu})$ is the fuzzy set $\mathcal{N}^-(v) = (X_v^-, m_v^-)$ where $X_v^- = \{u | \vec{\mu}(u, v) > 0\}$ and $m_v^- : X_v^- \rightarrow [0, 1]$ defined by $m_v^-(u) = \vec{\mu}(u, v)$.

Example 1: Let $\vec{\xi}$ be a directed fuzzy graph. Let the vertex set be $\{a, b, c\}$ with membership values $\sigma(a) = 0.4$, $\sigma(b) = 0.5$, $\sigma(c) = 0.6$. The membership values of arcs are $\vec{\mu}(a, b) = 0.3$, $\vec{\mu}(c, b) = 0.5$. So $\mathcal{N}^+(a) = \{(b, 0.3)\}$. $\mathcal{N}^-(b) = \{(a, 0.3), (c, 0.5)\}$. (Note that $(a, \sigma(a))$ represents the vertex a with membership value $\sigma(a)$). It is shown in Figure 1.

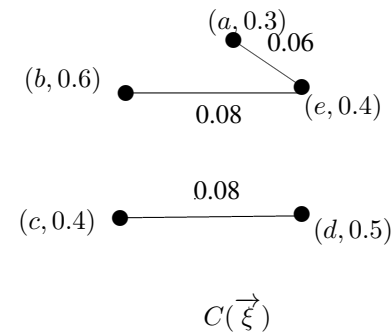
Now, we define fuzzy competition graph.

Definition 6: The fuzzy competition graph $\mathcal{C}(\vec{\xi})$ of a fuzzy digraph $\vec{\xi} = (V, \sigma, \vec{\mu})$ is an undirected fuzzy graph $\xi = (V, \sigma, \mu)$ which has the same fuzzy vertex set as in $\vec{\xi}$ and has a fuzzy edge between two vertices $x, y \in V$ in $\mathcal{C}(\vec{\xi})$ if and only if $\mathcal{N}^+(x) \cap \mathcal{N}^+(y)$ is non-empty fuzzy set in $\vec{\xi}$. The edge membership value between x and y in $\mathcal{C}(\vec{\xi})$ is $\mu(x, y) = (\sigma(x) \wedge \sigma(y))h(\mathcal{N}^+(x) \cap \mathcal{N}^+(y))$.

Example 2: Let $\vec{\xi}$ be a directed fuzzy graph. Let the vertices with membership values of $\vec{\xi}$ be $(a, 0.3)$, $(b, 0.6)$,



(a) : Directed fuzzy graph



(b) : Fuzzy competition graph

Fig. 2. Example of fuzzy competition graph

$(c, 0.4)$, $(d, 0.5)$, $(e, 0.4)$ with membership values of arcs be $\vec{\mu}(b, a) = 0.2$, $\vec{\mu}(c, b) = 0.35$, $\vec{\mu}(d, c) = 0.2$, $\vec{\mu}(e, d) = 0.2$, $\vec{\mu}(e, a) = 0.25$, $\vec{\mu}(a, d) = 0.3$ (shown in Figure 2(a)). The corresponding fuzzy competition graph is shown in Figure 2(b).

Edge in fuzzy competition graphs indicates that there is a competition between two vertices (species) for at least one prey. So the strengths of the edges are important to characterize the competitions.

Now an extension of fuzzy competition graph, called fuzzy k -competition graph is defined in the following.

Definition 7: Let k be a non-negative number. The fuzzy k -competition graph $\mathcal{C}_k(\vec{\xi})$ of a fuzzy digraph $\vec{\xi} = (V, \sigma, \vec{\mu})$ is an undirected fuzzy graph $\xi = (V, \sigma, \mu)$ which has the same fuzzy vertex set as $\vec{\xi}$ and has a fuzzy edge between two vertices $x, y \in V$ in $\mathcal{C}_k(\vec{\xi})$ if and only if $|\mathcal{N}^+(x) \cap \mathcal{N}^+(y)| > k$. The edge membership value between x and y in $\mathcal{C}_k(\vec{\xi})$ is $\mu(x, y) = \frac{(k' - k)}{k'} [\sigma(x) \wedge \sigma(y)] h(\mathcal{N}^+(x) \cap \mathcal{N}^+(y))$ where $k' = |\mathcal{N}^+(x) \cap \mathcal{N}^+(y)|$.

So fuzzy k -competition graph is simply fuzzy competition graph when $k = 0$. An example of fuzzy 0.15-competition graph is given below.

Example 3: Let $\vec{\xi}$ be a directed fuzzy graph (Figure 3(a)). Let vertices with membership values of $\vec{\xi}$ be $(x, 0.4)$, $(y, 0.6)$, $(a, 0.6)$, $(b, 0.7)$, $(c, 0.8)$, and the membership values of arcs be $\vec{\mu}(x, a) = 0.3$, $\vec{\mu}(x, b) = 0.35$, $\vec{\mu}(x, c) = 0.36$,

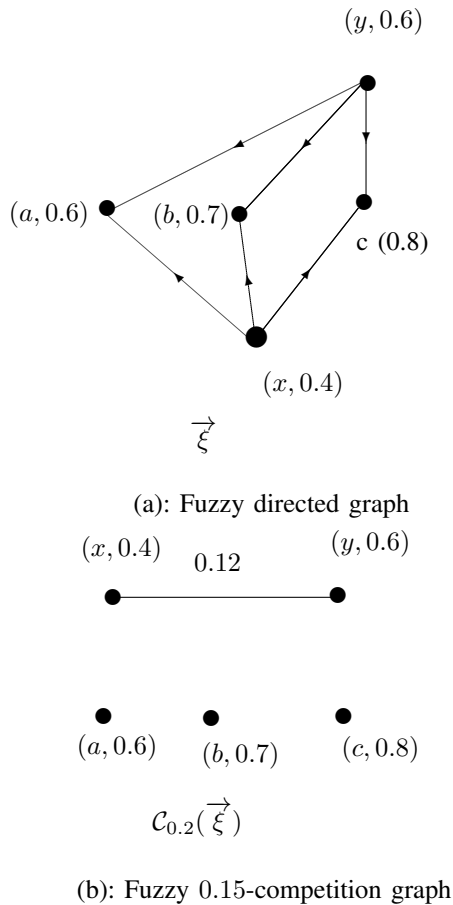


Fig. 3. Example of fuzzy 0.15-competition graph

$\vec{\mu}(y, a) = 0.6, \vec{\mu}(y, b) = 0.5, \vec{\mu}(y, c) = 0.45$. The corresponding fuzzy 0.15-competition graph is shown in Figure 3(b).

Theorem 1: Let $\vec{\xi} = (V, \sigma, \vec{\mu})$ be a fuzzy digraph. If $\mathcal{N}^+(x) \cap \mathcal{N}^+(y)$ is singleton set, then the edge (x, y) of $C(\vec{\xi})$ is strong if and only if $|\mathcal{N}^+(x) \cap \mathcal{N}^+(y)| > 0.5$.

Proof. Here $\vec{\xi} = (V, \sigma, \vec{\mu})$ is a fuzzy digraph. Let $\mathcal{N}^+(x) \cap \mathcal{N}^+(y) = \{(a, m)\}$, where m is the membership value of the element a . Here, $|\mathcal{N}^+(x) \cap \mathcal{N}^+(y)| = m = h(\mathcal{N}^+(x) \cap \mathcal{N}^+(y))$. So, $\mu(x, y) = m \times \sigma(x) \wedge \sigma(y)$. Hence the edge (x, y) in $C(\vec{\xi})$ is strong if and only if $m > 0.5$. \square

If all the edges of a fuzzy digraph are strong, then all the edges of the corresponding fuzzy competition graph may not be strong. This result is illustrated below. Let us consider two vertices x, y with $\sigma(x) = 0.3, \sigma(y) = 0.4$ in a fuzzy digraph such that the vertices have a common prey z with $\sigma(z) = 0.2$. Let $\vec{\mu}(x, z) = 0.2, \vec{\mu}(y, z) = 0.15$. Clearly, the edges (x, z) and (y, z) are strong. But membership value of the edge (x, y) in corresponding competition graph is $0.3 \times 0.15 = 0.045$. Hence the edge is not strong as $\frac{0.045}{0.3} = 0.15 < 0.5$. But if all the edges are strong of a fuzzy digraph, then a result can be found from the following theorem.

Theorem 2: If all the edges of a fuzzy digraph $\vec{\xi} = (V, \sigma, \vec{\mu})$ be strong, then $\frac{\mu(x, y)}{(\sigma(x) \wedge \sigma(y))^2} > 0.5$ for all edge (x, y)

in $C(\vec{\xi})$.

Proof. Let $\vec{\xi} = (V, \sigma, \vec{\mu})$ be a fuzzy digraph and every edge of $\vec{\xi}$ be strong i.e., $\frac{\vec{\mu}(x, y)}{\sigma(x) \wedge \sigma(y)} > 0.5$ for all edge (x, y) in $\vec{\xi}$.

Let the corresponding fuzzy competition graph be $C(\vec{\xi}) = (V, \sigma, \mu)$.

Case 1: Let $\mathcal{N}^+(x) \cap \mathcal{N}^+(y)$ be a null set for all $x, y \in V$. Then there exist no edge in $C(\vec{\xi})$ between x and y .

Case 2: $\mathcal{N}^+(x) \cap \mathcal{N}^+(y)$ is not a null set. Let $\mathcal{N}^+(x) \cap \mathcal{N}^+(y) = \{(a_1, m_1), (a_2, m_2), \dots, (a_z, m_z)\}$, where $m_i, i = 1, 2, \dots, z$ are the membership values of $a_i, i = 1, 2, \dots, z$, respectively. So $m_i = \min\{\vec{\mu}(x, a_i), \vec{\mu}(y, a_i)\}, i = 1, 2, \dots, z$. Let $h(\mathcal{N}^+(x) \cap \mathcal{N}^+(y)) = \max\{m_i, i = 1, 2, \dots, z\} = m_{max}$.

$\mu(x, y) = (\sigma(x) \wedge \sigma(y))h(\mathcal{N}^+(x) \cap \mathcal{N}^+(y)) = m_{max} \times \sigma(x) \wedge \sigma(y)$. Hence $\frac{\mu(x, y)}{(\sigma(x) \wedge \sigma(y))^2} = \frac{m_{max}}{\sigma(x) \wedge \sigma(y)} > 0.5$. \square

We have seen that if height of intersection between two out neighbourhoods of two vertices of a fuzzy digraph is greater than 0.5, the edge between the two vertices in corresponding fuzzy competition graph is strong. This result is not true in corresponding fuzzy k -competition graph. A related result is presented below.

Theorem 3: Let $\vec{\xi} = (V, \sigma, \vec{\mu})$ be a fuzzy digraph. If $h(\mathcal{N}^+(x) \cap \mathcal{N}^+(y)) = 1$ and $|\mathcal{N}^+(x) \cap \mathcal{N}^+(y)| > 2k$, then the edge (x, y) is strong in $C_k(\vec{\xi})$.

Proof. Let $\vec{\xi} = (V, \sigma, \vec{\mu})$ be a fuzzy digraph and $C_k(\vec{\xi}) = (V, \sigma, \mu)$ be the corresponding fuzzy k -competition graph. Also let, $h(\mathcal{N}^+(x) \cap \mathcal{N}^+(y)) = 1$ and $|\mathcal{N}^+(x) \cap \mathcal{N}^+(y)| > 2k$.

Now, $\mu(x, y) = \frac{k'-k}{k'} \sigma(x) \wedge \sigma(y) h(\mathcal{N}^+(x) \cap \mathcal{N}^+(y))$, where $k' = |\mathcal{N}^+(x) \cap \mathcal{N}^+(y)|$. So, $\mu(x, y) = \frac{k'-k}{k'} \sigma(x) \wedge \sigma(y)$. Hence $\frac{\mu(x, y)}{\sigma(x) \wedge \sigma(y)} = \frac{k'-k}{k'} > 0.5$ as $k' > 2k$. Hence the edge (x, y) is strong. \square

A. Fuzzy isolated vertex

Isolated vertex in crisp graph is a vertex which has no incident edge i.e. a vertex of degree 0. In fuzzy graph, degree of a vertex is the sum of the membership values of incident edges. If the degree of a vertex in fuzzy graph is zero approximately, then the vertex can be assumed as isolated vertex. The formal definition of fuzzy isolated vertex is given below.

Definition 8: Let $\xi = (V, \sigma, \mu)$ be a fuzzy graph and ϵ be a pre-assigned positive real number. A vertex x is said to be fuzzy isolated vertex if the degree of x is less than ϵ i.e. $d(x) < \epsilon$.

An example of isolated vertex is given as follows.

Example 4: Let $\epsilon = 0.05$. In Fig. 4, the degree of the vertex b is $0.01 + 0.03 = 0.04$. As $d(b) < \epsilon$, b is said to be fuzzy isolated vertex. By similar reason, a and c are fuzzy isolated vertices.

The fuzzy isolated vertices are not same like crisp isolated vertices. Fuzzy isolated vertices may have an edge of small strength. The definition of strong isolated vertices are given below.

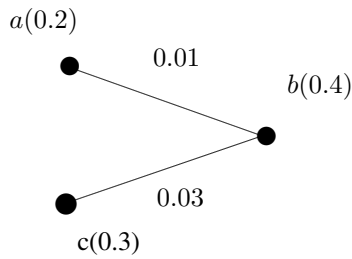


Fig. 4. An example of fuzzy isolated vertex.

Definition 9: Let $\xi = (V, \sigma, \mu)$ be a fuzzy graph. A vertex $x \in V$ is said to be strong isolated vertex in ξ if $d(x) = 0$.

In fuzzy graph, vertices which are not connected to any other vertices are called strong isolated vertices. So, strong isolated vertices are comparable with crisp isolated vertices.

B. Fuzzy competition number

Fuzzy competition number is associated with a fuzzy competition graph which is defined below.

Definition 10: Let $\vec{\xi}$ be an arbitrary fuzzy digraph and $C(\vec{\xi})$ be the corresponding fuzzy competition graph. The fuzzy competition number of a fuzzy graph ψ is the minimum number of isolated fuzzy vertices such that ψ along with these isolated fuzzy vertices (say ξ) is the fuzzy competition graph of $\vec{\xi}$ i.e. $C(\vec{\xi}) = \xi$.

This concept is illustrated in the following example.

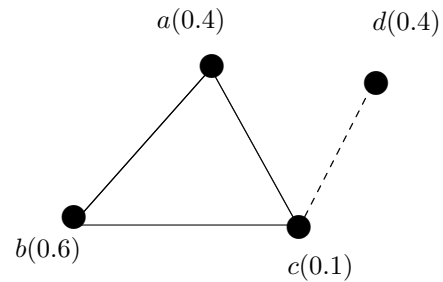
Example 5: Let $\psi = (V, \sigma, \mu)$ be a fuzzy graph (see Fig. 5(a)) with $V = \{(a, 0.4), (b, 0.6), (c, 0.1)\}$ and $E = \{((a, b), 0.2), ((b, c), 0.1), ((c, a), 0.1)\}$. Now this fuzzy graph along with an isolated fuzzy vertex $d(0.4)$ and an edge $((c, d), 0.04)$ is drawn. Let $\xi = \psi \cup \{(d, 0.4), ((c, d), 0.04)\}$. Now in Fig 5(b), a fuzzy multi-digraph $\vec{\xi}$ is shown. Clearly $C(\vec{\xi}) = \xi$. Also, d is said to be fuzzy isolated vertex if $\epsilon = 0.05$. Thus the fuzzy competition number of ψ is 1.

An important theorem related to strong isolated vertices is given below.

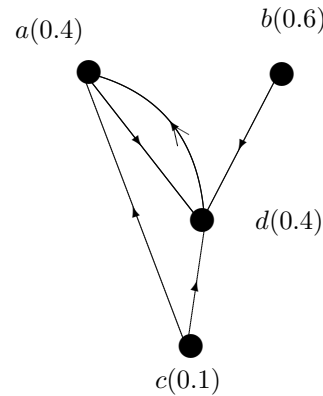
Theorem 4: A path of length m along with a strong isolated vertex may be a fuzzy competition graph of a fuzzy directed tree of $m + 1$ vertices.

Proof. Let $P_m = (V, \sigma, \mu)$ be a fuzzy path where $V = \{v_1, v_2, \dots, v_m\}$. We take another vertex u which is distinct from the vertices of P_m . So, the fuzzy path together with the strong isolated vertex has $m + 1$ vertices. Now, we construct the directed fuzzy graph whose fuzzy competition graph is $P_m \cup \{u\}$. Keeping the concept of fuzzy competition graph of a fuzzy digraph, we construct the directed fuzzy edges $(\overrightarrow{v_i, u})$, $i = 1, 2, \dots, m$. Now this directed fuzzy graph is a directed fuzzy tree T_{m+1} of $m + 1$ vertices. Also, $C(T_{m+1}) = P_m \cup \{u\}$. Hence the result. \square

The above theorem can be extended as follows. Some disjoint paths along with a strong isolated vertex may be a fuzzy competition graph of a fuzzy directed tree. Let the disjoint paths be $P_{m_1}, P_{m_2}, \dots, P_{m_n}$, then the number of vertices of the corresponding directed fuzzy graph is



(a): $\psi \cup \{(d, 0.4), ((c, d), 0.04)\}$



(b): $\vec{\xi}$

Fig. 5. Example of fuzzy competition number.

$$m_1 + m_2 + \dots + m_n + 1.$$

From Theorem 4, it is easy to observe that the fuzzy competition number of a path is 1. Like crisp graph the fuzzy competition numbers can be found as follows.

The competition number of a fuzzy chordal graph which has no strong isolated vertex is 1.

If a fuzzy graph is triangle free, then the fuzzy competition number is equal to two more than the difference between the number of edges and number of vertices.

The competition number of fuzzy complete graph is one.

C. Fuzzy neighbourhood graphs

The fuzzy open neighbourhood and fuzzy closed neighbourhood of a vertex in fuzzy graph are defined below.

Definition 11: Fuzzy open neighbourhood of a vertex v of a fuzzy graph $\xi = (V, \sigma, \mu)$ is the fuzzy set $\mathcal{N}(v) = (X_v, m_v)$ where $X_v = \{u | \mu(v, u) > 0\}$ and $m_v : X_v \rightarrow [0, 1]$ defined by $m_v(u) = \mu(v, u)$. For each vertex $v \in V$, we define fuzzy singleton set, $A_v = (\{v\}, \sigma')$ such that $\sigma' : \{v\} \rightarrow [0, 1]$ defined by $\sigma'(v) = \sigma(v)$. Fuzzy closed neighbourhood of a vertex v is $\mathcal{N}[v] = \mathcal{N}(v) \cup A_v$.

In this section, fuzzy open neighbourhood graphs are defined and then fuzzy closed neighbourhood graphs. Based on these fuzzy graphs fuzzy k -neighbourhood graphs of open and closed types are defined.

Definition 12: Let $\xi = (V, \sigma, \mu)$ be a fuzzy graph. Fuzzy open neighbourhood graph of ξ is a fuzzy graph $\mathcal{N}(\xi) = (V, \sigma, \mu')$ whose fuzzy vertex set is same as ξ and has a fuzzy edge between two vertices x and $y \in V$ in $\mathcal{N}(\xi)$ if and only if $\mathcal{N}(x) \cap \mathcal{N}(y)$ is non-empty fuzzy set in ξ and $\mu' : V \times V \rightarrow [0, 1]$ such that $\mu'(x, y) = [\sigma(x) \wedge \sigma(y)]h(\mathcal{N}(x) \cap \mathcal{N}(y))$.

Definition 13: Let $\xi = (V, \sigma, \mu)$ be a fuzzy graph. Fuzzy closed neighbourhood graph of ξ is a fuzzy graph $\mathcal{N}[\xi] = (V, \sigma, \mu')$ whose fuzzy vertex set is same as ξ and has a fuzzy edge between two vertices x and $y \in V$ in $\mathcal{N}[\xi]$ if and only if $\mathcal{N}[x] \cap \mathcal{N}[y]$ is non-empty fuzzy set in ξ and $\mu' : V \times V \rightarrow [0, 1]$ such that $\mu'(x, y) = [\sigma(x) \wedge \sigma(y)]h(\mathcal{N}[x] \cap \mathcal{N}[y])$.

Definition 14: Let $\xi = (V, \sigma, \mu)$ be a fuzzy graph. Fuzzy (k)-neighbourhood graph (read as open fuzzy k -neighbourhood graph) of ξ is a fuzzy graph $\mathcal{N}_k(\xi) = (V, \sigma, \mu')$ whose vertex set is same as ξ and has an edge between two vertices x and $y \in V$ in $\mathcal{N}_k(\xi)$ if and only if $|\mathcal{N}(x) \cap \mathcal{N}(y)| > k$ in ξ and $\mu' : V \times V \rightarrow [0, 1]$ such that $\mu'(x, y) = \frac{(k'-k)}{k'}[\sigma(x) \wedge \sigma(y)]h(\mathcal{N}(x) \cap \mathcal{N}(y))$ where $k' = |\mathcal{N}(x) \cap \mathcal{N}(y)|$.

Definition 15: Let $\xi = (V, \sigma, \mu)$ be a fuzzy graph. Fuzzy [k]-neighbourhood graph (read as fuzzy closed k -neighbourhood graph) of ξ is a fuzzy graph $\mathcal{N}_k[\xi] = (V, \sigma, \mu')$ whose fuzzy vertex set is same as ξ and has a fuzzy edge between two vertices x and $y \in V$ in $\mathcal{N}_k[\xi]$ if and only if $|\mathcal{N}[x] \cap \mathcal{N}[y]| > k$ in ξ and $\mu' : V \times V \rightarrow [0, 1]$ such that $\mu'(x, y) = \frac{(k'-k)}{k'}[\sigma(x) \wedge \sigma(y)]h(\mathcal{N}[x] \cap \mathcal{N}[y])$ where $k' = |\mathcal{N}[x] \cap \mathcal{N}[y]|$.

Theorem 5: For every edge of a fuzzy graph ξ , there exists one edge in $\mathcal{N}[\xi]$.

Proof. Let (x, y) be an edge of a fuzzy graph $\xi = (V, \sigma, \mu)$. Let the corresponding closed neighbourhood graph be $\mathcal{N}[\xi] = (V, \sigma, \nu)$. Then $x, y \in \mathcal{N}[x]$ and $x, y \in \mathcal{N}[y]$. So $x, y \in \mathcal{N}[x] \cap \mathcal{N}[y]$. Hence $h(\mathcal{N}[x] \cap \mathcal{N}[y]) \neq 0$. Now, $\nu(x, y) = \sigma(x) \wedge \sigma(y)h(\mathcal{N}[x] \cap \mathcal{N}[y]) \neq 0$. So for every edge (x, y) in ξ , there exists an edge (x, y) in $\mathcal{N}[\xi]$. \square

Definition 16: Let $\vec{\xi} = (V, \sigma, \vec{\mu})$ be a fuzzy digraph. The underlying fuzzy graph of $\vec{\xi}$ is denoted by $\mathcal{U}(\xi)$ and is defined as $\mathcal{U}(\xi) = (V, \sigma, \mu)$ where $\mu(u, v) = \min\{\vec{\mu}(u, v), \vec{\mu}(v, u)\}$ for all $u, v \in V$.

A relation between fuzzy (k)-neighbourhood graph and fuzzy k -competition graph is established below.

Theorem 6: If the symmetric fuzzy digraph $\vec{\xi}$ is loop less, $\mathcal{C}_k(\vec{\xi}) = \mathcal{N}_k(\mathcal{U}(\xi))$ where $\mathcal{U}(\xi)$ is the fuzzy graph underlying $\vec{\xi}$.

Proof. Let a directed fuzzy graph be $\vec{\xi} = (V, \sigma, \vec{\mu})$ and the corresponding underlying fuzzy graph be $\mathcal{U}(\xi) = (V, \sigma, \mu)$. Also let $\mathcal{C}_k(\vec{\xi}) = (V, \sigma, \nu)$ and $\mathcal{N}_k(\mathcal{U}(\xi)) = (V, \sigma, \nu')$. The fuzzy vertex set of $\vec{\xi}$ is equal to $\mathcal{C}_k(\vec{\xi})$. Also an underlying fuzzy graph has the same fuzzy vertex set as the directed fuzzy graph. Hence $\mathcal{N}_k(\mathcal{U}(\xi))$ has the same fuzzy vertex set as $\vec{\xi}$. Now we need to show that $\nu(x, y) = \nu'(x, y)$ for all $x, y \in V$. If $\nu(x, y) = 0$ in $\mathcal{C}_k(\vec{\xi})$ then $|\mathcal{N}^+(x) \cap \mathcal{N}^+(y)| \leq k$. As $\vec{\xi}$ is symmetric fuzzy set, $|\mathcal{N}[x] \cap \mathcal{N}[y]| \leq k$ in $\mathcal{U}(\xi)$. So $\nu'(x, y) = 0$.

If $|\mathcal{N}^+(x) \cap \mathcal{N}^+(y)| > k$ then $\nu(x, y) > 0$ in $\mathcal{C}_k(\vec{\xi})$. So $\nu(x, y) = \frac{(k'-k)}{k'}[\sigma(x) \wedge \sigma(y)]h(\mathcal{N}^+(x) \cap \mathcal{N}^+(y))$ where $k' = |\mathcal{N}^+(x) \cap \mathcal{N}^+(y)|$. As $\vec{\xi}$ is symmetric fuzzy digraph, $|\mathcal{N}[x] \cap \mathcal{N}[y]| > k$ in $\mathcal{U}(\xi)$. So $\nu' = \frac{(k''-k)}{k''}[\sigma(x) \wedge \sigma(y)]h(\mathcal{N}[x] \cap \mathcal{N}[y])$ where $k'' = |\mathcal{N}[x] \cap \mathcal{N}[y]|$. It is clear that $h(\mathcal{N}^+(x) \cap \mathcal{N}^+(y))$ in $\vec{\xi}$ is equal to $h(\mathcal{N}[x] \cap \mathcal{N}[y])$ in $\mathcal{U}(\xi)$ as $\vec{\xi}$ is symmetric. $k' = k''$ for similar reason. Hence $\nu(x, y) = \nu'(x, y)$ for all $x, y \in V$. \square

Similarly, a relation between fuzzy [k]-neighbourhood graph and fuzzy k -competition graph is established below.

Theorem 7: If the symmetric fuzzy digraph $\vec{\xi}$ has loop at every vertex, then $\mathcal{C}_k(\vec{\xi}) = \mathcal{N}_k[\mathcal{U}(\xi)]$ where $\mathcal{U}(\xi)$ is the loop less fuzzy graph underlying $\vec{\xi}$.

Proof. Let a directed fuzzy graph be $\vec{\xi} = (V, \sigma, \vec{\mu})$ and the corresponding underlying loop less graph be $\mathcal{U}(\xi) = (V, \sigma, \mu)$. Also let $\mathcal{C}_k(\vec{\xi}) = (V, \sigma, \nu)$ and $\mathcal{N}_k[\mathcal{U}(\xi)] = (V, \sigma, \nu')$. The fuzzy vertex set of $\vec{\xi}$ is equal to $\mathcal{C}_k(\vec{\xi})$. Also an underlying fuzzy graph has the same fuzzy vertex set as the directed fuzzy graph. Hence $\mathcal{N}_k[\mathcal{U}(\xi)]$ has the same fuzzy vertex set as $\vec{\xi}$. Now we need to show that $\nu(x, y) = \nu'(x, y)$ for all $x, y \in V$. As the directed fuzzy graph $\vec{\xi}$ has a loop at every vertex, out-neighbourhood of each vertex contains the vertex itself. Hence if $\nu(x, y) = 0$ in $\mathcal{C}_k(\vec{\xi})$ then $|\mathcal{N}^+(x) \cap \mathcal{N}^+(y)| \leq k$. As $\vec{\xi}$ is symmetric fuzzy set, $|\mathcal{N}(x) \cap \mathcal{N}(y)| \leq k$ in $\mathcal{U}(\xi)$. So $\nu'(x, y) = 0$.

If $|\mathcal{N}^+(x) \cap \mathcal{N}^+(y)| > k$ then $\nu(x, y) > 0$ in $\mathcal{C}_k(\vec{\xi})$. So $\nu(x, y) = \frac{(k'-k)}{k'}[\sigma(x) \wedge \sigma(y)]h(\mathcal{N}^+(x) \cap \mathcal{N}^+(y))$ where $k' = |\mathcal{N}^+(x) \cap \mathcal{N}^+(y)|$. As $\vec{\xi}$ is symmetric fuzzy digraph, $|\mathcal{N}(x) \cap \mathcal{N}(y)| > k$ in $\mathcal{U}(\xi)$. So $\nu' = \frac{(k''-k)}{k''}[\sigma(x) \wedge \sigma(y)]h(\mathcal{N}(x) \cap \mathcal{N}(y))$ where $k'' = |\mathcal{N}(x) \cap \mathcal{N}(y)|$. It is clear that $h(\mathcal{N}^+(x) \cap \mathcal{N}^+(y))$ in $\vec{\xi}$ is equal to $h(\mathcal{N}(x) \cap \mathcal{N}(y))$ in $\mathcal{U}(\xi)$ and $k' = k''$ as $\vec{\xi}$ is symmetric. Hence $\nu(x, y) = \nu'(x, y)$ for all $x, y \in V$. \square

IV. ISOMORPHISM IN FUZZY COMPETITION GRAPH

Isomorphism on fuzzy graphs are well known in literature. Here the isomorphism in fuzzy digraphs are introduced. A homomorphism of fuzzy digraphs $\vec{\xi}$ and $\vec{\xi}'$ is a map $h : S \rightarrow S'$ which satisfies $\sigma(x) \leq \sigma'(h(x))$ for all $x \in S$ and $\mu(x, y) \leq \mu'(h(x), h(y))$ for all $x, y \in S$ where S is the set of vertices of $\vec{\xi}$ and S' is that of $\vec{\xi}'$.

A weak isomorphism between fuzzy digraphs is a bijective homomorphism $h : S \rightarrow S'$ which satisfies $\sigma(x) = \sigma'(h(x))$ for all $x \in S$.

A co-weak isomorphism between fuzzy digraphs is a bijective homomorphism $h : S \rightarrow S'$ which satisfies $\mu(x, y) = \mu'(h(x), h(y))$ for all $x, y \in S$.

An isomorphism between fuzzy graphs of fuzzy digraphs is a bijective homomorphism $h : S \rightarrow S'$ which satisfies $\sigma(x) = \sigma'(h(x))$ for all $x \in S$ and $\mu(x, y) = \mu'(h(x), h(y))$ for all $x, y \in S$.

Isomorphism between fuzzy graphs is an equivalence relation. But, if there is an isomorphism between two fuzzy

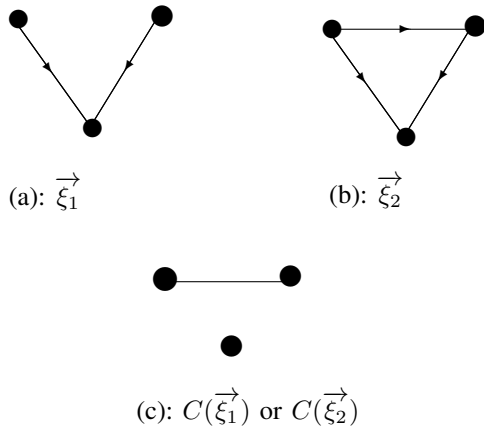


Fig. 6. Fuzzy competition graphs are isomorphic but corresponding digraphs are not isomorphic.

graph and one is fuzzy competition graph, then the other will be fuzzy competition graph. But, the corresponding digraphs may not be isomorphic. This result can be shown as follows.

Remark 1: Let $\vec{\xi}_1$ and $\vec{\xi}_2$ be two digraphs such that $C(\vec{\xi}_1)$ and $C(\vec{\xi}_2)$ are isomorphic. But $\vec{\xi}_1$ and $\vec{\xi}_2$ may not be isomorphic.

This remark can be illustrated from the following example. In Fig. 6(a) and Fig. 6(b), two fuzzy digraphs are shown. These fuzzy digraphs are not isomorphic as degree of vertices of these fuzzy digraphs are not same. But, the corresponding fuzzy competition graphs are isomorphic.

If two fuzzy digraphs are isomorphic, their corresponding fuzzy competition graphs must be isomorphic. This can be established in the following theorem.

Theorem 8: If two fuzzy digraphs $\vec{\xi}_1$ and $\vec{\xi}_2$ are isomorphic, then $C(\vec{\xi}_1)$ and $C(\vec{\xi}_2)$ are isomorphic.

Proof. Here two fuzzy digraphs $\vec{\xi}_1$ and $\vec{\xi}_2$ are isomorphic. Then there exists one to one correspondence between vertices and edges. Also the membership values of the vertices and edges are preserved. So the adjacency of edges are preserved. Then it is easy to observe that $C(\vec{\xi}_1)$ and $C(\vec{\xi}_2)$ are isomorphic. \square

Similarly, we can prove that if two fuzzy digraphs $\vec{\xi}_1$ and $\vec{\xi}_2$ are isomorphic, then $C_k(\vec{\xi}_1)$ and $C_k(\vec{\xi}_2)$ are isomorphic.

V. CONCLUSIONS

This study introduces fuzzy competition graphs and fuzzy k -competition graph. In these fuzzy graphs, if there is a common out neighbourhood of two vertices, then there will be an edge between the vertices. Thus the fuzzy competition graph can be stated as 1-step fuzzy competition graph. In future, m -step fuzzy competition graphs can be investigated as an extension of this study. Besides, fuzzy isolated vertices and fuzzy competition numbers are introduced. The competition numbers of paths and several graphs are investigated. But, fuzzy competition number of any fuzzy graphs is not calculated here. This can be investigated in future. Isomorphism in

fuzzy graphs is new in the research field. Isomorphism relation between two fuzzy competition graphs are established. Also, some fundamental results related to fuzzy competition graphs are presented. These results will be helpful in ecosystem, competitive markets, etc.

REFERENCES

- [1] B. D. Acharya and M. N. Vartak, Open neighbourhood graphs, Research Report 07, IIT Bombay, 1973.
- [2] M. Akram and W. A. Dudek, Interval-valued fuzzy graphs, *Computers and Mathematics with Applications*, 61(2), 289-299, 2011.
- [3] M. Akram, W. A. Dudek, Intuitionistic fuzzy hypergraphs with applications, *Information Sciences*, 218, 182-193, 2013.
- [4] M. Akram, Bipolar fuzzy graphs with applications, *Knowledge Based System*, 39, 1-8, 2013.
- [5] K. R. Bhutani and A. Battou, On M -strong fuzzy graphs, *Information Sciences*, 155(12), 103-109, 2003.
- [6] K. R. Bhutani and A. Rosenfeld, Strong arcs in fuzzy graphs, *Information Sciences*, 152, 319-322, 2003.
- [7] K. R. Bhutani, J. Moderson and A. Rosenfeld, On degrees of end nodes and cut nodes in fuzzy graphs, *Iranian Journal of Fuzzy Systems*, 1(1), 57-64, 2004.
- [8] R. C. Brigham and R. D. Dutton, On neighbourhood graphs, *Journal of Combinatorics, Information, and System Sciences*, 12, 75-85, 1987.
- [9] R.C. Brigham, F. R. McMorris and R. P. Vitray, Tolerance competition graphs, *Linear Algebra and its Application*, 217, 41-52, 1995.
- [10] C. Cable, K. F. Jones, J. R. Lundgren and S. Seager, Niche graphs, *Discrete Applied Mathematics*, 23(3), 231-241, 1989.
- [11] H. H. Cho, S. R. Kim and Y. Nam, The m -step competition graph of a diagraph, *Discrete Applied Mathematics*, 105(1-3), 115-127, 2000.
- [12] J. E. Cohen, Interval graphs and food webs: a finding and a problem, Document 17696-PR, RAND Corporation, Santa Monica, CA (1968).
- [13] C. Eslahchi and B. N. Onaghe, Vertex Strength of Fuzzy Graphs, *International Journal of Mathematics and Mathematical Sciences*, Volume 2006, Article ID 43614, Pages 1-9, DOI 10.1155/IJMMS/2006/43614.
- [14] P. Ghosh, K. Kundu and D. Sarkar, Fuzzy graph representation of a fuzzy concept lattice, *Fuzzy Sets and Systems*, 161(12), 1669-1675, 2010.
- [15] M. C. Gulumbic and A. Trenk, *Tolerance Graphs*, Cambridge University Press, (2004).
- [16] G. Isaak, S. R. Kim, T. A. McKee, F.R. McMorris and F. S. Roberts, 2-competition graphs, *SIAM J. Disc. Math.*, 5(4), 524-538, 1992.
- [17] J. B. Jenson and G. Z. Gutin, *Digraphs: Theory, Algorithms and Applications*, Springer-verlag, 2009.
- [18] S. R. Kim, Graphs with one hole and competition number one, *J. Korean Math. Soc.*, 42(6), 1251-1264, 2005.
- [19] S. R. Kim, T. A. McKee, F.R. McMorris and F. S. Roberts, p -competition graphs, *Linear Algebra and its Application*, 217, 167-178, 1995.
- [20] L. T. Koczy, Fuzzy graphs in the evaluation and optimization of networks, *Fuzzy Sets and Systems*, 46, 307-319, 1992.
- [21] J. R. Lundgren and J. S. Maybee, Food webs with interval competition graph, In *Graphs and Applications: Proceedings of the first colorado symposium on graph theory*, Wiley, Newyork, 1984.
- [22] S. Mathew and M.S. Sunitha, Types of arcs in a fuzzy graph, *Information Sciences*, 179, 1760-1768, 2009.
- [23] S. Mathew and M.S. Sunitha, Node connectivity and arc connectivity of a fuzzy graph, *Information Sciences*, 180(4), 519-531, 2010.
- [24] J. N. Mordeson and P. S. Nair, *Fuzzy graphs and hypergraphs*, Physica Verlag, 2000.
- [25] J. N. Mordeson and P. S. Nair, Successor and source of (fuzzy) finite state machines and (fuzzy) directed graphs, *Information Sciences*, 95(1-2), 113-124, 1996.
- [26] S. Muoz, M. T. Ortuio, J. Ramirez and J. Yez, Coloring fuzzy graphs, *Omega*, 33(3), 211-221, 2005.
- [27] A. Nagoorgani and K. Radha, On regular fuzzy graphs, *Journal of Physical Sciences*, 12, 33-40, 2008.
- [28] A. Nagoorgani and J. Malarvizhi, Isomorphism properties of strong fuzzy graphs, *International Journal of Algorithms, Computing and Mathematics*, 2(1), 39-47, 2009.
- [29] A. Nagoorgani and P. Vadivel, Relations between the parameters of independent domination and irredundance in fuzzy graph, *International Journal of Algorithms, Computing and Mathematics*, 2(1), 15-19, 2009.

- [30] A. Nagoorgani and P. Vijayalakshmi, Insestive arc in domination of fuzzy graph, *Int. J. Contemp. Math. Sciences*, 6(26), 1303-1309, 2011.
- [31] A. Nagoorgani and R. J. Hussain, Fuzzy effective distance k -dominating sets and their applications, *International Journal of Algorithms, Computing and Mathematics*, 2(3), 25-36, 2009.
- [32] P. S. Nair and S. C. Cheng, Cliques and fuzzy cliques in fuzzy graphs, IFSA World Congress and 20th NAFIPS International Conference, 4, 2277 - 2280, 2001.
- [33] P. S. Nair, Perfect and precisely perfect fuzzy graphs, *Fuzzy Information Processing Society*, 19-22, 2008.
- [34] C. Natarajan and S. K. Ayyasawamy, On strong (weak) domination in fuzzy graphs, *World Academy of Science, Engineering and Technology*, 67, 247-249, 2010.
- [35] A. Raychaudhuri and F. S. Roberts, Generalized competition graphs and their applications, *IX symposium on operations research*, Part I, Sections 14 (Osnabruck, 1984) Athenaum/Hain/Hanstein, Konigstein, Methods Oper. Res. 49,295-311, 1985.
- [36] A. Rosenfeld, Fuzzy graphs, in: L.A. Zadeh, K.S. Fu, M. Shimura (Eds.), *Fuzzy Sets and Their Applications*, Academic Press, New York, 77-95, 1975.
- [37] S. Samanta and M. Pal, Fuzzy tolerance graphs, *International Journal of Latest Trends in Mathematics*, 1(2), 57-67, 2011.
- [38] S. Samanta and M. Pal, Fuzzy threshold graphs, *CIIT International Journal of Fuzzy Systems*, 3(12), 360-364, 2011.
- [39] S. Samanta and M. Pal, Irregular bipolar fuzzy graphs, *International Journal of Applications of Fuzzy Sets*, 2, 91-102, 2012.
- [40] S. samanta and M. Pal, Bipolar fuzzy hypergraphs, *International Journal of Fuzzy Logic Systems*, 2(1), 17 – 28, 2012.
- [41] S. Samanta, M. Pal and A. Pal, Some more results on bipolar fuzzy sets and bipolar fuzzy intersection graphs, To appear in *The Journal of Fuzzy Mathematics*.
- [42] S. Samanta and M. Pal, A new approach to social networks based on fuzzy graphs, To appear in *Journal of Mass Communication and Journalism*.
- [43] Y. Sano, The competition-common enemy graphs of digraphs satisfying Conditions $C'(p)$ and $C''(p)$, arXiv:1006.2631v2 [math.CO], 2010.
- [44] Y. Sano, Characterizations of competition multigraphs, *Discrete Applied Mathematics*, 157(13), 2978-2982, 2009.
- [45] D. D. Scott, The competition-common enemy graph of a digraph, *Discrete Appl. Math.*, 17, 269-280, 1987.
- [46] M. Sonnatag and H. M. Teichert, Competition hypergraphs, *Discrete Appl. Math.*, 143, 324-329, 2004.
- [47] A. Somasundaram and S. Somasundaram, Domination in fuzzy graphs-1, *Pattern Recognition Letters*, 19(9), 787-791, 1998.

Zernike Moment Feature Extraction for Handwritten Devanagari (Marathi) Compound Character Recognition

Karbhari V. Kale, Senior Member, IEEE *, Prapti D. Deshmukh †, Shriniwas V. Chavan, Student Member, IEEE ‡,
Majharoddin M. Kazi, Student Member, IEEE §, Yogesh S. Rode, Student Member, IEEE ¶

*‡§Department of Computer Science and IT, Dr. B. A. M. University, Aurangabad, Maharashtra, India - 431004

†Dr. G. Y. Pathrikar College of Computer Science, MGM, Maharashtra, India - 431005

‡Department of Computer Science, MSS's ACS College, Ambad, Jalna, Maharashtra, India - 431203

*Email: kvkale91@gmail.com, †prapti.research@gmail.com, ‡shripc@gmail.com, §mazhar940@gmail.com, ¶ys.rode@gmail.com

Abstract—Compound character recognition of Devanagari script is one of the challenging tasks since the characters are complex in structure and can be modified by writing combination of two or more characters. These compound characters occurs 12 to 15% in the Devanagari Script. The moment based techniques are being successfully applied to several image processing problems and represents a fundamental tool to generate feature descriptors where the Zernike moment technique has a rotation invariance property which found to be desirable for handwritten character recognition. This paper discusses extraction of features from handwritten compound characters using Zernike moment feature descriptor and proposes SVM and k-NN based classification system. The proposed classification system preprocess and normalize the 27000 handwritten character images into 30x30 pixels images and divides them into zones. The pre-classification produces three classes depending on presence or absence of vertical bar. Further Zernike moment feature extraction is performed on each zone. The overall recognition rate of proposed system using SVM and k-NN classifier is upto 98.37%, and 95.82% respectively.

Keywords—Handwritten Character, Devanagari Compound, Zernike, SVM, k-NN.

I. INTRODUCTION

Handwritten character recognition is gaining popularity for many years and attracting researchers for the purpose of potential application development. These potential applications reduce the cost of human efforts and save the time. Some of its potential application areas are like bank automation, postal automation [1]–[3] etc. Similarly the biometric and criminal identification system uses scanned handwritten script for forensic and Historic Document Analysis (HDA) and represents an excellent study area within the research field of biometrics and forensic science.

The technical challenge in handwritten character recognition comes from three sources: *Symbol*: an ideal shape that occurs in hierarchy and symbol are arranged in complex form at different level in organization. *Deformation*: shape variation in each symbol to undergoes geometric transformation (translation, rotation, scaling, stretching) and complex representation. *Defect* flaw in image owing to print, scan, quantized, binary etc. Handwritten and Printing character demands diverse approach, handwritten consist of extended stroke and printed consist of normal shaped blobs.

Research in handwritten character recognition focuses on two main approaches i.e. on-line and off-line. In on-line character recognition system captures data by the sensors during writing process, which makes the information dynamically available according to the strokes. While, off-line character recognition takes place in static form where images are captured or scanned after completion of the writing process on paper/sheets. Both the tasks are challenging for automatic character recognition, specifically in off-line character recognition requires more efforts due to various reasons viz. large variations in shape of characters due to pen ink, pen width, and accuracy of devices, stroke size and location, effect of physical and mental situation of the writer on writing style, in turns effect the recognition accuracy.

Character recognition problem becomes more challenging even in on-line and off-line in Indian Language Scripts due to several reasons [4]. The Indian scripts have character set with large number of characters. The shape of the characters in Indian scripts is more complex and may have modifiers. These modifiers may found at above, below or in-line with the character. The modifiers are the vowel that changes their shapes when they get connected with the consonants. The scripts may have some character pairs that are looks alike and cause difficulty in classification. Some of Indian languages like Devanagari, Bangla are having the specific problem in compound characters where two or more consonants join with each other to form a special character [5], [6].

The research work on character recognition of Devanagari script was started in 1970, where Sinha and Mahabala [7] were presented a syntactic pattern analysis system for the recognition of Devanagari characters (DC). First research report on handwritten Devanagari Characters (HDC) was published in 1977 by Sethi and Chatterjee [8], very few work were reported on OCR in the literature and later on in the next decade S. Kumar and et. al. contributed more in this domain [9]. An extensive research work on printed Devanagari Characters and Handwritten Characters was carried out by Bansal [10]–[12] and Reena et.al, [13], [14] respectively. Recognition of characters in different languages using Zernike Moments was reported in [9], [15]–[22]. Researchers have proposed Chain Code Histogram and directional information gradient based feature extraction in [22]–[24]. A significant contribution

by Arora and et. al., proposed feature extraction techniques namely, intersection, shadow feature, chain code histogram and straight line fitting features in [25]–[28]. Deshpande and et. al. [29] has proposed fine classification and recognition of Devanagari characters. S. Kumar in [30] also extracted various features and performed comparison using SVM and MLP. Pal and et al. proposed SVM and MQDF based scheme for recognition of Devanagari Characters [31]. U. Pal and T. Wakabayashi [32] given a comparative study of different Devanagari Character recognizers which extracts features based on curvature and gradient information. Sushama Shelke and et. al. [33] presented a novel approach for recognition of unconstrained handwritten Marathi characters. Baheti M.J. and et al. [34] proposed a method based on Affine Invariant Moment (AIM) for Gujarati numerals using k-NN and PCA classifiers. Elastic matching (EM) technique based on an Eigen Deformation (ED) for recognition of handwritten Devanagari characters is proposed by V. Mane and et.al, [35]. Recognition of handwritten Bangla compound characters was attempted by U. Pal and et al. [36] using gradient features. S. Shelke and S. Apte have reported work on handwritten Marathi compound characters using multi-stage multi-feature classifier [5], [6].

The literature evidence shows that moment can be considered as potential features for recognition of characters and numerals, which motivate us to enrich the several orthogonal and discrete moment features and test the efficacy of the system for compound characters. While significant advances have been achieved in recognizing Roman-based scripts like English, ideographic characters Chinese, Japanese, Korean, and Arabic, only few works on some of the major Indian scripts like Devanagari, Bangla, Gurmukhi, Tamil, Telugu, are available in the literature [37]–[41].

This paper proposes a novel Zernike moment based feature descriptor followed by SVM and k-NN neural network approach for recognition of Marathi Script Basic and Compound Characters derived from Devanagari. The organization of the paper is as follows: Section 2 deals with properties of Devanagari derived Marathi script. Database designing and Proposed System has been discussed in Section 3. Section 4 deals with Zernike Moment based feature extraction technique. Details about the SVM and k-NN approach used for character recognition system are elaborated in Section 5. The experimental results are discussed in Section 6. Conclusion of the paper is given in Section 7.

II. PROPERTIES OF DEVANAGARI BASIC AND COMPOUND CHARACTER

The basic set of symbols of Devanagari script consists of 12 vowels (or swar), 36 consonants (or vyanjan). The alphabet of modern Devanagari script consists of 14 vowels and 33 consonants also called as basic characters. Writing style of the Devanagari script is from left to right and the concept of upper and lower case is absent in the script. In this script vowel following by a consonant takes a modified shape, these modified shapes are called modified characters. A consonant or vowel following a consonant sometime takes a compound orthographic shape, which we called as a compound character. Compound characters can be combination of two consonants as well as a consonant and a vowel. The compound characters are joined in various ways, by removing vertical line of the character and then to the other characters from the

left side like म्य, in another way it is joined side by side or one above the other like डू. The example of compound characters is shown in Fig (1). The split character is half of the basic character which gets connected to other characters. The example of split component of compound character is shown in Fig (2). Compounding of three or four characters also exists in the script. There are about 280 compound characters in the Devanagari script [4], [31].

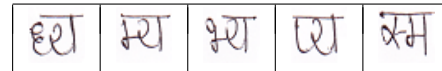


Figure 1. Sample images of Compound Character

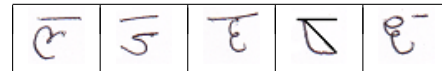


Figure 2. Sample images of Split Component of Compound Character

Marathi script is one of the derived script from Devanagari, and it is an official language of Maharashtra. Marathi script consists of 16 vowels and 36 consonants making 52 alphabets. Marathi script is written from left to right, which does not have upper and lower case characters. Similar to Devanagari it has nearly the similar type of compound characters property. However, the occurrence of compound characters in Marathi is found to be about 11 to 12%, whereas in other scripts of Devanagari, it is about 5 to 7% [42].

III. DATABASE DESIGNING AND PROPOSED SYSTEM

A. Database

At present no dataset of handwritten compound characters is available for Marathi script derived from Devanagari and hence we have created handwritten compound characters dataset for this work and it has been tested with our proposed system for its recognition, this adds a new contribution in the literature. Details of this database are provided in Table I.

The database of Handwritten Characters of Marathi from Devanagari script is created for the purpose of this work, which contains basic, compound and split components of compound characters. These data characters were recorded in written form on special paper sheet from 250 different volunteers of different age group. (in between 20-40 year old). The recorded character is then scanned with Flatbed Scanner at 300 dpi. The size of the image of each character is considered 90x90 pixels and it is stored in TIFF image format.

Table I. DATASET OF HANDWRITTEN DEVANAGARI BASIC AND COMPOUND CHARACTERS

Property	Descriptions
Number of subjects	250
Number of basic character	48
Number of compound characters	45
Number of split compound characters	15
Number of images given by each subject	48+45+15=108
Gray/Color	Color
Resolution	90*90 pixels
DPI	300
Format	TIFF
Total Number of images	27000

B. Proposed System

In the proposed system, we aim at recognizing handwritten Marathi Devanagari compound characters. This is done by employing Zernike moment feature extraction using SVM and k-NN neural network approach. Fig. (3) shows the basic block diagram of the proposed recognition system, which consists of different phases begin with input character images, preprocessing, pre-classification of the characters, Zernike moment based feature extraction and character recognition. The brief phase wise explanation of the recognition system as follows:

Fig. (3) shows the basic block diagram of the recognition system. It shows that the handwritten Devanagari character are scanned and a digitized document is obtained. From it a particular character is selected, the image character is cropped and resized into fix row and columns. Each block of the recognition system is elaborated in following sections.

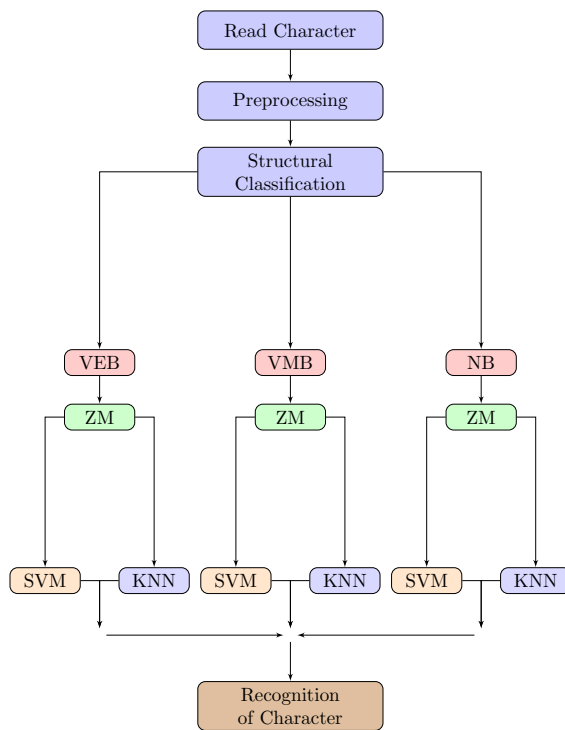


Figure 3. Block Diagram of Proposed Character Recognition System

C. Preprocessing

Pre-processing step is performed on the character image to remove the noise from it and also to minimize the variations in character styles. Occasionally, the document while scanning was not clean and so it has produced small dots in the images. Noise generated by the shaded areas and dots must be filtered during preprocessing step. Moreover, the characters in scanned images may found to be skewed, slant and varied in sizes due to cropping. This has been processed in this step. The typical flow of preprocessing step is shown in following Fig (4).

1) *RGB to Gray Image*: The database contains color character images. In preprocessing the character images are converted to binary images using rgb2gray utility in MATLAB.

2) *Thresholding*: This preprocessing step also termed as binarization process and converts the pixels that are above the threshold to white and those which are below the threshold to black. We have set the threshold value $Th= 190$ to produce good quality binarized images.

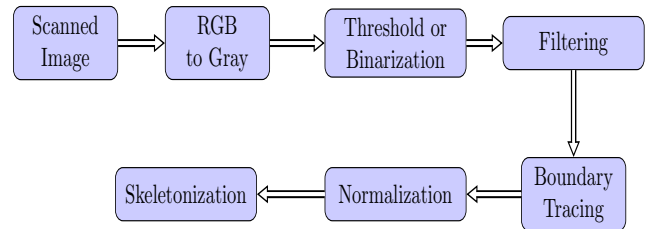


Figure 4. Steps in Preprocessing of Image

3) *Filtering*: To remove the noise present in the binarized image filtering has been done. We have used Median filter to remove small black spot in the image and the black shade appearing at the edges. Further, the documents were cropped from the edges. Thresholding and filtering steps often resulted in some broken characters. To rejoin the broken characters, image dilation operation on the filtered images has performed.

4) *Boundary Tracing*: Tracing of the boundary identifies the connected components of the characters in the filtered images and stores it in array. To find the connected components, the algorithm starts by traversing the rows of filtered image. It searches for a foreground pixel, and then it marks that pixel and picks it. Similarly, marking of all the neighbors of found pixel in all search directions completed till all the pixels of the possible character have been traversed and marked. Otherwise, it will continue the search in the next row. If the size of any picked connected component is too small than the actual required size, then the algorithm treats that component as noise and neglects that component.

5) *Normalization*: During normalization step, slant in characters is removed and resized to a window. Slant is the average divergence of the vertical strokes of the character from the right side of the character. To remove the slant, we used imrotate with angle θ . At each angle the sum of vertical projection of the transformed character is calculated. The angle with maximum sum of vertical projection is used to finally perform shear transformation on the character and estimated the slant angle.

6) *Skeletonization*: In skeletonization, the thickness of the character is reduced to one-pixel character bound. We have applied the thinning operation on the character and taken the precaution, do not to break the character. These operations were used not only to find the vertical bar and position of vertical bar in the character, but also to extract endpoints, junction in the character. This features helps in the pre-classification of the characters. A sample output of the preprocessed character क is shown in Fig. (5).

D. Pre-classification

Character Images after preprocessing stage consists of some global and local features. The global feature consists of presence of vertical line, position of vertical bar in the

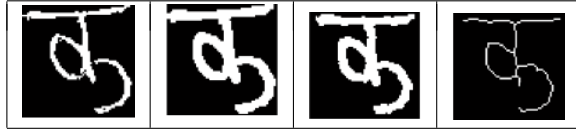


Figure 5. Character Images after Preprocessing

character and enclosed region in the character. The local features consists of the end points and junction position in the character. On the basis of global feature, the character is classified into three major categories based on the presence of vertical bar i.e. a) character with vertical bar at right (**VEB: Vertical End Bar**), b) character with vertical bar at middle (**VMB: Vertical Mid Bar**), and c) the character with absence of vertical bar (**NB: No Bar**). Vertical bar at right are further classified into two categories based on whether the vertical bar and rest of the character are connected or not to the bar. These pre-classification of characters are shown in the following Table II and III.

Table II. CLASSIFICATION OF DEVANAGARI BASIC CHARACTER

Sr. No.	Pre Classification	Character
1	Character connected vertical bar at right side	ख, घ, च, ज, झ, ञ, त, थ, द, ध, न, प, ब, भ, म, य, र, ल, व, स, ष, क्ष, ज्ञ
2	Character not connected with vertical bar at right side	ग, ण, श
3	Character with absence of vertical bar	ङ, छ, ट, ठ, ड, ढ, द, र, ह, ळ

Table III. CLASSIFICATION OF DEVANAGARI COMPOUND CHARACTER

Sr. No.	Pre Classification	Character
1	Character connected vertical bar at right side	प्य, ज्य, व्य, त्य, ध्य, भ्य, ल्य, व्य, ध्य, म्य, व्य, न्य, च्य, स्य, स्म, न्म, ज्म, त्म, स्य, ल्य, क्य, क्ल, फ्य, ग्य, ण्य, श्व, ज्व, स्व, भ्व, म्म, व्य, प्त, व्ज, ख्व, त्त, न्न
2	Character not connected with vertical bar at right side	स्क, ल्क, स्फ
3	Character with absence of vertical bar	ध्द, च्छ, म्ह, न्ह, छ, व्द, व्द

E. Local Structural Classification

The local features are detected on the basis of the end points of the character. We have firstly partitioned the character into 3x3 image i.e. 9 quadrants and extracted the end points and junctions in each individual block as shown in Fig. (6).

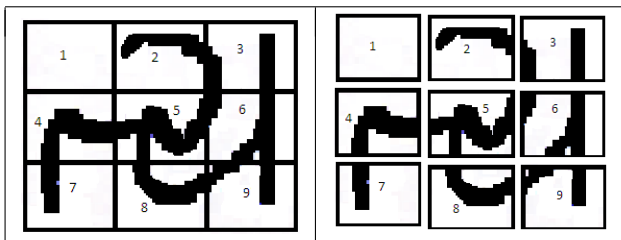


Figure 6. Presence of End Points in partition block of Character

Thus pre-classification of character is done and put the character in proper class like VEB, VMB and NB and then Zernike moment features are extracted for its final classification under SVM and k-NN.

IV. ZERNIKE MOMENT BASED FEATURE EXTRACTION

Zernike moments are complex number by which an image is mapped on to a set of two-dimensional complex Zernike polynomials. The magnitude of Zernike moments is used as a rotation invariant feature to represent a character image patterns [43]. Zernike moments are a class of orthogonal moments and have been shown effective in terms of image representation. The orthogonal property of Zernike polynomials enables the contribution of each moment to be unique and independent of information in an image. A Zernike moment does the mapping of an image onto a set of complex Zernike polynomials. These Zernike polynomials are orthogonal to each other and have characteristics to represent data with no redundancy and able to handle overlapping of information between the moments [26]. Due to these characteristics, Zernike moments have been utilized as feature sets in applications such as pattern recognition [27] and content-based image retrieval [28]. These specific aspects and properties of Zernike moment are supposed to found to extract the features of compound handwritten characters. Teague [16] has introduced the use of Zernike moments to overcome the shortcomings of information redundancy due to geometric moments.

The Zernike moment were first proposed in 1934 by Zernike [44]. Their moment formulation appears to be one of the most popular, outperforming the alternatives [45] (in terms of noise resilience, information redundancy and reconstruction capability). Complex Zernike moments [46] are constructed using a set of complex polynomials which form a complete orthogonal basis set defined on the unit disc $(x^2+y^2) \leq 1$. They are expressed as A_{pq} . Two dimensional Zernike moments:

$$A_{mn} = \frac{m+1}{\pi} \int_x \int_y f(x,y)[V_{mn}(x,y)]^* dx dy$$

where $x^2 + y^2 \leq 1 \nabla_y (x_i + h, y_j + k)$

(1)

where $m = 0, 1, 2, \dots, \infty$ and defines the order, $f(x, y)$ is the function being described and $*$ denotes the complex conjugate. While n is an integer (that can be positive or negative) depicting the angular dependence, or rotation, subject to the conditions:

$$m - |n| = \text{even}, |n| \leq m \quad (2)$$

and $A_{mn}^* = A_{m,-n}$ is true. The Zernike polynomials [20] $V_{mn}(x, y)V_{mn}(x, y)$ Zernike polynomial expressed in polar coordinates are:

$$V_{mn}(r, \theta) = R_{mn}(r)exp(jn\theta) \quad (3)$$

where (r, θ) are defined over the unit disc, $j = \sqrt{-1}$ and $R_{mn}(r)$ and is the orthogonal radial polynomial, defined as $R_{mn}(r)$ Orthogonal radial polynomial:

$$R_{mn}(r) = \sum_{s=0}^{\frac{m-|n|}{2}} (-1)^s F(m, n, s, r) \quad (4)$$

where:

$$F(m, n, s, r) = \frac{(m-s)!}{s! \left(\frac{m+|n|}{2} - s\right)! \left(\frac{m-|n|}{2} - s\right)!} r^{m-2s} \quad (5)$$

where $R_{mn}(r) = R_{m,-n}(r)$ and it must be noted that if the conditions in Eq. 2 are not met, then $R_{mn}(r) = 0$. The first six orthogonal radial polynomials are:

$$\begin{aligned} R_{00}(r) &= 1 & R_{11}(r) &= r \\ R_{20}(r) &= 2r^2 - 1 & R_{22}(r) &= r^2 \\ R_{31}(r) &= 3r^3 - 2r & R_{33}(r) &= r^3 \end{aligned} \quad (6)$$

So for a discrete image, if P_{xy} is the current pixel then Eq. (1) becomes:

$$A_{mn} = \frac{(m+1)}{\pi} \sum_x \sum_y P_{xy} [V_{mn}(x, y)]^* \quad \text{where } x^2 + y^2 \leq 1 \quad (7)$$

To calculate the Zernike moments, the image (or region of interest) is first mapped to the unit disc using polar coordinates, where the centre of the image is the origin of the unit disc. Those pixels falling outside the unit disc are not used in the calculation. The coordinates are then described by the length of the vector from the origin to the coordinate point, r , and the angle from the x axis to the vector r . r Polar co-ordinate radius, θ Polar co-ordinate angle, by convention measured from the positive x axis in a counter clockwise direction. The mapping from Cartesian to polar coordinates is:

$$x = r \cos \theta \quad y = r \sin \theta \quad (8)$$

where,

$$r = \sqrt{x^2 + y^2} \quad \theta = \tan^{-1} \left(\frac{y}{x} \right) \quad (9)$$

However, \tan^{-1} in practice is often defined over the interval $\frac{\pi}{2} \leq \theta \leq \frac{3\pi}{2}$, so care must be taken as to which quadrant the Cartesian coordinates appear in. Translation and scale invariance can be achieved by normalising the image using the Cartesian moments prior to calculation of the Zernike moments [47]. Translation invariance is achieved by moving the origin to the image's COM, causing $m_{01} = m_{10} = 0$. Following this, scale invariance is produced by altering each object so that its area (or pixel count for a binary image) is $m_{00} = \beta$, where β is a predetermined value. Both invariance properties (for a binary image) can be achieved using :

$$h(x, y) = f \left(\frac{x}{a} + \bar{x}, \frac{y}{a} + \bar{y} \right) \quad \text{where } a = \sqrt{\frac{\beta}{m_{00}}} \quad (10)$$

and $h(x, y)$ is the new translated and scaled function. The error involved in the discrete implementation can be reduced by interpolation. If the coordinate calculated by Equation 58 does not coincide with an actual grid location, the pixel value associated with it is interpolated from the four surrounding pixels. As a result of the normalization, the Zernike moments $|A_{00}|$ and $|A_{11}|$ are set to known values. $|A_{11}|$ is set to zero, due to the translation of the shape to the center of the coordinate system. This however will be affected by a discrete

implementation where the error in the mapping will decrease as the shape (being mapped) size (or pixel-resolution) increases. $|A_{00}|$ is dependent on m_{00} , and thus on β

$$|A_{00}| = \frac{\beta}{\pi} \quad (11)$$

Further, the absolute value of a Zernike moment is rotation invariant as reflected in the mapping of the image to the unit disc. The rotation of the shape around the unit disc is expressed as a phase change, if ϕ is the angle of rotation, A_{mn}^R is the Zernike moment of the rotated image and A_{mn} is the Zernike moment of the original image then:

$$A_{mn}^R = A_{mn} \exp(-jn\phi) \quad (12)$$

Moment based features are extracted from the each zone of the scaled character bitmapped image. The image is partitioned into zone and features are extracted from each zone. In this paper Zernike moments based feature extraction is proposed for off-line Devnagari Handwritten Basic and Compound Character. To get the feature set, at first, the image is segmented to 30 x 30 blocks, and partitioned as feature set as follows and the List of the first 8 order Zernike moments is given in Table IV.

Feature set 1: Fig. 7 (a) is considered as a whole character image.

Feature set 2: Fig. 7 (b) shows the image divided into four equal zones.

Feature set 3: Fig. 7 (c) shows the image divided into three vertical equal zones.

Feature set 4: Figure 7 (d) shows the image divided into three horizontal equal zones.

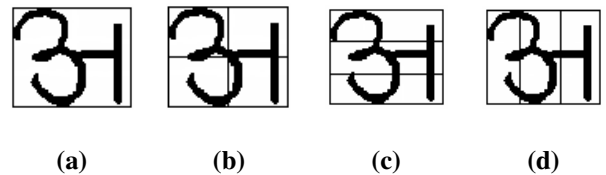


Figure 7. Partition of Devanagari Character into feature set

Table IV. THE FIRST 8 ORDER ZERNIKE MOMENTS

Order	Dimensionality	Zernike Moments
0	1	$A_{0,0}$
1	2	$A_{1,1}$
2	4	$A_{2,0}, A_{2,2}$
3	6	$A_{3,1}, A_{3,3}$
4	9	$A_{4,0}, A_{4,2}, A_{4,4}$
5	12	$A_{5,1}, A_{5,3}, A_{5,5}$
6	16	$A_{6,0}, A_{6,2}, A_{6,4}, A_{6,6}$
7	20	$A_{7,1}, A_{7,3}, A_{7,5}, A_{7,7}$

V. CLASSIFICATION AND RECOGNITION

The classification stage is the decision making part of a recognition system and it uses the features extracted in the previous stage. We have used Support Vector Machine (SVM) and k-NN for the purpose of Classification and recognition.

A. Support Vector Machine (SVM)

The support vector machine (SVM) is capable of learning and to achieve good generalization performance. If SVM is given a finite amount of training data, it is striking a balance between the goodness of fit on a given training and testing datasets. The SVM shows high ability to achieve error-free recognition. With this concept as the basis, support vector machines have proved to achieve good generalization performance with no prior knowledge of the data. The SVM is nonlinearly map the input data onto a higher dimensional feature space and determines a separating hyper plane with maximum margin between the two classes. A support vector machine is a maximal margin hyper plane in feature space built by using a kernel function. This results a nonlinear boundary in the input space. The optimal separating hyper plane can be determined without any computations in the higher dimensional feature space by using kernel functions in the input space [48].

The SVM produces a model (based on the training data) which predicts the target values of the test data features. Given a training set of instance-label pairs $(x_i, y_i), i = 1, 2, \dots, l$ where $x_i \in R^n$ and $y \in \{1, -1\}$, the SVM require the solution of the following optimization problem:

$$\min_{w,b,\xi} = \frac{1}{2}w^T w + C \sum_{i=1}^l \xi_i$$

Subject to $y_i(w^t \phi(x_i) + b) \geq 1 - \xi_i, \xi_i > 0$

(13)

Here the training vectors x_i is mapped into a higher dimensional space by the function ϕ . SVM finds the optimal hyper-plane which maximizes the distance, or more specifically the margin, between the nearest examples of both the classes. These nearest examples are called as support vectors (SVs). Where, $C > 0$ is the penalty parameter of the error term. Furthermore, $K(x_i, x_j) \equiv \phi(x_i)^T \phi(x_j)$ is called the kernel function. We have used the radial basis function (RBF) kernel in our work given by

$$K(x_i, x_j) \equiv e^{(-\gamma \|x_i - x_j\|)}, \gamma > 0 \quad (14)$$

A search is applied to find the value of γ which is parameter of RBF. The value of both variance parameter are selected in the range of (0, 1) for gamma γ and (0, 1000) for cost (c) for support vectors and examines the recognition rate.

B. k-Nearest Neighbor (k-NN) Classifier

In the k-NN based classification similar observations belongs to similar classes. The test numeral feature vector is classified to a class, depending upon nearest neighbor distance. The nearest factor is based on minimum Euclidean Distance. Prior features are used to decide the k-nearest neighbor of the given feature vector. The most common similarity measure for k-NN classification is the Euclidian distance metric, defined between feature vectors as:

$$euc(x^p, y^p) = \sqrt{\sum_{i=1}^f (x_i - y_i)^2} \quad (15)$$

Where, f represents the number of features. The less distance values represent greater similarity [18], [19].

VI. EXPERIMENTS AND RESULTS

The performance evaluation using SVM and k-NN based classification has be performed on the database of Handwritten Devanagari Marathi Characters. The training dataset consists of 9600 basic character, 9000 Compound and 3000 split component of compound characters. The testing images are preprocessed and pre-classified as discussed in Section III (A). This gives 30x30 blocks segmented images of each character. Depending on the zones decided in the preprocessing step we have classified the feature sets as discussed in Section V. Then, moment based features are extracted from the each zone of the scaled character bitmapped image. Table IV shows first eight ordered Zernike moments extracted from each character using equation Zernike Moment. The Zernike moments are further divided into five folded cross validation parameters for each Devanagari Marathi Basic and Compound Characters shown in Table II and III. We experiment with different 2 values of the gamma (γ) and cost function c . The value of gamma (γ) = 0.5 and cost (c) = 1000. For the value of k-NN with K=3 is selected. The results are promising for both basic and compound character. The overall recognition accuracy is 98.37% for SVM, and 95.82% for k-NN for basic character and 98.32% for SVM and 95.42% for k-NN towards Compound character. The results on some sample are placed in Table V and VI.

The performance of the proposed method in terms of the recognition rate is compared with the other reported work and is given in Table VII. On the basis of the Table VII our proposed method shows the enhancement in the recognition rate i.e. 98.37% for basic characters and 98.32% for compound characters.

Table V. RECOGNITION RESULT FOR BASIC CHARACTER

Basic Character	Classifier		Basic Character	Classifier	
	SVM	k-NN		SVM	k-NN
क	99.26	95.14	घ	98.49	96.12
ख	98.45	95.39	न	98.82	96.57
ग	99.12	96.00	प	98.78	96.62
घ	98.40	95.30	फ	99.23	96.21
ङ	97.66	94.73	ब	98.58	95.82
च	98.73	94.50	भ	98.61	97.26
छ	97.84	95.19	म	98.59	96.36
ज	98.62	95.87	य	98.50	95.45
झ	98.53	95.09	र	98.53	96.33
ञ	97.43	95.94	ल	98.62	96.10
ट	98.43	95.43	व	98.63	96.06
ठ	98.52	95.02	श	99.27	97.25
ड	97.40	95.29	स	98.76	96.00
ढ	98.29	95.30	ह	97.74	94.49
ण	99.23	96.36	ळ	98.13	95.51
त	98.82	95.95	ष	98.20	95.36
थ	97.79	96.37	क्ष	98.23	96.94
द	98.09	95.90	ज्ञ	98.48	96.26
Average Recognition Rate SVM: 98.37 and k-NN: 95.82					

VII. CONCLUSION

This paper presents a system for offline handwritten simple and compound character recognition for Marathi derived Devanagari script. Huge compound a basic and compound character dataset is collected from various age groups of writers and which has been used for database creation and named as KVKPR2013. This database further utilize for classification and recognition purpose specifically for compound characters.

Table VI. RECOGNITION RESULT FOR COMPOUND CHARACTER

Compound Character	Classifier		Compound Character	Classifier	
	SVM	k-NN		SVM	k-NN
क्य	98.86	96.13	व्य	98.80	96.82
त्त	98.50	96.48	स्व	98.04	96.56
प्य	98.75	96.90	त्स	98.63	96.36
कल	98.56	96.30	न्ह	97.71	93.45
ज्य	97.76	96.78	ष्ट	97.06	93.28
स्म	97.99	94.55	घ्य	98.54	96.09
त्त	98.09	94.25	म्य	98.70	94.66
ध्द	97.85	94.86	न्य	98.86	94.31
ज्व	97.33	94.92	द्व	98.52	94.42
ग्य	98.64	96.14	म्न	98.28	94.49
च्छ	97.24	95.28	स्फ	98.48	94.62
फ्य	98.92	95.02	अं	98.59	95.36
व्य	98.62	94.28	त्त	98.79	96.54
त्य	98.76	95.26	न्न	98.37	96.46
स्क	98.36	95.76	च्य	98.47	95.67
क्त	98.18	95.45	ख्व	97.64	94.48
म्ह	97.88	94.72	प्य	98.56	96.57
न्म	98.49	94.86	स्य	98.54	96.74
ध्र्य	98.36	95.42	स्य	98.60	95.64
ज्म	98.38	96.57	त्य	98.51	95.76
भ्य	98.72	95.78	द्व	97.89	94.29
ल्य	98.89	95.54	श्व	98.47	95.47
			भ्व	97.25	94.45
Average Recognition Rate SVM: 98.32 and k-NN: 95.42					

Table VII. COMPARISON OF RESULTS OF PROPOSED METHOD WITH OTHER METHODS IN LITERATURE

Method	Features	Classifier	Dataset (size)	Accuracy (%)
Sharma [22]	Chain Code	Quadratic	11270	80.36
Deshpande [29]	Chain Code	RE and MED	5000	82.00
Arora [26]	Structural	FFNN	50000	89.12
Hanmandlu [23]	Vector Distance	Fuzzy set	4750	90.65
Arora [28]	Shadow and CH	NKO and MED	7154	90.74
Kumar [9]	Gradient	SVM	25000	94.10
Pal et. al [24]	Gradient and Gaussian Filter	Quadratic	36172	94.24
Mane [35]	Eigen Deformation (ED)	Elastic Matching	3600	94.91
Pal [26]	Gradient	SVM and MQDF	36172	95.13
Pal [32]	Gradient	MIL	36172	95.19
Arora [27]	Chain code, Shadow	MLP	1500	98.16
S. Shelke and S. Apte [49]	NPD, ED, Wavelet	MLP	37000	97.95
Proposed (Basic)	Zernike Moment	SVM	12000	98.37
Proposed (Compound)	Zernike Moment	SVM	15000	98.32

Prior to feature extraction the character is pre-classified into three categories using structural features. Various complex features of compound characters from the database has been created through Zernike moment approach and implemented successfully for its classification and recognition under SVM and k-NN approach. Zernike moment feature for Devnagari has given better result for compound character. The proposed system gives improved recognition rate of 0.37% than other handwritten character recognition system. The system has been evaluated on a huge amount of Handwritten Character Database i.e. 12000 basic and 15000 compound character dataset created in our laboratory. Since, no work has been reported on Devnagari Compound Character recognition in the last decade, the system handles the problem with structural and statistical features of compound character. The system handles

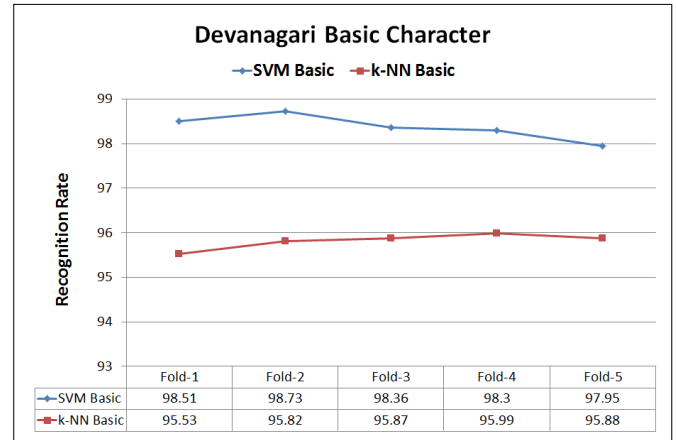


Figure 8. Recognition Rate of Basic Characters through SVM and k-NN Classifiers

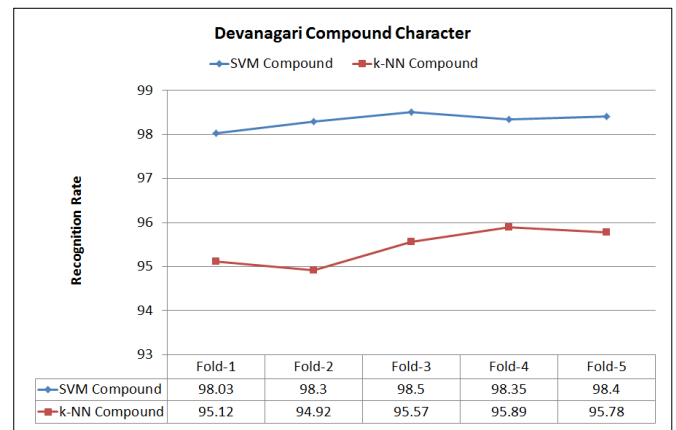


Figure 9. Recognition Rate of Basic Characters through SVM and k-NN Classifiers

only 45 compound characters that extracts Zernike moment features and classified using SVM and k-NN approach. In future the system can be extended to handle more compound characters with other features like orthogonal moments and can classified through advanced patterns classification and neural network approaches.

ACKNOWLEDGMENT

Authors would like to acknowledge and thanks to University Grants Commission (UGC), India for granting UGC SAP (II) DRS Phase-I F. No.-3-42/2009 Biometrics: Multimodal System Development Laboratory facility and One Time Research Grant F. No. 4-10/2010 (BSR) supporting to this work.

REFERENCES

[1] K. Roy, S. Vaidya, U. Pal, B. B. Chaudhuri, and A. Belaid, "A system for indian postal automation," in *Proc. 8th Int. Conf. Document Analysis and Recognition, Seoul, Korea, Aug. 31-Sep. 1, 2005*, pp. 1060-1064.
 [2] U. Pal, R. K. Roy, and F. Kimura, "Indian multi script full pin-code string recognition for postal automation," in *Proc. 10th Int. Conf. Document Analysis and Recognition, Barcelona, Spain, Jul. 26-29, 2009*, pp. 456-460.

- [3] B. B. Chaudhari, "Digital document processing - major directions and recent advances," *London:Springer*, 2007.
- [4] U. Pal and B. B. Chaudhari, "Indian script character recognition: a survey," *Pattern Recognition*, vol. 37, pp. 1887–1899, 2004.
- [5] S. Shelke, S. Apte, and et. al., "A novel multistage classification and wavelet based kernel generation for handwritten marathi compound character recognition," in *Proc. Int. Conf. Communications and Signal Processing, Kerala, India*, 2011, pp. 193–197.
- [6] S. Shelke and S. Apte, "A multistage handwritten marathi compound character recognition scheme using neural networks and wavelet features," *International Journal of Signal Processing, Image Processing and Pattern Recognition*, vol. 4, pp. 81–94, 2011.
- [7] R. K. Sinha and Mahabala, "Machine recognition of devnagari script," *IEEE Trans. System Man Cyber*, pp. 435–441, 1979.
- [8] I. K. Sethi and B. Chatterjee, "Machine recognition of constrained hand printed devnagari," *Pattern Recognition*, vol. 9, pp. 69–75, 1977.
- [9] S. Kumar and C. Singh, "A study of zernike moments and its use in devnagari handwritten character recognition," in *Proc. Intl. Conf. Cognition and Recognition, Mandya (India)*, 2005, pp. 514–520.
- [10] V. Bansal and et. al., *Integrating Knowledge Sources in Devanagari Text Recognition*. IIT, Kharagpur: Ph.D. Thesis, 1999.
- [11] V. Bansal and R. M. K. Sinha, "Partitioning and searching dictionary for correction of optically read devanagari character strings," in *Proc. 5th Int. Conf. Document Analysis and Recognition, Bangalore, India, Sept. 20-22, 1999*, pp. 53–656.
- [12] V. Bansal. and R. M. K. Sinha., "On how to describe shapes of devanagari characters and use them for recognition," in *Proc. 5th Int. Conf. Document Analysis and Recognition, Bangalore, India, Sept. 20-22, 1999*, pp. 410–413.
- [13] R. Bajaj, L. Dey, and S. Chaudhury, "Devnagari numeral recognition by combining decision of multiple connectionist classifiers," *Sadhana*, vol. 27, pp. 59–72, 2002.
- [14] P. M. Patil and T. R. Sontakke, "Rotation, scale and translation invariant handwritten devanagari numeral character recognition using general fuzzy neural network," *Pattern Recognition*, vol. 40, pp. 2110–2117, 2007.
- [15] L. C. Barczak, M. J. Johnson, and C. H. Messom, "Revisiting moment invariant: Rapid feature extraction and classification for handwritten digit," in *Proceeding of Image and Vision Computing, Hamilton, New Zealand, December, 2007*, pp. 137–142.
- [16] R. O. Duda, P. E. Hart, and D. G. Stork, *Pattern Classification, Second ed.* John Wiley and Sons, Inc. 14, 2001.
- [17] H. R. Boveiri and et. al., "Persian printed numeral character recognition using geometrical central moments and fuzzy min max neural network," *International Journal of Signal Processing*, pp. 226–232, 2009.
- [18] H. R. Boveiri., "Persian printed numeral classification using extended moment invariants," *World Academy of Science, Engineering and Technology 63*, pp. 167–174, 2010.
- [19] S. Arora, D. Bhattacharjee, M. Nasipuri, D. K. Basu, and M. Kundu, "Application of statistical features in handwritten devanagari character recognition," *International Journal of Recent Trends in Engineering*, vol. 2, pp. 40–42, 2009.
- [20] R. S. Kunte and R. D. S. Samuel, "A simple and efficient optical character recognition system for basic symbols in printed kannada text," *Sadhana*, vol. 32, pp. 21–533, 2007.
- [21] S. N. Nawaz and et. al., "An approach to offline arabic character recognition using neural network," in *Proceeding of IEEE ICECS*, 2003, pp. 1325–1331.
- [22] N. Sharma, U. Pal, F. Kimura, and S. Pal, "Recognition of offline handwritten devnagari characters using quadratic classifier," in *Proc. Indian Conf. Computer Vision Graphics and Image Processing, Madurai (India)*, 2006, pp. 805–816.
- [23] M. Hanmandlu, O. V. R. Murthy, and V. K. Madasu, "Fuzzy model based recognition of handwritten hindi characters," in *Proc. Ninth Biennial Conf. Australian Pattern Recognition Society on Digital Image Computing Techniques and Applications, Glenelg (Australia)*, 2007, pp. 454–461.
- [24] U. Pal, N. Sharma, T. Wakabayashi, and F. Kimura, "Off-line handwritten character recognition of devnagari script," in *Proc. Ninth Intl. Conf. Document Analysis and Recognition, Curitiba (Brazil)*, 2007, pp. 496–500.
- [25] S. Arora, D. Bhattacharjee, M. Nasipuri, D. K. Basu, and M. Kundu, "Combining multiple feature extraction techniques for handwritten devnagari character recognition," in *Proc. IEEE Region 10 Colloquium and Third Intl. Conf. Industrial and Information Systems, Kharagpur (India)*, 2008.
- [26] S. Arora, D. Bhattacharjee, M. Nasipuri, and L. Malik, "A two stage classification approach for handwritten devanagari characters," in *Proc. Intl. Conf. Comput. Intell. Multimedia Appl.*, 2007, pp. 399–403.
- [27] S. Arora, D. Bhattacharjee, M. Nasipuri, D. K. Basu, M. Kundu, and L. Malik, "Study of different features on handwritten devnagari character," in *Proc. 2nd Emerging Trends Eng. Technol.*, 2009, pp. 929–933.
- [28] S. Arora, D. Bhattacharjee, M. Nasipuri, D. K. Basu, and M. Kundu, "Recognition of non-compound handwritten devnagari characters using a combination of mlp and minimum edit distance," *Int. J. Comput. Sci. Security*, vol. 4, pp. 1–14, 2010.
- [29] P. S. Deshpande, L. Malik, and S. Arora, "Fine classification and recognition of hand written devnagari characters with regular expressions and minimum edit distance method," *Journal of Computers*, vol. 3, pp. 11–17, 2008.
- [30] S. Kumar, "Performance comparison of features on devanagari hand-printed dataset," *Int. J. Recent Trends*, vol. 1, pp. 33–37, 2009.
- [31] U. Pal, S. Chanda, T. Wakabayashi, and F. Kimura, "Accuracy improvement of devnagari character recognition combining svm and mqdf," in *Proc. Eleventh Intl. Conf. Frontiers in Handwriting Recognition, Montreal (Canada)*, 2008, pp. 367–372.
- [32] U. Pal, T. Wakabayashi, and F. Kimura, "Comparative study of devnagari handwritten character recognition using different feature and classifiers," in *Proc. Tenth Intl. Conf. Document Analysis and Recognition, Barcelona (Spain)*, 2009, pp. 1111–1115.
- [33] S. Shelke and S. Apte, "A novel multi-feature multi-classifier scheme for unconstrained handwritten devanagari character recognition," in *12th International Conference on Frontiers in Handwriting Recognition*, 2010.
- [34] M. J. Baheti, K. V. Kale, and M. E. Jadhav, "Comparison of classifiers for gujarati numeral recognition," *International Journal of Machine Intelligence (IJMI)*, vol. 3, pp. 160–163, 2011.
- [35] V. Mane and L. Ragha, "Handwritten character recognition using elastic matching and pca," in *Proc. Int. Conf. Adv. Comput., Commun. Control*, 2009, pp. 410–415.
- [36] U. Pal, T. Wakabayashi, and F. Kimura, "Handwritten bangla compound character recognition using gradient feature," in *Proc. 10th Intl. Conf. Information Technology, Orissa, India*, 2007, pp. 208–213.
- [37] B. B. Chaudhuri and U. Pal, "A complete printed bangla ocr system," *Pattern Recognition*, vol. 31, pp. 531–549, 1998.
- [38] K. Roy, T. Pal, U. Pal, and F. Kimura, "Oriya handwritten numeral recognition system," in *Proc. 8th Intl. Conf. Document Analysis and Recognition, vol. 2, Seoul, Korea, Aug. 31-Sep. 1, 2005*, pp. 770–774.
- [39] A. Pujari, C. D. Naidu, M. S. Rao, and B. C. Jinaga, "An intelligent character recognizer for telugu scripts using multi resolution analysis and associative memory," *Image and Vision Computing*, vol. 22, pp. 1221–1227, 2004.
- [40] U. Bhattacharya, S. K. Ghosh, and S. K. Parui, "A two stage recognition scheme for handwritten tamil characters," in *Proc. 9th Intl. Conf. Document Analysis and Recognition, Parana, Sept. 23-26, 2007*, pp. 511–515.
- [41] M. Hasnat, S. M. Habib, and M. Khan, "A high performance domain specific ocr for bangla script," in *Novel Algorithms and Techniques In Telecommunications, Automation and Industrial Electronics*. Springer Netherland, 2008, pp. 174–178.
- [42] U. ., G. ., and B. B. Chaudhari, "Segmentation of touching character in printed devanagari and bangla script using fuzzy multifactorial analysis," *IEEE Trans. Systems, Man and Cybernetics-Part C, Applications and Reviews*, vol. 32, pp. 449–459, 2002.
- [43] H. J. Kim and W.-Y. Kim, "Eye detection in facial images using zernike moments with svm," *ETRI Journal*, vol. 32, pp. 335–337, 2008.
- [44] F. Zernike, "Beugungstheorie des schneidenverfahrens und seiner verbesserten form, der phasenkontrastmethode (diffraction theory of

the cut procedure and its improved form, the phase contrast method),” *Physica*, vol. 1, pp. 689–704, 1934.

- [45] C. Teh and R. T. Chin, “On image analysis by the method of moments,” *IEEE Trans. on Pattern Analysis and Machine Intelligence*, vol. 10, pp. 496–513, 1988.
- [46] M. R. Teague, “Image analysis via the general theory of moments,” *Journal of the Optical Society of America*, vol. 70, pp. 920–930, 1979.
- [47] A. Khotanzad and Y. H. Hongs, “Invariant image recognition by zernike moments,” *IEEE Trans. on Pattern Analysis and Machine Intelligence*, vol. 12, pp. 489–497, 1990.
- [48] V. Vapnik., “The nature of statistical learning theory,” *Springer, N.Y. ISBN 0-387-94559-8*, 1995.
- [49] S. Shelke and S. Apte, “Multistage handwritten marathi compound character recognition using neural networks,” *Journal of Pattern Recognition Research 2 (JPPR)*, pp. 253–268, 2011.



Dr. Karbhari V. Kale, M.Sc, MCA Ph.D. FIETE, Presently working as a professor and head, Department of Computer Science and Information Technology, Dr Babasaheb Ambedkar Marathwada University, Aurangabad, MS-India. He is a fellow of IETE, Life member of CSI, IAPR, ISCA, senior member of CSI and IEEE. He is a member and Faculty of Board of Studies of various universities in India and designed and developed new courses in computer science at UG and PG level. He is recipient of VIJAY SHREE Award. He is actively engage in research and development and has over than 218 research papers in reputed national/international journals and conferences and three books to his credit. He has produced 21 Ph. D. Student under his able guidance. He is reviewer and editor of several journals for India and aboard. He has organized several workshops and conferences. His areas of interests are Image Processing, Pattern Recognition, Biometrics, Bioinformatics, S/W Engg., Artificial Intelligence, Computer vision, Neural Networks etc. He has completed three major research projects and currently working on to specifically area of multimodal Biometrics and Bioinformatics.



Dr. Prapti D. Deshmukh (Patil), M.Sc, Ph.D. MIETE, Presently working as a Principal, Dr. G. Y. Pathrikar’s College of Computer Science, MGM, Aurangabad, MS-India. He is a member of IETE, Life member ISCA. Her research interests are Biometrics, Advanced Pattern Recognition and Neural Network, and Advanced Image Processing.



Mr. Shrinivas V. Chavan, M.Sc, M. Phil, Presently working as Assistant Professor, Department of Computer Science, MSS’s ACS College, Ambad, Jalna, Maharashtra, India. He is a student member of IEEE. His research interests are Character Recognition, Neural Network and Image Processing.



Mr. Majharoddin M. Kazi, UGC MANF Research Fellow (Ministry of Minority Affairs Scholar), Department of Computer Science and IT, Dr Babasaheb Ambedkar Marathwada University, Aurangabad, MS-India. He is a student member of IEEE. His research interests are Biometrics, Pattern Recognition, Neural Network and Image Processing.



Mr. Yogesh S. Rode, M. Phil, Presently working as UGC BSR Meritorious Research Fellow, Department of Computer Science and IT, Dr Babasaheb Ambedkar Marathwada University, Aurangabad, MS-India. He is a student member of IEEE. His research interests are Biometrics, Pattern Recognition, Neural Network and Image Processing.